

T-3366

STABILITY OF OIL/WATER INTERFACE DURING IMMISCIBLE
DISPLACEMENT IN POROUS MEDIA

by

Majeed H. Yousif

ARTHUR LAKES LIBRARY
COLORADO SCHOOL of MINES
GOLDEN, COLORADO 80401

ProQuest Number: 10796315

All rights reserved

INFORMATION TO ALL USERS

The quality of this reproduction is dependent upon the quality of the copy submitted.

In the unlikely event that the author did not send a complete manuscript and there are missing pages, these will be noted. Also, if material had to be removed, a note will indicate the deletion.



ProQuest 10796315

Published by ProQuest LLC (2019). Copyright of the Dissertation is held by the Author.

All rights reserved.

This work is protected against unauthorized copying under Title 17, United States Code
Microform Edition © ProQuest LLC.

ProQuest LLC.
789 East Eisenhower Parkway
P.O. Box 1346
Ann Arbor, MI 48106 – 1346

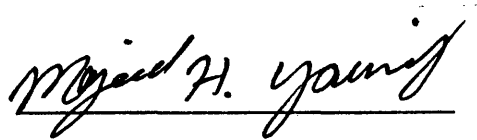
T-3366

A thesis submitted to the Faculty and the Board of Trustees of the Colorado School of Mines in partial fulfillment of the requirements for the degree of Doctor of Philosophy (Petroleum Engineering).

Golden, Colorado

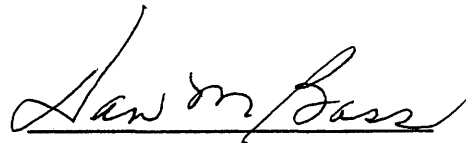
Date 12/22/1987

Signed:



Majeed H. Yousif

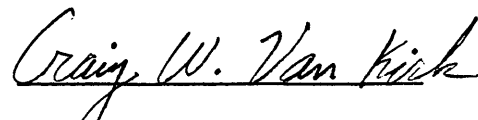
Approved:



Dr. Dan M. Bass
Thesis Advisor

Golden, Colorado

Date Dec. 17, 1987



Dr. Craig W. Van Kirk
Department Head
Petroleum Engineering

DEDICATION

To my mother and father whose lives of hard work have been an inspiration to myself and whose unending love has been a source of support all my life.

ABSTRACT

The stability of immiscible displacement in porous media was investigated theoretically and experimentally in order to delineate the boundaries of stable displacement and to determine the variables pertinent to the process.

A total of 18 runs were conducted in a rectangular cell packed with a nearly homogeneous and isotropic porous medium. The floods were performed at favorable and adverse viscosity ratios. The motion of the oil/water interface was tracked using 55 sets of electrodes located on opposite sides of the cell. The electric resistivity across these electrodes was converted to water saturation using Archie's equation.

No fingering was observed in all the displacements. The only manifestation of instability reported during the displacements conducted in this work was gravity tonguing. However, neither tonguing nor fingering were observed in some displacements, although, the values of breakthrough recovery indicated instability.

A multi-dimensional inspectional analysis was undertaken in order to determine a complete set of similarity groups for two phase immiscible displacements in a rectangular system.

The results of the displacements, conducted in various sand-fluid systems, were analyzed using various derived scaling groups. It was found that the group F_s , representing the combination of the ratio of capillary to gravity forces and the viscosity ratio successfully

predicted the boundaries of instability encountered in immiscible displacement in porous media. The correlation of this dimensionless group, called the stability factor, with the breakthrough recovery showed that the displacement is stable if

$$F_s = 10066 \frac{\sigma \sqrt{\phi/k}}{\Delta\rho g M} > 1.83 \times 10^5 \quad (6.1)$$

In applying the stability criterion shown above, interfacial tension should be in dynes/cm, permeability in darcies and density in gm/cc.

Other scaling groups produced through the method of inspectional analysis showed no meaningful results when correlated with the recovery at breakthrough.

TABLE OF CONTENTS

	<u>Page</u>
ABSTRACT	iv
TABLE OF CONTENTS	vi
LIST OF FIGURES	viii
LIST OF TABLES	xi
ACKNOWLEDGMENTS	xiii
INTRODUCTION	1
CHAPTER ONE - THE NATURE OF STABILITY PHENOMENA	3
CHAPTER TWO - THEORY OF IMMISCIBLE DISPLACEMENT	9
2.1 Mathematical Description of Immiscible Displacement	9
2.1.1 Darcy Law for Two-Phase Flow	9
2.1.2 The Equation of Continuity	10
2.1.3 Capillary Pressure Equation	10,
2.2 Fractional Flow Formula	14
2.3 Normalized One-Dimensional Displacement Equations	14
2.4 The Lagrangian and Eulerian Forms of the Displacement Equation	16
CHAPTER Three - REVIEW OF RELATED RESEARCH	19
CHAPTER FOUR - DIMENSIONAL AND INSPECTIONAL ANALYSIS	34
4.1 Inspectional Analysis	37
4.2 The Physical Significance of the Derived Scaling Groups	40
CHAPTER FIVE - EXPERIMENTAL EQUIPMENT AND PROCEDURE	42
5.1 Model	42

	<u>Page</u>
5.1.1 Model Scaling	42
5.2 Porous Media	45
5.3 Fluids	46
5.4 Saturation Recording System	53
5.4.1 Data Acquisition System	53
5.5 Displacement Procedure	59
CHAPTER SIX - EXPERIMENTAL RESULTS AND DISCUSSIONS	61
6.1 Oil Flooding and the Establishment of Connate Water Saturation	61
6.2 Polymer and Water Flooding	63
6.2.1 Low Permeability Sand Packs	63
6.2.2 Medium Permeability Sand Packs	86
6.2.3 High Permeability Sand Packs	96
6.3 The Boundaries of Stability	107
CONCLUSIONS AND RECOMMENDATIONS	113
REFERENCES CITED	116
APPENDIX A - LISTING OF EXPERIMENTAL DATA	120
APPENDIX B - NOMENCLATURE	138

LIST OF FIGURES

<u>Figure</u>		<u>Page</u>
1.1	Three Types of Equilibrium	4
1.2	4
1.3	Flow in a Cylindrical Tube	6
1.4	A Stable Displacement in Porous Media	6
1.5	Types of Unstable Immiscible Displacement in Porous Media	7
5.1	Rectangular Cell	43
5.2	Schematic Diagram of the Apparatus	44
5.3	Grain Size Distribution of Ottawa Sand	47
5.4	Kerosene Viscosity	49
5.5	Mineral Oil Viscosity	50
5.6	Viscosity of Pusher 500 Solution in Brine	51
5.7	Rheology of Pusher 500 Polymer	52
5.8	Electric Circuitry of a Pair of Electrodes	54
5.9	Data Acquisition/Control System Setup	56
5.10	Diagram of Complete Electric Circuitry	57
5.11	Comparison of Water Saturation Calculated from Resistivity with Water Saturation Measured Volumetrically	58
6.1	Connate Water Saturation. Run No. 1	62
6.2	Saturation Contours of Run Number 1. Oil Flood. Low Permeability Sand	64
6.3	Saturation Contours of Run Number 11. Oil Flood. Medium Permeability Sand	65
6.4	Saturation Contours of Run Number 1. Polymer Flood. Low	

<u>Figure</u>	<u>Page</u>
Permeability Sand	67
6.5 Saturation Contours of Run Number 2. Polymer Flood. Low	
Permeability Sand	69
6.6 Saturation Contours of Run Number 3. Polymer Flood. Low	
Permeability Sand	71
6.7 Saturation Contours of Run Number 4. Water Flood. Low	
Permeability Sand	74
6.8 Saturation Contours of Run Number 5. Water Flood. Low	
Permeability Sand	76
6.9 Saturation Contours of Run Number 6. Water Flood. Low	
Permeability Sand	78
6.10 Saturation Contours of Run Number 7. Water Flood. Low	
Permeability Sand	80
6.11 Saturation Contours of Run Number 8. Water Flood. Low	
Permeability Sand	82
6.12 Saturation Contours of Run Number 9. Water Flood. Low	
Permeability Sand	84
6.13 Saturation Contours of Run Number 10. Water Flood. Low	
Permeability Sand	87
6.14 Saturation Contours of Run Number 11. Water Flood.	
Medium Permeability Sand	89
6.15 Saturation Contours of Run Number 12. Water Flood.	
Medium Permeability Sand	91
6.16 Saturation Contours of Run Number 13. Water Flood.	

<u>Figure</u>	<u>Page</u>
Medium Permeability Sand	93
6.17 Saturation Contours of Run Number 14. Water Flood.	
Medium Permeability Sand	97
6.18 Saturation Contours of Run Number 15. Water Flood.	
High Permeability Sand	99
6.19 Saturation Contours of Run Number 16. Water Flood.	
High Permeability Sand	101
6.20 Saturation Contours of Run Number 17. Water Flood.	
High Permeability Sand	103
6.21 Saturation Contours of Run Number 18. Water Flood.	
High Permeability Sand	105
6.22 Boundaries of Stability as Defined by the Stability	
Factor, F_s	108
6.23 Correlation of the Stability Factor F_s with the	
Breakthrough Oil Recovery. Data from Allam (1979) and	
Peggs (1973)	109
6.24 Effect of Viscosity Ratio on Breakthrough Oil Recovery .	110
6.25 Correlation of Dimensionless Factor G with Breakthrough	
Oil Recovery	111

LIST OF TABLES

<u>Table</u>	<u>Page</u>
5.1 Properties of Porous Medium	46
5.2 Properties of Oil Phase at 72°F	48
6.1 Summary of Experimental Data. Low Permeability Sand . .	66
6.2 Summary of Experimental Data. Medium and High Permeability Sand	95
A1 RUN NO. 1. POLYMER FLOOD	121
A2 RUN NO. 2. POLYMER FLOOD	122
A3 RUN NO. 3. POLYMER FLOOD	123
A4 RUN NO. 4. WATER FLOOD	124
A5 RUN NO. 5. WATER FLOOD	125
A6 RUN NO. 6. WATER FLOOD	126
A7 RUN NO. 7. WATER FLOOD	127
A8 RUN NO. 8. WATER FLOOD	128
A9 RUN NO. 9. WATER FLOOD	129
A10 RUN NO. 10. WATER FLOOD	130
A11 RUN NO. 11. WATER FLOOD	131
A12 RUN NO. 12. WATER FLOOD	132
A13 RUN NO. 13. WATER FLOOD	133
A14 RUN NO. 14. WATER FLOOD	134
A15 RUN NO. 15. WATER FLOOD	135
A16 RUN NO. 16. WATER FLOOD	136
A17 RUN NO. 17. WATER FLOOD	137

T-3366

Table

Page

A18	RUN NO. 18. WATER FLOOD	138
-----	-----------------------------------	-----

ACKNOWLEDGMENTS

I would like to express my gratitude to Dr. D.M. Bass, for suggesting the topic of this work and acting as thesis advisor and for his continuous support and encouragement throughout this study despite his retirement from Colorado School of Mines. His guidance and constructive criticism were invaluable.

The author deeply appreciates the kind support and understanding of Dr. Craig Van Kirk, head of the Petroleum Engineering Department, throughout this work.

Appreciation is extended to Dr. R.M. Graves, Dr. B.J. Mitchell, Dr. J.S. Chung, and Prof. D.I. Dickinson for serving as committee members.

Also, many thanks are due to Mr. W.E. Robbins for his continuous help in maintaining the experimental apparatus. I also extend appreciation to my friend Mr. F.H. Thamir, the electronics wizard, who kindly helped in setting up the data acquisition system used in this work.

The author is greatly obliged to the Ministry of Higher Education and Scientific Research of Iraq for their generous assistance throughout his graduate studies in the United States.

INTRODUCTION

Ever since enhanced oil recovery became a common practice in the oil industry, the displacement of one fluid by another has received a great deal of attention. Whether the displacement process be a water flood, a steam flood, a polymer flood, or a surfactant flood, maximum displacement efficiency is always the goal. This requirement has promoted extensive research toward more understanding of the mechanism of the displacement process and the variables contributing the most to an efficient displacement.

Conventionally, it is recognized that an efficient and stable displacement is the one with a uniform fluid velocity and saturation in any cross section perpendicular to the direction of bulk flow and a thin transition zone separating the two fluids. However, frequently, the displacing phase is less viscous than the displaced one. Under such circumstances the displacing phase penetrates the displaced phase irregularly in a form of viscous fingers or a gravity tongue resulting in a non-uniform velocity and saturation in the transverse direction to bulk flow. This type of displacement, which is said to be unstable, occurs in a homogeneous and isotropic porous media, and should be differentiated from that legitimately caused by permeability stratification or other gross inhomogeneities in the system.

Although it is commonly believed that an adverse viscosity or mobility ratio is a necessary condition for instability, several experimental observations indicated that it is not a sufficient

condition. Other parameters, such as the displacement rate, the capillary forces, the gravity forces, and the system geometry, have a significant effect on the stability of the displacement.

As a consequence of front instability, a premature breakthrough of the displacing phase occurs and the validity of the mathematical predictions of the displacement behavior will be undermined. Therefore, a thorough investigation of the stability phenomena of two phase immiscible displacement would achieve two goals: First, it would pinpoint the parameters that control the stability of the displacements, so that the right flood design could be chosen to ensure a stable and efficient displacement; and second, it would delineate the boundaries of a stable displacement, the region in which the mathematical predictions may be applied with confidence.

The broad objective of this study is to investigate the stability of two phase immiscible displacement in a horizontal rectangular system and to obtain, by means of the method of inspectional analysis, a dimensionless scaling group and its critical value to predict the boundaries of the region where the displacement is stable.

CHAPTER ONE

THE NATURE OF STABILITY PHENOMENA

Numerous analogous examples are available to help understand the stability phenomena encountered in the process of immiscible displacement in porous media. Interesting examples can be obtained from the field of mechanics where stability of various mechanical systems have been investigated. Consider the three balls shown in Figure 1.1, where each ball is in a different state of equilibrium. Ball A inside a hemisphere, ball B on a flat surface and ball C on top of a hemisphere. Suppose that a small disturbance is introduced to each ball. Ball A returns to its original position, ball B moves to a new position and remains there, and ball C moves away from its original position to an unknown destination with a new state of equilibrium. Based on the reaction of the three balls, A, B, and C, to the introduced disturbance, their state of equilibrium can be categorized as stable, neutral and unstable, respectively. In the stable and neutral states of equilibrium the initial disturbance damped away with time, whereas in the case of unstable state of equilibrium the magnitude of disturbance increased in order of magnitude compared to that initially applied as time passed.

Another example is a metal beam supported at its lower end in a state of equilibrium, but its condition of equilibrium changes to unstable if a certain weight is attached to its free end (Figure 1.2). A slight displacement of the beam from the vertical position may cause it to buckle and bend. The preceding examples represented relatively

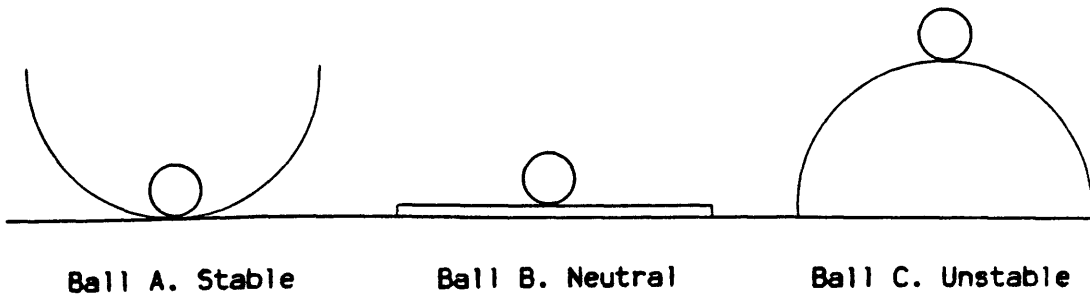


Figure 1.1. Three Types of Equilibrium.

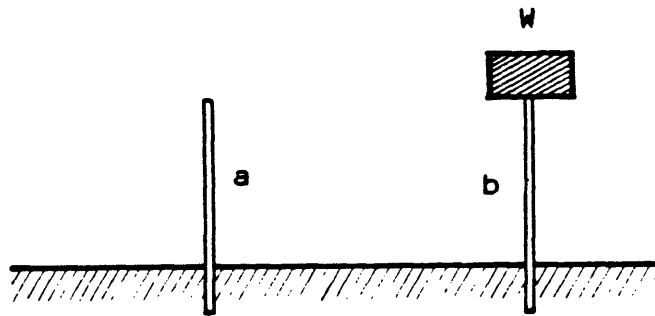
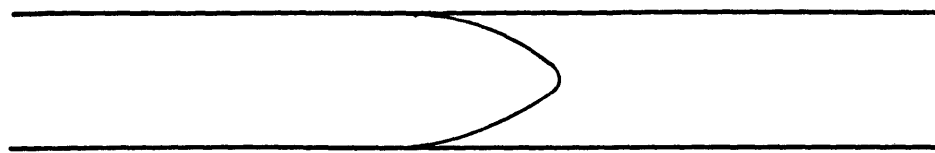


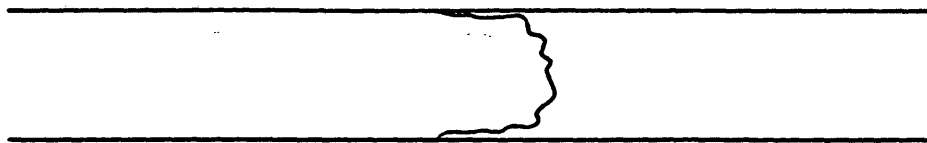
Figure 1.2

simple mechanical systems. When dealing with fluids, stability refers to a more complicated but analogous phenomenon. In hydrodynamics, the flow of a liquid in a cylindrical tube represents a well known example. At Reynolds numbers below the critical value, the velocity of the liquid particles is described by the parabolic function (Figure 1.3a) where Poiseuille's formula represents a solution to such a problem. This type of flow, normally called laminar, is stable to infinitesimal disturbances. However, as the Reynolds number exceeds the critical value, the flow becomes highly vulnerable to quite small disturbances, which grow so rapidly that the parabolic function representing the velocity distribution of the liquid particles can no longer exist and are replaced by large eddies or turbulent spots. This type of flow is unstable and normally called turbulent flow (Figure 1.3b).

In statics, the system approaches stability as its potential energy approaches a minimum. However, this simple criterion fails to describe such a process involving viscous friction, diffusion and surface attraction encountered in hydrodynamics and flow in porous media. In the latter, a stable displacement is conventionally described as the one with a uniform fluid velocity and saturation in any cross section perpendicular to the direction of fluid motion and a thin transition zone separating the two immiscible fluids (Figure 1.4). Several experimental observations performed on immiscible displacements in porous media have shown different behavior at certain flow conditions; i.e., the displacing phase penetrated the displaced phase in a form of viscous fingers (Figure 1.5a), resulting in a premature breakthrough of



a. Laminar Flow (stable)



b. Turbulent Flow (unstable).

Figure 1.3. Flow in a Cylindrical Tube.

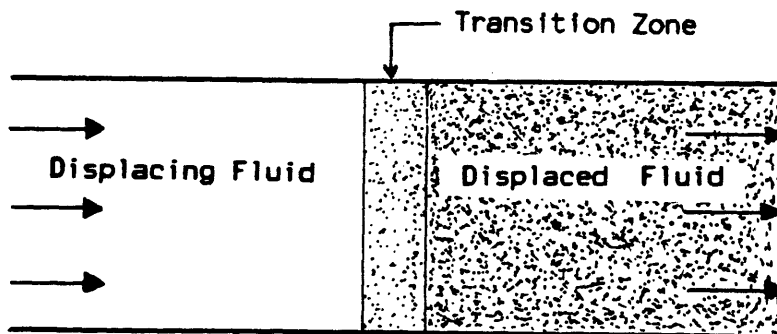
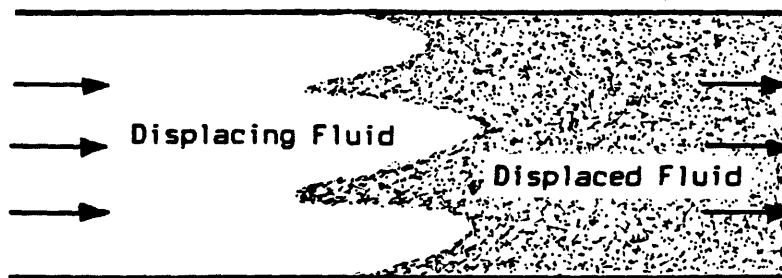
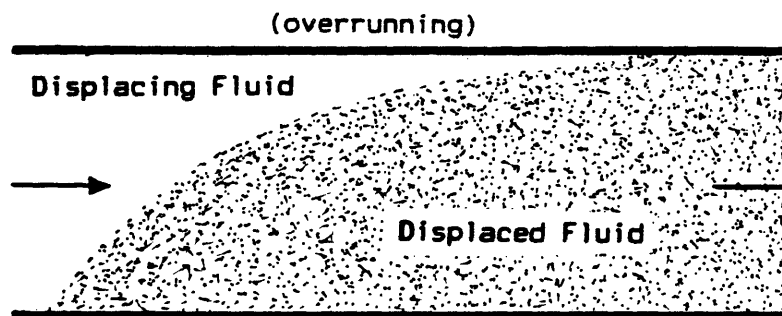
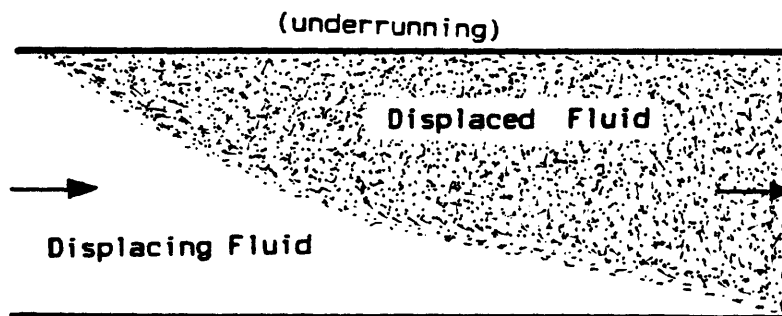


Figure 1.4. A Stable Displacement in Porous Media.



a. Fingering



b. Gravity Tongues

Figure 1.5. Types of Unstable Immiscible Displacements in Porous Media.

ARTHUR LAKES LIBRARY
COLORADO SCHOOL of MINES
GOLDEN, COLORADO 80401

the displacing phase, leaving behind considerable volumes of the displaced phase. These fingers, which characterize unstable displacements, are not related to the ones legitimately caused by the macroscopic heterogeneity of the porous medium. A similar unstable displacement manifests itself in a single finger (gravity tongue) representing the displacing phase, underrunning or overrunning the displaced phase (Figure 1.5b).

CHAPTER TWO

THEORY OF IMMISCIBLE DISPLACEMENT2.1. Mathematical Description of Immiscible Displacement

The differential equations describing the theory of immiscible displacement as currently formulated are based on two physical principles and one auxiliary relationship:

- 1) Conservation of momentum (Darcy's law written for both the displacing and the displaced phases).
- 2) Conservation of mass (continuity equation written for both phases).
- 3) The defining equation for capillary pressure, which links the two flow relationships.

2.1.1. Darcy Law for Two-Phase Flow

Let two immiscible fluids flowing in a homogeneous and isotropic porous medium be denoted as oil and water, where the water is the displacing phase. A general form of Darcy's law can be written for each of the two immiscible fluids as

$$\vec{v}_w = - \frac{k'_w k_{rw}}{\mu_w} (\nabla p_w + \rho_w g \nabla z) \quad (2.1)$$

and

$$\vec{v}_o = - \frac{k'_o k_{ro}}{\mu_o} (\nabla p_o + \rho_o g \nabla z) \quad (2.2)$$

The z-axis is directed upward, and k'_w and k'_o are some base permeabilities used to define water and oil relative permeabilities. Commonly, three different types of base permeabilities are used (Craig,

1980): (1) the absolute permeability to air; (2) the absolute permeability to water; and (3) the permeability to oil at connate water saturation. The choice among these three base permeabilities is a matter of convenience.

2.1.2. The Equation of Continuity

Applying the law of conservation of mass to both oil and water phases results in two additional equations. Assuming that no sources or sinks are present, the two continuity equations can be written as

$$\frac{\partial(S_w \rho_w \phi)}{\partial t} + \nabla \cdot (\rho_w \mathbf{v}_w) = 0 \quad (2.3)$$

and

$$\frac{\partial(S_o \rho_o \phi)}{\partial t} + \nabla \cdot (\rho_o \mathbf{v}_o) = 0 \quad (2.4)$$

2.1.3. Capillary Pressure Equation

Leverett's (1941) definition of the capillary pressure is employed:

$$p_c(S_w) = p_o - p_w \quad (2.5)$$

Since only two fluids are considered, namely oil and water, their respective saturations should sum up to unity:

$$S_o + S_w = 1 \quad (2.6)$$

The above six equations provide in principle the required relationships to mathematically describe two-phase immiscible displacement theory.

For homogeneous and incompressible fluids, the densities and viscosities can be treated as constants. Furthermore, in a non-deformable, homogeneous porous medium, the porosity can also be

considered constant. With these assumptions in mind, the continuity equations simplify to

$$\phi \frac{\partial S_w}{\partial t} + \nabla \cdot \vec{v}_w = 0 \quad (2.7)$$

and

$$\phi \frac{\partial S_o}{\partial t} + \nabla \cdot \vec{v}_o = 0 \quad (2.8)$$

Adding Eqs. 2.7 and 2.8 and using Eq. 2.6

$$\nabla \cdot (\vec{v}_w + \vec{v}_o) = \nabla \cdot \vec{v} = 0 \quad (2.9)$$

where

$$\vec{v} = \vec{v}_w + \vec{v}_o \quad (2.10)$$

Equations 2.1 and 2.2 may be rewritten as

$$\frac{\vec{v}_w}{\frac{k'_w k_{rw}}{\mu_w}} = - (\nabla p_w + \rho_w g \nabla z) \quad (2.11)$$

and

$$- \frac{\vec{v}_o}{\frac{k'_o k_{ro}}{\mu_o}} = - (\nabla p_o + \rho_o g \nabla z) \quad (2.12)$$

Now, subtracting Eq. 2.12 from Eq. 2.11 yields

$$\begin{aligned} \frac{\vec{v}_w}{k'_w k_{rw} / \mu_w} - \frac{\vec{v}_o}{k'_o k_{ro} / \mu_o} &= - \nabla p_w - \rho_w g \nabla z + \nabla p_o + \rho_o g \nabla z \\ &= \nabla p_o - \nabla p_w - (\rho_w - \rho_o) g \nabla z \end{aligned} \quad (2.13)$$

Using the definition of the capillary pressure and assuming that the following equation is valid

$$\nabla p_o - \nabla p_w = \nabla p_c \quad (2.14)$$

Equation 2.13 becomes

$$\frac{\vec{v}_w}{k'_w k_{rw} / \mu_w} - \frac{\vec{v}_o}{k'_o k_{ro} / \mu_o} = \nabla p_c - \Delta \rho g \nabla z \quad (2.15)$$

Using Eq. 2.10 and rearranging

$$\vec{v}_w \left[\frac{1}{k'_w k_{ro} / \mu_w} + \frac{1}{k'_o k_{ro} / \mu_o} \right] = \frac{\vec{v}}{k'_o k_{ro} / \mu_o} + \nabla p_c - \Delta \rho g \nabla z \quad (2.16)$$

$$\vec{v}_w = \frac{k'_w k_{rw} / \mu_w}{k'_w k_{rw} / \mu_w + k'_o k_{ro} / \mu_o} \vec{v} + \frac{(k'_o k_{ro} / \mu_o)(k'_w k_{rw} / \mu_w)}{k'_w k_{rw} / \mu_w + k'_o k_{ro} / \mu_o} \nabla p_c - \frac{(k'_o k_{ro} / \mu_o)(k'_w k_{rw} / \mu_w)}{k'_w k_{rw} / \mu_w + k'_o k_{ro} / \mu_o} \Delta \rho g \nabla z \quad (2.17)$$

Now defining

$$\begin{aligned} F_w(S_w) &= \frac{k'_w k_{rw} / \mu_w}{k'_w k_{rw} / \mu_w + k'_o k_{ro} / \mu_o} \\ &= \frac{M k_{rw}}{k'_w k_{rw} + k_{ro}} \end{aligned} \quad (2.18)$$

where

$$M = \frac{k'_w \mu_o}{k'_o \mu_w} \quad (2.19)$$

Using the above definitions, Eq. 2.17 can be written as

$$\vec{v}_w = F_w \vec{v} + \frac{k'_w F_w k_{ro}}{\mu_w M} \nabla p_c - \frac{k'_w \Delta \rho g F_w k_{ro}}{\mu_w M} \nabla z \quad (2.20)$$

Substituting Eq. 2.20 into Eq. 2.7 gives

$$\begin{aligned} \phi \frac{\partial S_w}{\partial t} + \nabla \cdot (F_w \vec{v}) + \nabla \cdot \left(\frac{k'_w F_w k_{ro}}{\mu_w M} \nabla p_c \right) \\ - \nabla \cdot \left(\frac{k'_w \Delta \rho g F_w k_{ro}}{\mu_w M} \nabla z \right) = 0 \end{aligned} \quad (2.21)$$

Noting that

$$\begin{aligned} \nabla \cdot (F_w \vec{v}) &= F_w \nabla \cdot \vec{v} + \vec{v} \cdot \nabla F_w \\ \nabla \cdot (F_w \vec{v}) &= \vec{v} \cdot \nabla F_w \end{aligned} \quad (2.22)$$

then Eq. 2.21 simplifies to

$$\begin{aligned} \phi \frac{\partial S_w}{\partial t} + \vec{v} \cdot \nabla F_w + \nabla \cdot \left(\frac{k'_w F_w k_{ro}}{\mu_w M} \nabla p_c \right) \\ - \nabla \cdot \left(\frac{k'_w \Delta \rho g F_w k_{ro}}{\mu_w M} \nabla z \right) = 0 \end{aligned} \quad (2.23)$$

Commonly, F_w , p_c , k_{ro} and k_{rw} are considered functions of S_w only (Leverett, 1939). Eq. 2.23 was further modified to give the saturation equation:

$$\phi \frac{\partial S_w}{\partial t} + \frac{dF_w}{dS_w} \vec{v} \cdot \nabla S_w + \nabla \cdot \left(\frac{k'_w F_w k_{ro}}{\mu_w M} \frac{dp_c}{dS_w} \nabla S_w \right)$$

$$-\frac{k'_w}{\mu_w} \frac{\Delta \rho g \nabla z}{M} \frac{d}{dS_w} (F_w k_{ro}) \nabla S_w = 0 \quad (2.24)$$

2.2. Fractional Flow Formula

Dividing every term of Eq. 2.20 by the total velocity vector, $|\vec{v}|$, the fractional flow formula evolves :

$$\vec{f}_w = \frac{\vec{v}_w}{\vec{v}} = F_w \frac{\vec{v}}{\vec{v}} + \frac{k'_w F_w k_{ro}}{\mu_w \vec{v} M} \nabla p_c - \frac{k'_w \Delta \rho g F_w k_{ro}}{\mu_w \vec{v} M} \nabla z \quad (2.25)$$

Written in terms of the fractional flow, Eq. 2.7 becomes

$$\frac{\phi}{\vec{v}} \frac{\partial S_w}{\partial t} + \nabla \cdot \vec{f}_w = 0 \quad (2.26)$$

Eq. 2.26 is a general form of the Buckley-Leverett (1942) displacement model with the capillary and gravity terms retained.

2.3. Normalized One-Dimensional Displacement Equations

Displacement tests performed in laboratory cores are essentially, or at least meant to be one-dimensional. Define a coordinate system ξ , η and ζ along the dimensions of the core, which makes the angles α , β and γ with the three rectangular coordinates x , y and z , respectively. Suppose that the unidirectional displacement is specified to be in an ξ -direction which makes an angle, α , with the horizontal. Then,

$$\frac{\partial f_{w\eta}}{\partial \eta} = 0 \quad , \quad \frac{\partial f_{w\zeta}}{\partial \zeta} = 0$$

and

$$\frac{\partial f_w}{\partial \xi} = \frac{\partial f_w}{\partial \xi} \quad f_w(\xi, t)$$

Furthermore, for a core of constant cross-section

$$v = \frac{Q}{A} = V$$

and

$$\nabla p_c = \frac{dp_c}{d\xi} \quad \nabla z = \frac{\partial z}{\partial \xi} = \sin \alpha$$

Then, Eq. 2.25 can be written for a one-dimensional displacement as

$$f_w = F_w + \frac{k'_w F_w k_{ro}}{\mu_w V M} \frac{dp_c}{d\xi} - \frac{k'_w \Delta \rho g F_w k_{ro}}{\mu_w V M} \sin \alpha \quad (2.27)$$

Using a notation somewhat similar to those of Fayers and Sheldon (1959),

one may normalize the above equation by defining the following

normalized variables :

$$X = \frac{\xi}{L} ; \quad T = \frac{V t}{L \phi (1 - S_{wi} - S_{or})} ; \quad p_c = \frac{\sigma \cos \theta}{\sqrt{k/\phi}} J(S_w)$$

$$\text{and} \quad S = \frac{S_w - S_{wi}}{(1 - S_{wi} - S_{or})}$$

With the above definitions, the fractional flow formula, Eq. 2.27 takes

the following normalized form :

$$f_w = F_w \left[1 - \frac{k'_w \Delta \rho g k_{ro}}{\mu_w V M} \sin \alpha \right] + \frac{k'_w k_{ro} \sigma \cos \theta F_w}{\mu_w L V M \sqrt{k/\phi}} \frac{dJ}{dS} \frac{\partial S}{\partial X} \quad (2.28)$$

In a compact form Eq. 2.28 is written as

$$f_w = G(S) + N_c C(S) \frac{\partial S}{\partial X} \quad (2.29)$$

where

$$G(S) = \left(1 - N_g \frac{k_{ro}}{M} \right) F_w$$

$$N_c = \frac{k'_w \sigma \cos \theta}{\mu_w L V \sqrt{k/\phi}}$$

$$C(S) = \frac{F_w k_{ro}}{M} \frac{dJ}{dS}$$

If the core is oriented horizontally, then

$$N_g = 0$$

Eq. 2.26 can be written for one-dimensional, horizontal displacement as

$$\frac{\phi}{V} \frac{\partial S_w}{\partial t} + \frac{\partial f_w}{\partial x} = 0 \quad (2.30)$$

Now, substituting Eq. 2.29 into Eq. 2.30 results in a normalized two phase immiscible displacement equation:

$$\frac{\partial S}{\partial T} + \frac{\partial f_w}{\partial X} = 0 \quad (2.31)$$

2.4. The Lagrangian and Eulerian Forms of the Displacement Equation

Substitution of Eq. 2.29 into Eq. 2.31 gives

$$\frac{\partial S}{\partial T} + \frac{\partial}{\partial X} \left(G(S) + N_g C(S) \frac{\partial S}{\partial X} \right) = 0$$

$$\frac{\partial S}{\partial T} + \frac{dG(S)}{dS} \frac{\partial S}{\partial X} + \frac{\partial}{\partial X} \left(C(S) \frac{\partial S}{\partial X} \right) = 0 \quad (2.32)$$

In this partial differential equation, $S = S(X,T)$. It is called the Eulerian form of the fluid flow system, wherein S is a property of the system and measurements are made at a fixed point in space as a function of time. Essentially this equation was obtained by Rapoport and Leas (1953). Equation 2.31 can be transformed to

$$\left(\frac{\partial S}{\partial T} \right)_X = - \left(\frac{\partial f_w}{\partial S} \right)_T \left(\frac{\partial S}{\partial X} \right)_T$$

$$\left(\frac{\partial f_w}{\partial S} \right)_T = - \left(\frac{\partial S}{\partial T} \right)_X \left(\frac{\partial X}{\partial S} \right)_T$$

Such that

$$\left(\frac{\partial f_w}{\partial S} \right)_T = \left(\frac{\partial X}{\partial T} \right)_S \quad (2.33)$$

Now, substituting Eq. 2.29 into Eq. 2.33 gives

$$\frac{\partial X}{\partial T} = \frac{dG(S)}{dS} + \frac{\partial}{\partial S} \left(\frac{C(S)}{\frac{\partial X}{\partial S}} \right) \quad (2.34)$$

Eq. 2.34 is similar to that derived by Buckley and Leverett (1942) and is called the Lagrangian form of the displacement equation wherein an element with a specific saturation S is observed as it changes location X over the course of time T . i.e. $X = X(S,T)$.

Buckley and Leverett's (1942) original solution to Eq. 2.34 excluded the effects of capillary pressure and gravity. Later studies showed

that this solution with the modifications introduced by Welge (1952), is not applicable for two- or three-dimensional systems where cross flow becomes possible (Hawthorne, 1960, and Peggs, 1973).

No analytical solution has been reported in the literature to Equations 2.32 and 2.34 with the capillary and gravity terms retained. However, numerous studies have resorted to numerical methods to solve the two equations (Fayers and Sheldon, 1959, Hovanessian and Fayers, 1961, Bentsen, 1978, and Allen and Puckett, 1986).

CHAPTER THREE

REVIEW OF RELATED RESEARCH

The subject of interface stability associated with the process of immiscible displacement has been the focus of many theoretical and experimental studies aimed at improving the efficiency of the displacement process. Instability as it is reported in the literature often refers to the phenomena when the displacing phase penetrates through the displaced phase in the form of viscous fingers or as a tongue underrunning or overrunning the displaced phase.

Engelbert and Klinkenberg (1951) approached the problem by investigating the influence of the following dimensionless groups on the displacement process

$$\alpha, \frac{L}{H}, \frac{\Delta\rho g k}{V \mu_w}, \frac{\mu_o}{\mu_w}, \frac{\Delta\rho g L/k}{\sigma \cos \theta}$$

They used several cylindrical tubes packed with coarse sand with a permeability of 200 darcies and a porosity of 38%. The sand tubes were initially fully saturated with oils of different viscosities and displaced with water. The authors observed that at low rates of injection none of the groups above had a significant effect on the recovery at breakthrough, whereas at high rates of injection breakthrough recovery was primarily dependent on the viscosity ratio and to some extent on L/H.

Their observations concerning the manner with which the water invaded the oil zone led to the following conclusions. At a viscosity

ratio of one, the water uniformly invaded the oil zone with thin transition zone and was significantly independent of the rate of injection. This was reflected in a stable displacement with high recovery at breakthrough. At viscosity ratios of 4 and 24 and high rates of injection, the water penetrated the oil zone with several fingers haphazardly distributed across the sand pack, severely reducing the recovery at breakthrough. At intermediate rates, the fingers were replaced by a single water tongue underrunning the oil phase. This type of displacement signifies instability.

The observations cited above are mainly qualitative because of the uncertainty encountered in determining oil and water saturations in the model.

Dietz (1953) presented a two-dimensional mathematical analysis of water drive in a monoclinial reservoir, assuming an initially horizontal sharp interface between two fluids flowing in a homogeneous, isotropic porous media.

In his mathematical development, Dietz combined Darcy's equation and the equation of continuity to obtain the following equation:

$$\Delta\rho g \left(\tan \alpha + \frac{dy}{dx} \right) \cos \alpha = \left(\frac{\mu_o}{k_{ocw}} - \frac{\mu_w}{k_{wro}} \right) v \quad (3.1)$$

To arrive at the above equation, the following assumptions had to be made:

- 1) Constant or no pressure drop across the interface.
- 2) $v = v_o = v_w = \text{constant}$.

3) The flow potential is in the direction of the dip of the layer.

For the interface to remain stable (horizontal), either μ_o/k_{ocw} has to be equal to μ_w/k_{wro} or ρ_o equal to ρ_w . Otherwise (i.e. $\rho_o \neq \rho_w$ or $\mu_o/k_{ocw} > \mu_w/k_{wro}$), the interface underruns the oil zone in the form of a 'water tongue'. Dietz defined a critical velocity, V_c , above which the interface is no longer stable, as

$$V_c = \frac{\Delta \rho g \sin \alpha}{\mu_o/k_{ocw} - \mu_w/k_{wro}} \quad (3.2)$$

In a horizontal system where $\alpha = 0$, the interface is unstable no matter how small the rate of injection is because $V_c = 0$.

At rates greater than the critical value, where v_o and v_w are not equal, Dietz derived an equation for unstable conditions wherein at any cross section along the system

$$Q_o + Q_w = Q \quad (3.3)$$

With the above stipulation, the continuity equation and Darcy's law, the following equation was derived describing the location of the interface as a function of x and t

$$\frac{k_{ocw} \Delta \rho g}{\mu_o} \cos \alpha \frac{\partial^2 y}{\partial x^2} = \left[\frac{1}{(H-y)^2} + \left\{ \frac{a}{y^2} - \frac{1}{(H-y)^2} \right\} \frac{y}{a(H-y)+y} \right]$$

$$Q \frac{\partial y}{\partial x} + \left(\frac{a}{y} + \frac{1}{H-y} \right) \phi \Delta S \frac{\partial y}{\partial t} \quad (3.4)$$

This equation is a parabolic, nonlinear, second order partial differential equation. A solution for y as a function of x and t would involve mathematical difficulties. To alleviate this obstacle, Dietz assumed the curvature of the interface to be very small, and hence, the left-hand side of the equation was eliminated. In a horizontal system, this assumption becomes unacceptable because the left hand side has a maximum value when $\alpha = 0$. However, for a vertical system ($\alpha = 90$), the left-hand side is already zero and the analytical solution is correct. Using the chain rule, Eq. 3.4 can be solved for the updip velocity of the oil/water interface as

$$\frac{\partial x}{\partial t} = \frac{aH}{\{a(H - y) + y\}^2} \frac{Q}{\phi \Delta S} \quad (3.5)$$

Equation 3.5 led Dietz to conclude that the shape of the water tongue depends neither on gravity effects nor on the rate of production, but only on the mobility ratio, the cumulative production and to some extent on the dip angle.

Dietz further examined Eq. 3.4 to find that the error introduced by neglecting the left-hand side term diminished when $y = 0$ or $y = H$, but he failed to estimate the error when y is between those two limits (i.e. $0 < y < H$). However, later studies (Peggs, 1973, Croes and Schwarz, 1955) showed that this error renders Dietz' theory unsatisfactory when gravity effects are significant in horizontal or nearly horizontal systems.

Van Meurs (1957) confirmed the observations of Engelbert and

Klinkenberg (1951) using a transparent model packed with glass powder and fully saturated with oil (no connate water). The glass powder and the oil were selected to have the same refractive index to permit visual observations of the displacement.

All runs with an oil-water viscosity ratio of one showed high recovery at breakthrough and a uniformly progressing oil/water interface, which is an obvious sign of interface stability. However, for a viscosity ratio of 80, the interface broke up into several well-defined fingers, resulting in a markedly low recovery at water breakthrough.

Based upon these observations, van Meurs and van der Poel (1958) questioned the validity of the relative permeability concepts of the conventional theory of immiscible displacement to displacements dominated by viscous fingering. They accordingly developed a theory specially tailored to viscous fingering. This theory, which parallels the conventional Buckley-Leverett theory in several respects, has received little or no attention.

Lewis (1951) published his observations on immiscible displacement experiments conducted in closely-spaced parallel plates (Hele-Shaw cell). He reported the tendency of the interface to break up into several fingers penetrating the more viscous displaced phase.

Using the same experimental technique, these observations were confirmed by the work of Saffman and Taylor (1958), who presented a theoretical study of viscous fingering by introducing a small disturbance to an otherwise plane interface and examining the behavior

of this disturbance over the course of time spanning the progress of the displacement.

Chuoque et al. (1959) presented the most recognized theoretical study of viscous fingering from the standpoint of stability. They treated the phenomenon as a manifestation of hydrodynamic instability analogous to that encountered in the field of hydrodynamics.

The authors specified the following inequality as a necessary condition for instability

$$\left(\frac{\mu_o}{k_{ocw}} - \frac{\mu_w}{k_{wro}} \right) V + \Delta \rho g \cos \alpha > \sigma^* n^2 \quad (3.6)$$

Several conditions for instability may be extracted from the above inequality. It is convenient to define the critical velocity as

$$\left(\frac{\mu_o}{k_{ocw}} - \frac{\mu_w}{k_{wro}} \right) V_c + \Delta \rho g \cos \alpha = 0 \quad (3.7)$$

i.e.

$$V_c = \frac{k_{wro} \Delta \rho g \cos \alpha}{\mu_w \left(M - \frac{k_{ocw}}{k_{wro}} \right)} \quad (3.8)$$

Subtracting Eq. 3.7 from Eq. 3.6 yields

$$\left(\frac{\mu_o}{k_{ocw}} - \frac{\mu_w}{k_{wro}} \right) (V - V_c) > 0 \quad (3.9)$$

The wavelength is defined as

$$\lambda = \frac{2 \pi}{n} \quad (3.10)$$

Substituting Eq. 3.10 into Eq. 3.9, another condition for instability

evolves as

$$\lambda > 2\pi \left[\frac{k_{wro} / \mu_w \sigma^*}{(M - 1)(V - V_c)} \right]^{1/2} \quad (3.11)$$

Let a critical wavelength be defined as

$$\lambda_c = 2\pi \left[\frac{k_{wro} / \mu_w \sigma^*}{(M - 1)(V - V_c)} \right]^{1/2} \quad (3.12)$$

For instability to manifest itself in viscous fingering requires the following conditions be met simultaneously

$$V > V_c$$

$$M > 1$$

and

$$\lambda > \lambda_c$$

In a horizontal system, the critical rate is zero. Consequently, the first condition for instability is always met, leaving the satisfaction of the other two conditions to decide whether instability should exist. Their mathematical development was verified by experimental observations performed on three displacement systems namely, an inclined Hele-Shaw cell without a porous media, van Meurs' (1957) transparent model packed with glass powder in the presence of connate water, and the same model without connate water.

In the parallel-plate displacements, the experimental observations closely matched the mathematical predictions. At a viscosity ratio of 3.52, they reported a stable displacement interface at rates below the critical rate predicted by Eq. 3.8. At rates above the critical value,

the interface broke up into several sinusoidal fingers penetrating the oil zone. A comparison between the average wavelength of these fingers measured experimentally and the mathematically predicted wavelength revealed good agreement between the two, specifically for rates several times greater than critical.

This close agreement between the theoretical predictions and the experimental findings from the displacements conducted in the Hele-Shaw cell could be attributed to the fact that the authors have founded their stability theory on the hydrodynamic equations

$$\vec{v} = - \frac{k}{\mu} \nabla (p + \rho g z \cos \alpha) \quad (3.13)$$

$$\nabla \cdot \vec{v} = 0 \quad (3.14)$$

which constitute an accurate mathematical representation of flow between parallel plates.

In the displacements conducted in the transparent model with no connate water, viscous fingers were again clearly visible. But, in contrast to the parallel-plate displacements, the fingers lost their sinusoidal characteristics and smooth appearance. In these runs, the mathematically predicted most probable wavelength diverted from that measured experimentally. To force a match between theory and observation, the authors defined an effective interfacial tension which was directly proportional to the interfacial tension between the two fluids in the absence of porous media.

$$\sigma^* = C^* \sigma \quad (3.15)$$

They found the best fit when the constant C in their Eq. 24 is taken equal to 30, where C is defined as

$$C = 2\pi \sqrt{3 C^*} \quad (3.16)$$

These displacements were repeated on the same transparent model but with connate water present. No clear-cut results and observations were cited to verify the theory. The photographs shown by the authors to demonstrate fingering in connate water bearing porous media revealed fingers lacking any definite pattern. Consequently, they did not attempt any measurements that might lead to quantitative predictions of instability in the system under consideration. However, the authors made a remarkable comment on the stability of such systems.

In a water-wet, connate water-bearing, porous medium which spontaneously imbibes water, the effective interfacial tension, σ^* is very large, making the critical wavelength, λ_c , obtained through Eq. 3.11 far exceed the model dimensions. Under such conditions the displacement shows a significant stability even when other conditions for instability are satisfied. This explains the motive behind using both a high viscosity ratio and a high injection rate by the authors in the displacements performed on connate water bearing systems for which the mentioned photographs were displayed.

Rachford (1964) used a finite difference solution of the two-dimensional equations of displacement in connate water-bearing, porous media. Running his model on six hypothetical field and laboratory-

scale floods in a rectangular reservoir, he stated that in all the cases studied, no tendency towards instability was found. Furthermore, high displacement rates and unfavorable viscosity ratios were beneficial to stability as the perturbations damped more rapidly. Further, Rachford, supported by his earlier findings, questioned the applicability of a stability theory based on displacements conducted in the Hele-Shaw cells to immiscible displacements in water-wet porous media containing connate water. He argued that a real porous medium has a pore-size distribution, and consequently, different parts of an initially plane interface will move at different velocities through the porous medium, i.e., a distribution of saturation (often called the transition zone) will evolve to separate the two parts of the porous medium where only one fluid is moving in the presence of a minimum saturation of the other. Acting as a damper, the transition zone will force a saturation higher than the frontal saturation to move with a lower velocity, hence, insulating the incipient protrusions of a perturbation from the high mobility displacing phase. The lack of a transition zone in the parallel plate model displacement makes it more vulnerable to instability and the subsequent development of viscous fingering than real porous media.

Later, Perkins and Johnston (1969) confirmed the findings of Rachford (1964) concerning the inherent stability of connate water-bearing porous medium. They investigated the problem experimentally, employing the Hele-Shaw and glass bead packed models.

In all systems studied, no fingering was reported with favorable

In all systems studied, no fingering was reported with favorable viscosity ratios. But, with unfavorable viscosity ratios, numerous fingers were noticeable in the Hele-Shaw displacements, with and without beads, with no connate water models.

A noticeable difference was reported when the displacements were conducted in a bead-packed model with connate water. At favorable viscosity ratios, a distinct front with a steep saturation gradient was visible. Oil saturation behind the front was low, and little production after breakthrough was reported. At unfavorable viscosity ratios, numerous small fingers developed early in the displacement near the inlet end of the model. These fingers soon coalesced to form a dendritic network of channels that then formed a graded saturation zone. The authors attributed this damping behavior of the observed fingers to the flow of the two fluids in a direction transverse to the direction of gross fluid movement. Adding to their experimental findings, Perkins and Johnston, contributed two major conclusions:

1. The Hele-Shaw cells are not adequate to model the important characteristics of immiscible displacement, namely such aspects as relative permeability and transition zone effects.
2. Fingering studies would be more representative of a water-wet reservoir if performed in connate water bearing porous media.

Motivated by the apparent controversy in the literature regarding stability of immiscible displacement in water-wet connate water-bearing porous media, Hagoort (1974) investigated the process presenting a stability analysis parallel to that of Chuoke et al. (1959), introducing

a small first-order perturbation (disturbance) to an otherwise plane interface and observing the subsequent behavior of the perturbation over the course of time of the displacement. However, his analysis differs from that of Chuoke et al. (1959) in two important respects. Hagoort performed his stability analysis based on the Buckley-Leverett's (1942) displacement model rather than the piston-like displacement model adapted by Chuoke et al. (1959). The mobility ratio condition for instability was based on a so-called shock mobility ratio instead of the end point mobility ratio. He defined the shock mobility ratio as

$$M_s = \left[\frac{k_{ocw} k_{ro}(S_s)}{\mu_o} + \frac{k_{wro} k_{rw}(S_s)}{\mu_w} \right] / \frac{k_{ocw}}{\mu_o} \quad (3.17)$$

His theoretical analysis led him to the conclusion that the displacement is unstable if the shock mobility ratio is greater than one, provided that the wavelength of the instabilities is smaller than the width of the model.

As recently as 1981, Peters and Flock (1981) investigated the problem of interface stability, aiming at a dimensionless scaling group that could be used to predict the onset of instability during immiscible displacement. They argued that none of the previous studies regarding stability have succeeded in combining all the variables pertinent to the process in one lumped group. In order to achieve this task, they presented a stability analysis which is basically an extension to the stability theory proposed by Chuoke et al. (1959). Their stability

analysis produced two dimensionless groups defining the conditions for instability in cylindrical and rectangular systems. For a horizontal cylindrical system, the displacement is unstable if

$$\frac{(M - 1) V \mu_w D^2}{C^* \sigma k_{wro}} > 13.56$$

and for a horizontal rectangular system

$$\frac{(M - 1) V \mu_w W^2 H^2}{C^* \sigma k_{wro} (W^2 + H^2)} > 9.87$$

Assuming that the endpoint permeabilities are approximately equal to the absolute permeability, then the dimensionless groups can be written as

$$\left(\frac{\mu_o}{\mu_w} - 1 \right) \frac{V \mu_w D^2}{C^* \sigma k} > 13.56$$

and

$$\left(\frac{\mu_o}{\mu_w} - 1 \right) \frac{V \mu_w W^2 H^2}{C^* \sigma k (W^2 + H^2)} > 9.87$$

Similar to Chuoke et al. (1959), they defined an effective interfacial tension directly related to the oil-water interfacial tension through the wettability number, C^* :

$$\sigma^* = C^* \sigma$$

C^* is determined experimentally by measuring the fastest growing finger wavelength, λ_m . Substituting this value into their Eq. 20, they estimated wettability numbers of 5.45 for the oil-wet system and 306.25 for the water-wet system.

Peters and Flock (1981) verified their theory by several experiments

performed in cylindrical cores which measured 23 cm in length and 4.8 cm in diameter packed with 80-120 mesh Ottawa sand. Their results showed that all the oil-wet floods with no connate water were unstable, while the water-wet floods showed a region of constant recovery at breakthrough (stable displacement) and a region of declining recovery (unstable displacement). The transition from one region to the other occurred in the vicinity of the number 13.56 predicted by their theoretical analysis. No experimental data were reported for the rectangular system.

Despite the good agreement between the theory and the experimental findings, the work of Peters and Flock (1981) involved several limitations. The wettability number, C^* , is required to be known a priori for stability conditions to be determined. Furthermore, the effects of gravity were neglected in their analysis and hence did not show up in their dimensionless groups. Also, the experiments were conducted at a single viscosity ratio of 102.5, so it is difficult to generalize the conclusions of the work cited.

Several conclusions may be drawn, regarding stability and interface behavior during immiscible displacement in porous media, based on the literature presented. The stability analysis conducted for a first-order perturbation shows an excellent agreement with the experiments performed in the Hele-Shaw and van Meurs (1957) models with no connate water present. On the other hand, the experiments conducted on connate water bearing porous media have failed to confirm the theoretical predictions based on these stability analyses. As was cited earlier, no

clear-cut observations of viscous fingering in these experiments were made even with instability conditions being satisfied, and a marked reduction in breakthrough recoveries was reported. The reported damping of fingers early in the course of the displacement was attributed by several authors to the effect of capillary forces which tend to smear out the incipient fingers. However, in many occasions gravity tongues were reported to indicate instability in displacements conducted in a horizontal or slightly dipping porous medium. Therefore, it may be inferred that immiscible displacements conducted in a connate water-bearing, porous medium can be unstable (based on the reduction in breakthrough recovery) without conspicuous fingers. Instead, a macroscopic deformation of the interface in the form of a gravity tongue is the observed manifestation of instability in such displacements.

The objectives of this study were, first, to investigate, experimentally, the behavior of the interface through the course of immiscible displacement, and second, to conduct a multi-dimensional, inspectional analysis in order to determine a complete set of dimensionless scaling groups that may help identify the boundaries of a stable displacement.

CHAPTER FOUR

DIMENSIONAL AND INSPECTIONAL ANALYSIS

In general, two methods may be used to derive dimensionless groups for the investigation of the displacement process in a porous medium: Inspectional analysis, which requires the differential equations describing the displacement process to be known a priori; and dimensional analysis, which requires the knowledge of the relevant variables controlling the displacement.

The method of inspectional analysis makes use of the fact that all physical equations are relations between independent variables, dependent variables and constants, all with the same dimensions. Accordingly, the dependent variables, independent variables and the constant terms can be brought into a dimensionless form by dividing them by some value of the same dimension, characteristic of the system.

As an outcome to this process, dimensionless independent groups, dimensionless dependent groups and dimensionless similarity groups will emerge.

Unlike inspectional analysis, dimensional analysis can be performed whenever the process being investigated is lacking a mathematical description. Relying on the physical common sense of the user, the key variables governing the physical phenomena are used to form dimensionless groups. In order to derive these dimensionless groups, it is required that the power products of the pertinent variables be also dimensionless, which results in a homogeneous system of linear

equations, the solution of which yields a complete set of mutually independent, dimensionless groups. The number of these dimensionless groups, according to the Buckingham rule, is equal to the total number of variables minus the number of fundamental dimensions, e.g. mass, length and time.

Both methods of deriving the dimensionless groups have their advantages and limitations. Inspectional analysis usually produces a set of dimensionless groups whose physical meaning is readily apparent, whereas the groups obtained by dimensional analysis may be quite obscure. Further, inspectional analysis may result in two or more dimensionless groups coupled together. This combination then can be considered as a single dimensionless group, which means fewer groups including larger number of variables and hence giving a better description of the process. However, inspectional analysis cannot be applied to a process whose mathematical description is unavailable, whereas, under the same conditions, dimensional analysis can still be functional to yield valuable information in setting up experiments to initiate a study. However, dimensional analysis is so general that the inclusion of unnecessary variables in the menu of the pertinent variables will give rise to some supplemental and confusing groups that complicate the process.

Extensive literature exists regarding the application of the two methods to the process of immiscible displacement in porous media. Leverett et al. (1942) took the initiative in their model studies in which dimensionless groups were used to scale laboratory experiments to

field prototypes. Later, Engelbert and Klinkenberg (1951) extended the work of Leverett (1942) making extensive use of dimensionless groups derived by dimensional analysis to investigate the influence of specific variables on immiscible displacement in laboratory models. Further, they employed the various groups as a general aid in presenting their experimental findings.

Croes and Schwarz (1955) continued the latter work using the same dimensionless groups, putting the emphasis on the influence of the group representing the oil-water viscosity ratio on the displacement.

Rapoport (1955) presented a complete derivation of the dimensionless groups controlling immiscible displacement in three dimensional porous medium, whereas Geertsma et al. (1956) have matched the advantages of the two methods to develop a set of scaling groups for three types of displacements in porous media.

Craig et al. (1957) reproduced the dimensionless groups of Rapoport (1955) and Geertsma et al. (1956) and employed them in the investigation of the effect of gravity forces on the volumetric sweep efficiency of frontal drives.

The relevant dimensionless groups for the present work are best derived by the method of inspectional analysis. Eq. 2.23 provides a convenient starting point for such a derivation.

4.1. Inspectional Analysis

Starting with Eq. 2.23

$$\phi \frac{\partial S_w}{\partial t} + v \cdot \nabla F_w + \nabla \cdot \left(\frac{k'_w}{\mu_w M} F_w k_{ro} \nabla P_c \right) - \nabla \cdot \left(\frac{k'_w \Delta \rho g}{\mu_w M} F_w k_{ro} \nabla z \right) = 0 \quad (2.23)$$

In a horizontal system $\nabla z = 0$

and Eq. 2.23 becomes

$$\phi \frac{\partial S_w}{\partial t} + v \cdot \nabla F_w + \nabla \cdot \left(\frac{k'_w}{\mu_w M} F_w k_{ro} \nabla P_c \right) = 0 \quad (4.1)$$

Define the capillary pressure using the Leverett function

$$P_c = \frac{\sigma}{\sqrt{k/\phi}} J(S_w) \quad (4.2)$$

and let k'_w be equal to the absolute permeability, k .

Then

$$M = \mu_o / \mu_w$$

To describe the displacement in a horizontal rectangular system, Eq.

4.1 is expanded in rectangular x -, y - and z -coordinates to give

$$\phi \frac{\partial S_w}{\partial t} + \left[v_x \frac{\partial S_w}{\partial x} + v_y \frac{\partial S_w}{\partial y} + v_z \frac{\partial S_w}{\partial z} \right] \frac{dF_w}{dS_w} + \frac{k \sigma}{\mu_w M \sqrt{k/\phi}} \left[\frac{\partial}{\partial x} \left(F_w k_{ro} \frac{dJ}{dS_w} \nabla S_w \right) + \frac{\partial}{\partial y} \left(F_w k_{ro} \frac{dJ}{dS_w} \nabla S_w \right) + \right.$$

$$\frac{\partial}{\partial z} \left(F_w k_{ro} \frac{dJ}{dS_w} \nabla S_w \right) = 0 \quad (4.3)$$

Now, define the following dimensionless variables.

$$X = \frac{x}{L}$$

$$Y = \frac{y}{W}$$

$$Z = \frac{z}{H}$$

$$V = \frac{v}{V}$$

and

$$T = \frac{\Delta \rho g k t}{\mu_w L \phi}$$

Substituting these dimensionless variables into Eq. 4.3 yields

$$\begin{aligned} & \phi \frac{\frac{\partial S_w}{\mu_w L \phi}}{\Delta \rho g k} \frac{dF_w}{dT} + \left[\frac{V}{L} V_x \frac{\partial S_w}{\partial X} \frac{dF_w}{dS_w} + \frac{V}{W} V_y \frac{\partial S_w}{\partial Y} \frac{dF_w}{dS_w} + \right. \\ & \frac{V}{H} V_z \frac{\partial S_w}{\partial Z} \frac{dF_w}{dS_w} + \frac{k \sigma}{\mu_w M \sqrt{k/\phi}} \left[\frac{1}{L} \frac{\partial}{\partial X} \left\{ F_w k_{ro} \frac{dJ}{dS_w} \left(\frac{1}{L} \frac{\partial S_w}{\partial X} + \right. \right. \right. \\ & \left. \left. \frac{1}{W} \frac{\partial S_w}{\partial Y} + \frac{1}{H} \frac{\partial S_w}{\partial Z} \right) \right\} + \frac{1}{W} \frac{\partial}{\partial Y} \left\{ F_w k_{ro} \frac{dJ}{dS_w} \left(\frac{1}{L} \frac{\partial S_w}{\partial X} + \frac{1}{W} \frac{\partial S_w}{\partial Y} + \right. \right. \\ & \left. \left. + \frac{1}{H} \frac{\partial S_w}{\partial Z} \right) \right\} + \frac{1}{H} \frac{\partial}{\partial Z} \left\{ F_w k_{ro} \frac{dJ}{dS_w} \left(\frac{1}{L} \frac{\partial S_w}{\partial X} + \frac{1}{W} \frac{\partial S_w}{\partial Y} + \right. \right. \\ & \left. \left. \frac{1}{H} \frac{\partial S_w}{\partial Z} \right) \right\} \right] = 0 \quad (4.4) \end{aligned}$$

Rearranging gives

$$\begin{aligned}
 & \frac{\partial S_w}{\partial T} + \left(\frac{\mu_w V}{\Delta \rho g k} \right) V_x \frac{\partial S_w}{\partial X} \frac{dF_w}{dS_w} + \left(\frac{\mu_w V}{\Delta \rho g k} \right) \left(\frac{L}{W} \right) V_y \frac{\partial S_w}{\partial Y} \frac{dF_w}{dS_w} + \left(\frac{\mu_w V}{\Delta \rho g k} \right) \\
 & \left(\frac{L}{H} \right) V_z \frac{\partial S_w}{\partial Z} \frac{dF_w}{dS_w} + \left(\frac{\sigma \sqrt{\phi/k}}{\Delta \rho g L} \right) \left(\frac{1}{M} \right) \frac{\partial}{\partial X} \left[F_w k_{ro} \frac{dJ}{dS_w} \left(\frac{\partial S_w}{\partial X} + \right. \right. \\
 & \left. \left. \frac{L}{W} \frac{\partial S_w}{\partial Y} + \frac{L}{H} \frac{\partial S_w}{\partial Z} \right) \right] + \left(\frac{\sigma \sqrt{\phi/k}}{\Delta \rho g W} \right) \left(\frac{1}{M} \right) \frac{\partial}{\partial Y} \left[F_w k_{ro} \frac{dJ}{dS_w} \right. \\
 & \left. \left(\frac{\partial S_w}{\partial X} + \frac{L}{W} \frac{\partial S_w}{\partial Y} + \frac{L}{H} \frac{\partial S_w}{\partial Z} \right) \right] + \left(\frac{\sigma \sqrt{\phi/k}}{\Delta \rho g H} \right) \left(\frac{1}{M} \right) \frac{\partial}{\partial Z} \left[F_w k_{ro} \right. \\
 & \left. \frac{dJ}{dS_w} \left(\frac{\partial S_w}{\partial X} + \frac{L}{W} \frac{\partial S_w}{\partial Y} + \frac{L}{H} \frac{\partial S_w}{\partial Z} \right) \right] = 0 \tag{4.5}
 \end{aligned}$$

Writing Eq. 4.5 in a more compact form yields

$$\begin{aligned}
 & \frac{\partial S_w}{\partial T} + \left(\frac{\mu_w V}{\Delta \rho g k} \right) \left[V_x \frac{\partial S_w}{\partial X} + \frac{L}{W} V_y \frac{\partial S_w}{\partial Y} + \frac{L}{H} V_z \frac{\partial S_w}{\partial Z} \right] \frac{dF_w}{dS_w} \\
 & + \left(\frac{\sigma \sqrt{\phi/k}}{\Delta \rho g L} \right) \left(\frac{1}{M} \right) \frac{\partial I}{\partial X} + \left(\frac{\sigma \sqrt{\phi/k}}{\Delta \rho g W} \right) \left(\frac{1}{M} \right) \frac{\partial I}{\partial Y} + \left(\frac{\sigma \sqrt{\phi/k}}{\Delta \rho g H} \right) \\
 & \left(\frac{1}{M} \right) \frac{\partial I}{\partial Z} = 0 \tag{4.6}
 \end{aligned}$$

where

$$I = F_w k_{ro} \frac{dJ}{dS_w} \left(\frac{\partial S_w}{\partial X} + \frac{L}{W} \frac{\partial S_w}{\partial Y} + \frac{L}{H} \frac{\partial S_w}{\partial Z} \right)$$

The following dimensionless groups emerge from the above development using inspectional analysis:

- a) Independent variables: T, X, Y and Z.
- b) Dependent variables: S_w , V_x , V_y and V_z .

c) similarity (scaling) groups: L/W , L/H , $\mu_w V/\Delta\rho gk$,
 $\sigma \sqrt{\phi/k/\Delta\rho gL}$, $\sigma \sqrt{\phi/k/\Delta\rho gW}$, $\sigma \sqrt{\phi/k/\Delta\rho gH}$, dJ/dS_w and $1/M$.

4.2. The Physical Significance of the Derived Scaling Groups

The first two terms represent the geometric similarity groups. $\mu_w V/\Delta\rho gk$ is the well-known ratio of viscous forces to gravity forces, which has been reported in the literature by several authors (Engelbert and Klinkenberg, 1951, Allam, 1979, Craig et al., 1957, Croes and Schwarz, 1955, and George et al., 1982).

The groups $\sigma \sqrt{\phi/k/\Delta\rho gL}$, $\sigma \sqrt{\phi/k/\Delta\rho gW}$ and $\sigma \sqrt{\phi/k/\Delta\rho gH}$ are the ratio of capillary forces to gravity forces in the three rectangular coordinates x , y and z . macroscopically, the system can be considered as homogeneous and isotropic. Therefore, these three scaling groups could be reduced to a single group by removing the space dimensions from the denominator. i.e., L , H and W . The resulting group represents the ratio of capillary to gravity forces in any direction inside the system under consideration.

Since instability is attributed to fluid movement in a transverse direction to the commonly-assumed, one-dimensional flow, the group $\sigma\sqrt{\phi/k/\Delta\rho g}$ should provide good correlation coefficient to specify whether the displacement is stable or not.

As the scaling group $\sigma\sqrt{\phi/k/\Delta\rho g}$ controls the transverse motion of the displacing phase to prevent tonguing or fingering, it should be anticipated that the magnitude of this group may have a profound effect on the behavior of the interface.

The group $1/M$ is the water-oil viscosity ratio. This group is also expected to effect the oil recovery at breakthrough. As the method of inspectional analysis permits the combination of two or more dimensionless groups into a single group, the group $1/M$ is combined with the group $\sigma\sqrt{\phi/k}/\Delta\rho g$ to give

$$F_s = \frac{\sigma \sqrt{\phi/k}}{\Delta\rho g M} \quad (4.7)$$

In the present work, the above scaling groups will be basically used to investigate the influence of the displacement parameters on instability (tonguing or fingering) of immiscible displacement in water-wet, connate water bearing porous medium.

CHAPTER FIVE
EXPERIMENTAL EQUIPMENT AND PROCEDURE

5.1. Model

The model used to run the experiment is a rectangular cell (Figure 5.1) measuring 6 feet in length, 9 inches in height and 6 inches in width. Figure 5.2 shows a schematic diagram of the flow system which is basically the same as the one employed by Allam (1979). A detailed description of the apparatus can be found in this reference.

5.1.1. Model Scaling

Displacement experiments are widely used to investigate, directly or indirectly, water flooding behavior of petroleum reservoirs. Laboratory model studies can be useful in predicting fluid flow behavior in these reservoirs (prototypes) if they are properly scaled. Rapoport and Leas (1953) showed theoretically and experimentally that linear water floods are not only governed by the properties of the porous medium and the fluids flowing through it, but also by the rate of injection and the length of the system. They observed that water floods become independent of the rate of injection, the length of the system, and the fluid viscosities above a critical value of the product $LV\mu_w$, which they called "scaling coefficient", and the floods with a scaling coefficient greater than the critical value are said to be stabilized. A stabilized flood, conducted in identical porous media using the same water-oil viscosity ratio and initial saturation distribution, should behave similarly and yield the same relation between injected and produced

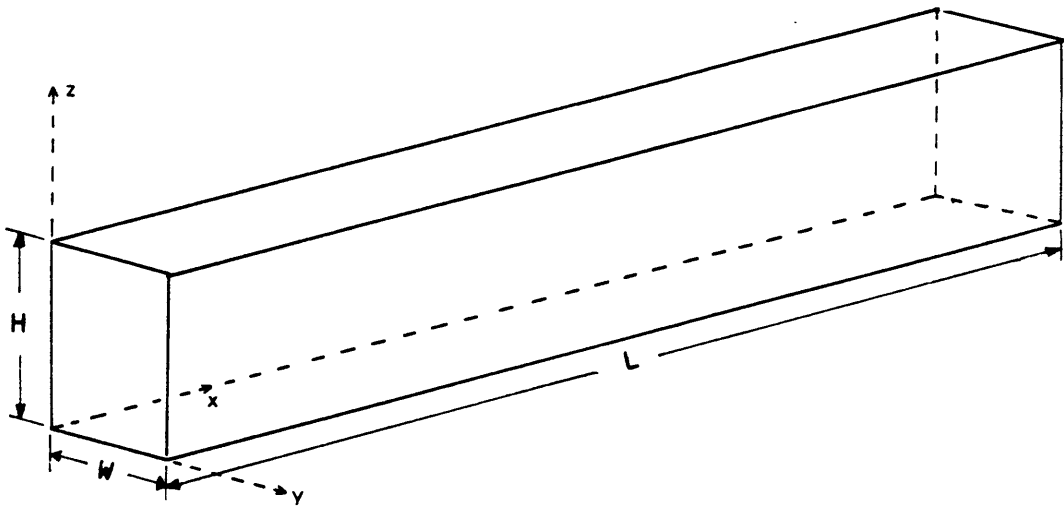


Figure 5.1. Rectangular Cell.

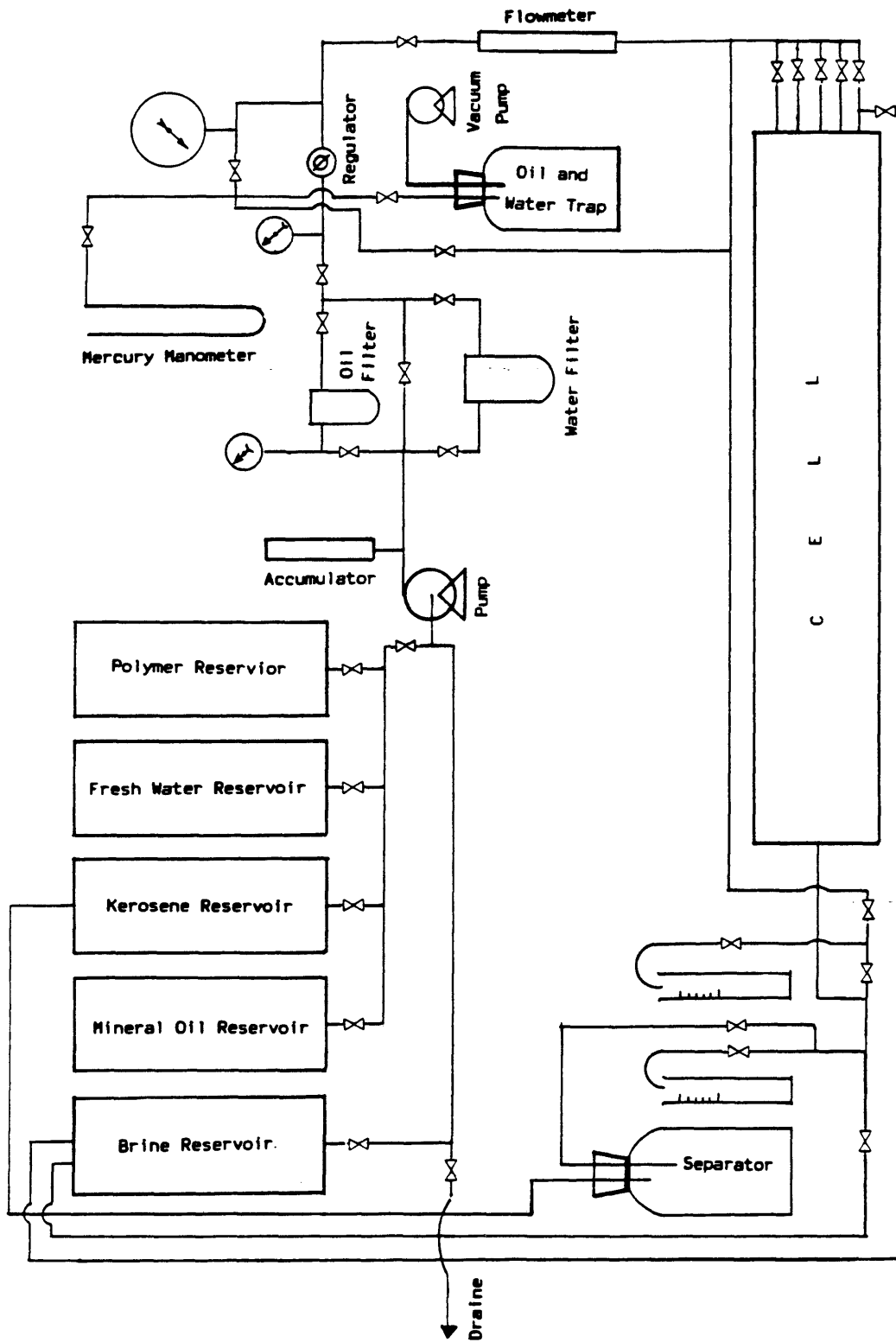


Figure 5.2. Schematic Diagram of the Apparatus.

volumes. Based on their data, a scaling coefficient greater than 1.5 signifies stability of the flood.

In contrast to the work cited, the data obtained by Richardson and Perkins (1957) show that recovery is substantially constant at values of the scaling coefficient in the range of 0.053 to 530.

McWilliams (1962) investigated the scaling coefficient proposed by Rapoport and Leas over a greater range of values of the relevant variables using cores of various diameters. He concluded that stability can be attained at a scaling coefficient in the range of 200 to 1000 and that the value of the scaling coefficient gets bigger for cores of larger diameters.

The divergence of McWilliams' data from those of Rapoport and Leas is pertinent to the large core permeabilities used by the former author which made gravitational segregation appreciable and hence enlarged the values of the scaling coefficient that ensures stability, as well as the fact that Rapoport and Leas neglected gravitational segregation in their derivation of the scaling coefficient $LV\mu_w$.

In this work, the values of the scaling coefficient $LV\mu_w$ were in the range of 2.75 to 329. It is noticed that floods performed under this range of scaling coefficient were significantly independent of the rate of injection.

5.2. Porous Media

The cell was packed with three different mesh sizes of Ottawa sand from Dowell-Schlumberger. The packing was done by filling the cell

vertically with the dry sand while hammering and shaking the cell until full. A de-aerated brine was pumped into the sand pack after vacuuming the cell. Later, additional hammering and shaking were applied to ensure good packing. Additional sand was added during this stage to fill any cavities through a hole near the inlet end of the cell.

Figure 5.3 shows the grain-size distribution of the sand obtained from sieve analysis and Table 5.1 shows the measured porosities and permeabilities.

Table 5.1. Properties of Porous Medium.

Mesh Size	Porosity %	Permeability darcy
10 - 20	34.93	106
20 - 40	34.77	67.83
80 - 100	33.53 - 35.11	6.72 - 8.82

5.3. Fluids

Four types of fluids were used. De-aerated brine, polymer, kerosene, and Silico T-75 mineral oil. City of Golden tap water was used to make the brine solution, after extracting air, by adding food quality salt. The salt concentration was varied between 10000 ppm and 33000 ppm to obtain different brine specific weights and viscosities.

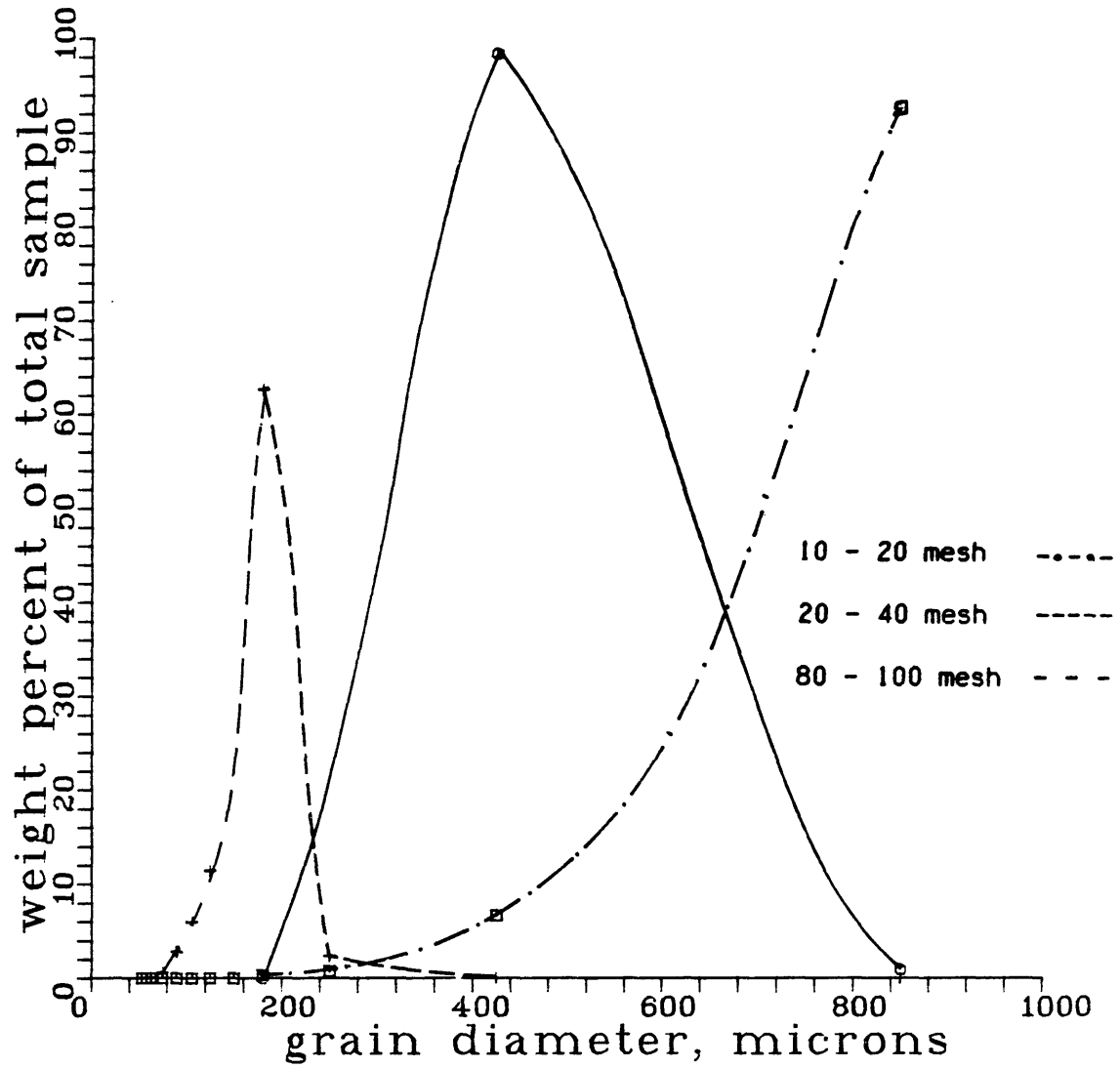


Figure 5.3. Grain Size Distribution of Ottawa Sand.

High quality Conoco kerosene (0.807 sp. gr.) represented the oil phase in runs 1 to 6, 11 to 13 and 15 to 16. Kerosene viscosity as a function of temperature is shown in Figure 5.4. Silico T-75 colorless mineral oil represented the oil phase in runs 7 to 10 and 14. Figure 5.5 shows the change of mineral oil viscosity with temperature variation. For runs 17 and 18, a mixture of 5% kerosene with mineral oil was used as the oil phase. The properties of the different types of oils used in this work are listed in Table 5.2.

Table 5.2. Properties of Oil Phase at 72°F.

Oil Type	Sp. Wt. gm/cc	Viscosity cp.
Kerosene	0.800	1.48
Silico T-75	0.833	23.80
Silico T-75 with 5% Kerosene mixture	0.827	14.20

Pusher-500 polymer was used as a mobility control agent in runs 1, 2 and 3 to obtain variable mobility conditions. Pusher-500 is a commercial polyacrylamide polymer supplied by Dow Chemical. A Brookfield viscometer with a UL adapter was employed to determine the rheological properties of the polymer. Figures 5.6 and 5.7 show these properties. Polymer solution viscosities of 37.8 cp., 7.87 cp. and 3.55 cp. were used in runs 1, 2 and 3, respectively.

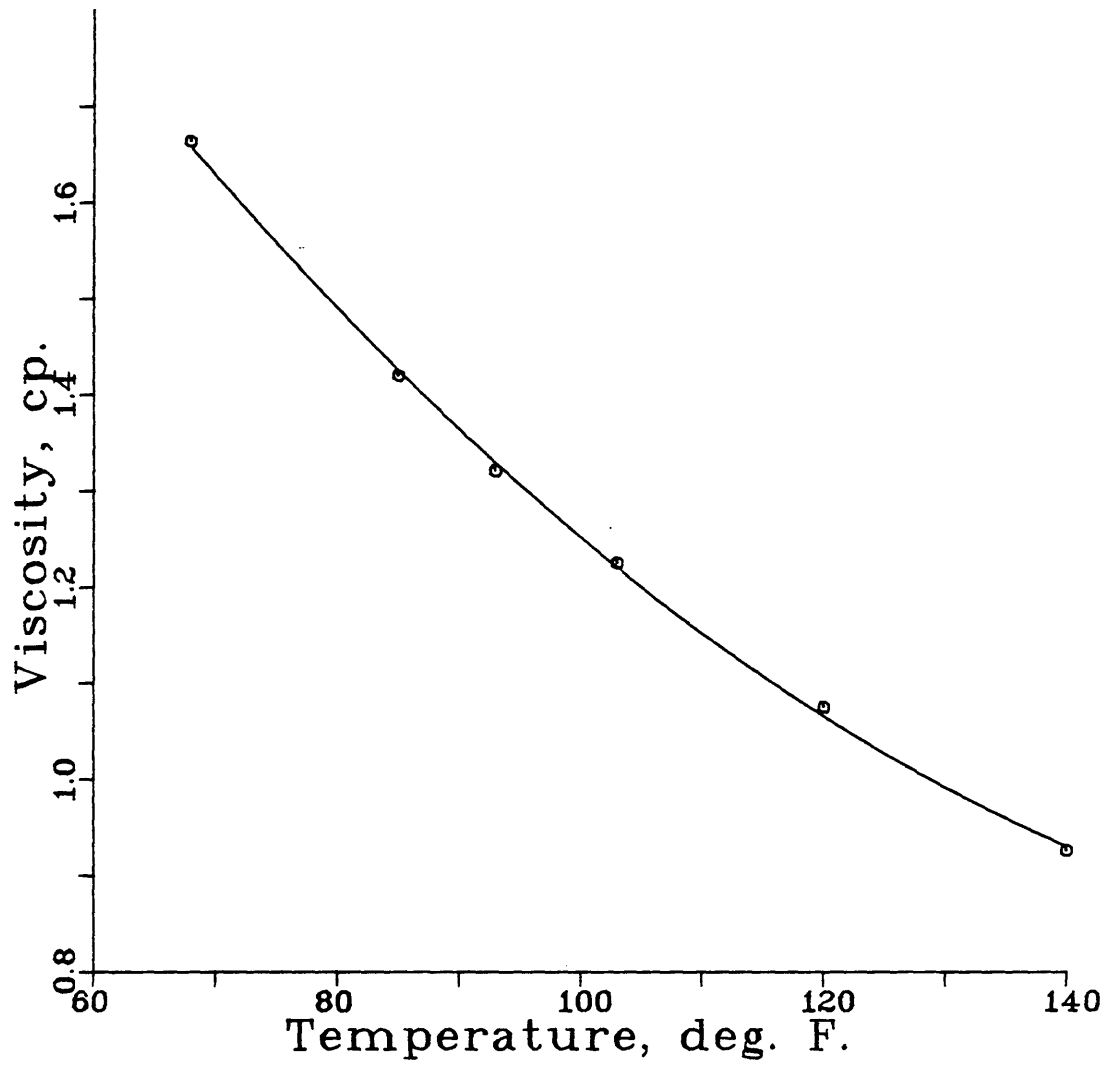


Figure 5.4. Kerosene Viscosity.

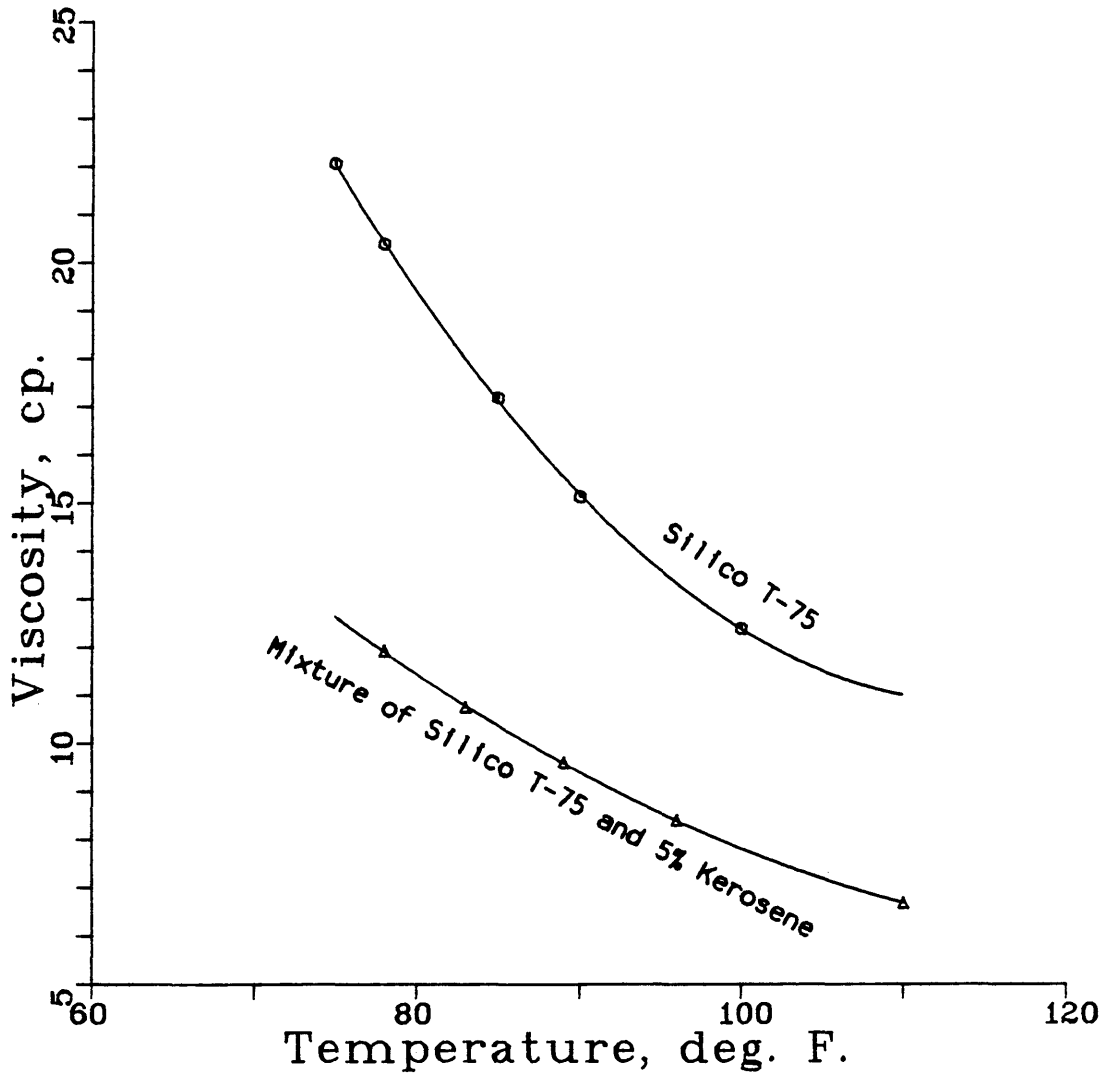


Figure 5.5. Mineral Oil Viscosity.

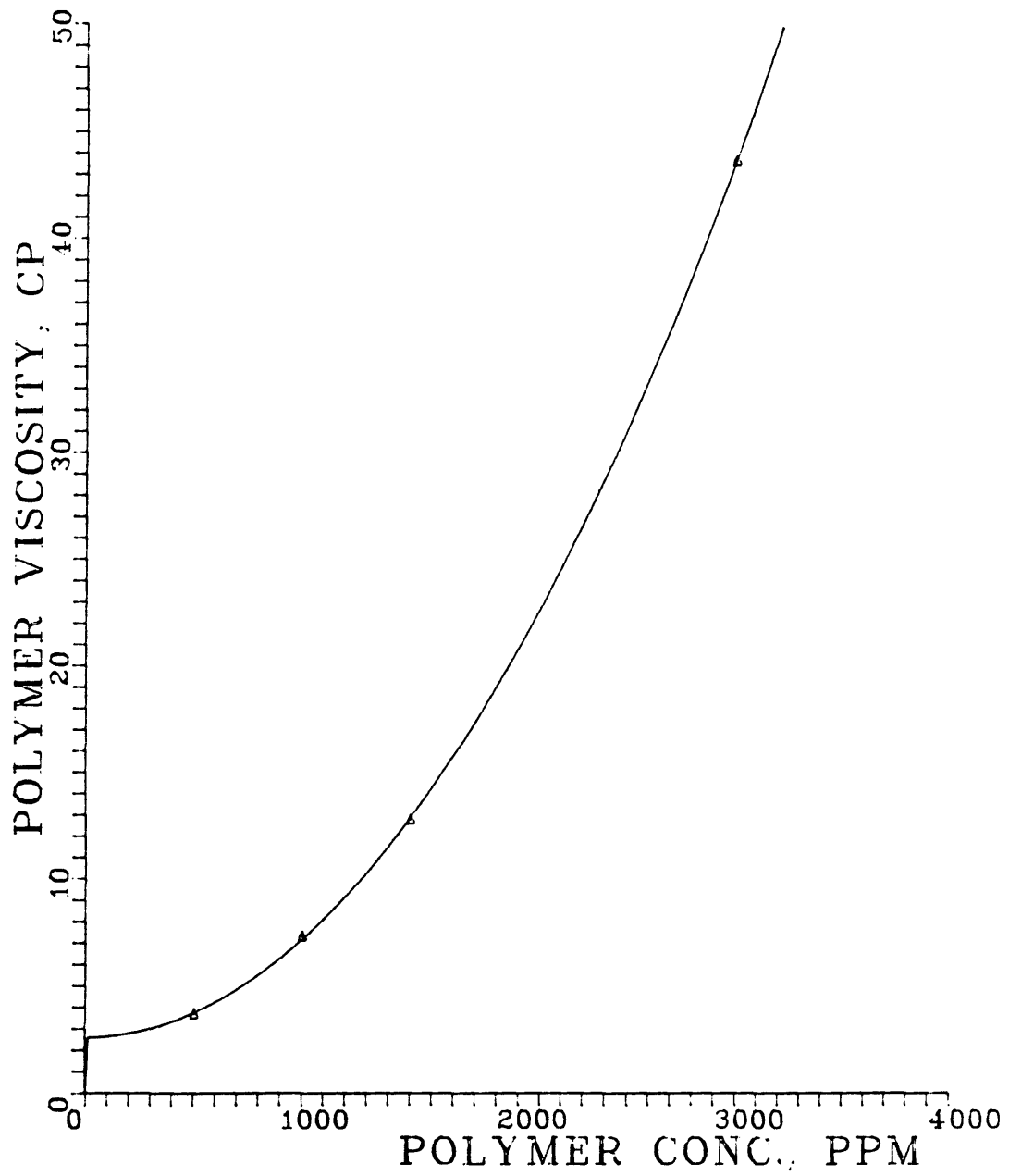


Figure 5.6. Viscosity of Pusher 500 Solution in Brine.

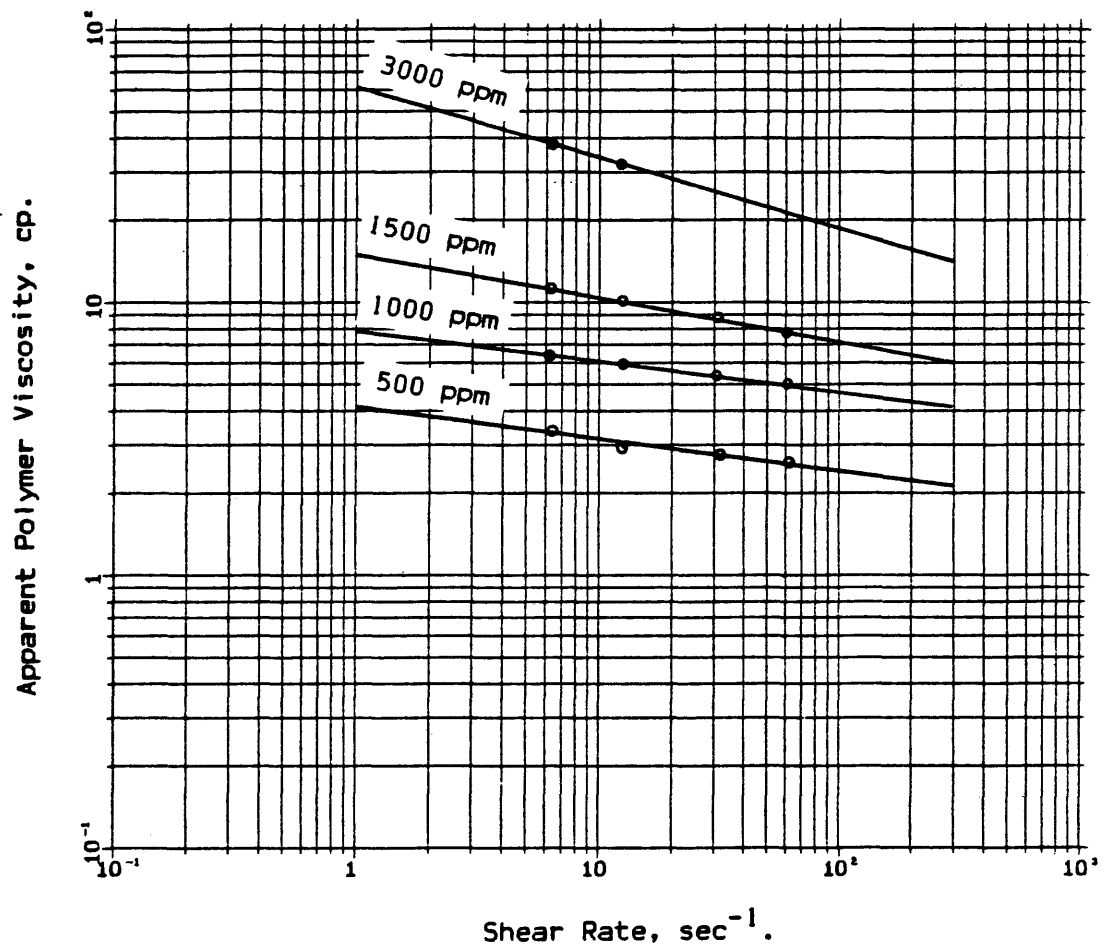


Figure 5.7. Rheology of Pusher-500 Polymer.

5.4. Saturation Recording System

55 pairs of electrodes were installed on opposite sides of the cell 2 1/2 in. apart in 11 columns. A 2000 CPS AC current was passed through the electric circuit of each electrode (Figure 5.8) and the voltage drop across a known resistance was measured and then used in the following equation to calculate the unknown resistance of the fluid saturated porous medium:

$$R_t = \frac{R_k (V_{osc} - V_k)}{V_k} \quad (5.1)$$

The water saturation across each pair of electrodes was then calculated from Archie's equation (1942)

$$S_w^m = \frac{R_o}{R_t} \quad (5.2)$$

In order to solve this equation for water saturation, the exponent, m , has to be initially determined. This was done by substituting $R_t(S_{or})$ and $R_t(S_{wi})$ twice in the following equation:

$$\ln S_w = \frac{1}{m} \ln R_o - \frac{1}{m} \ln R_t \quad (5.3a)$$

or

$$\ln S_w = \text{Cont.} - \frac{1}{m} \ln R_t \quad (5.3b)$$

5.4.1. Data Acquisition System

An HP 3054A computer-based automatic data acquisition and control system was employed to measure the electric resistance across the 55

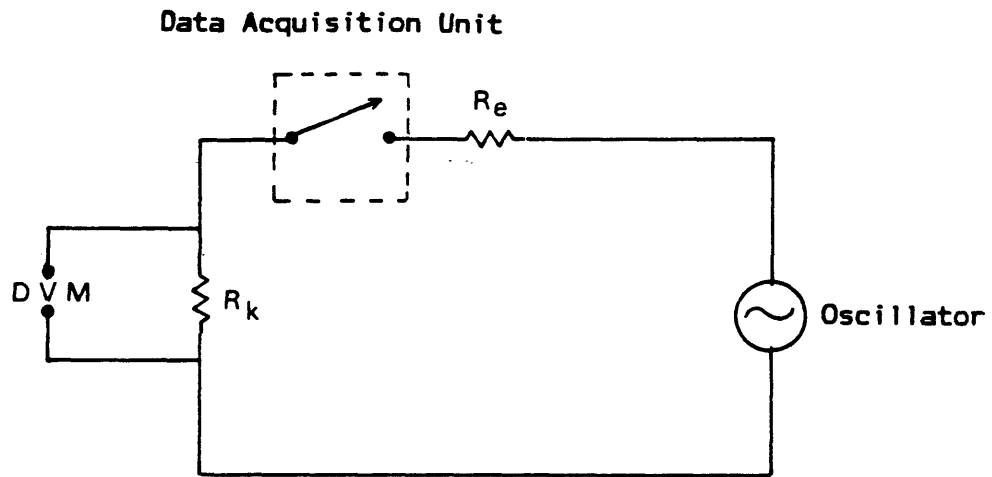


Figure 5.8. Electric Circuitry of a Pair of Electrodes.

pairs of electrodes. This system consisted of:

- HP 3497A data acquisition/control unit
- HP 3456A digital voltmeter
- HP 3437A system voltmeter.

The data acquisition system is interfaced to a desktop HP 9836 computer in the manner shown in Figure 5.9. The computer was programmed to activate and control the data acquisition system. Each pair of electrodes is connected to a channel on the data acquisition/control unit, i.e., 55 channels for the 55 pairs of electrodes. The computer closes one channel at a time and triggers the digital voltmeter to measure the voltage drop across the known resistance, R_k and then sends the reading back to the computer, which in turn runs a program to calculate R_t using Eq. 5.1 and stores the value of R_t on a data disc. Then the following channel is closed until all 55 channels are scanned. This is repeated at a preset time intervals over the course of the displacement. A full sweep took less than 20 seconds. Figure 5.10 shows a diagram of the electric circuitry.

In order to establish confidence in the values of water saturation measured electrically using the method explained above, these values were compared with those obtained volumetrically. The two values were plotted against each other in Figure 5.11. As the plot indicates, the water saturation obtained from resistivity measurements corresponds adequately to that determined volumetrically. This provides the confidence required to proceed with the resistivity method as a means

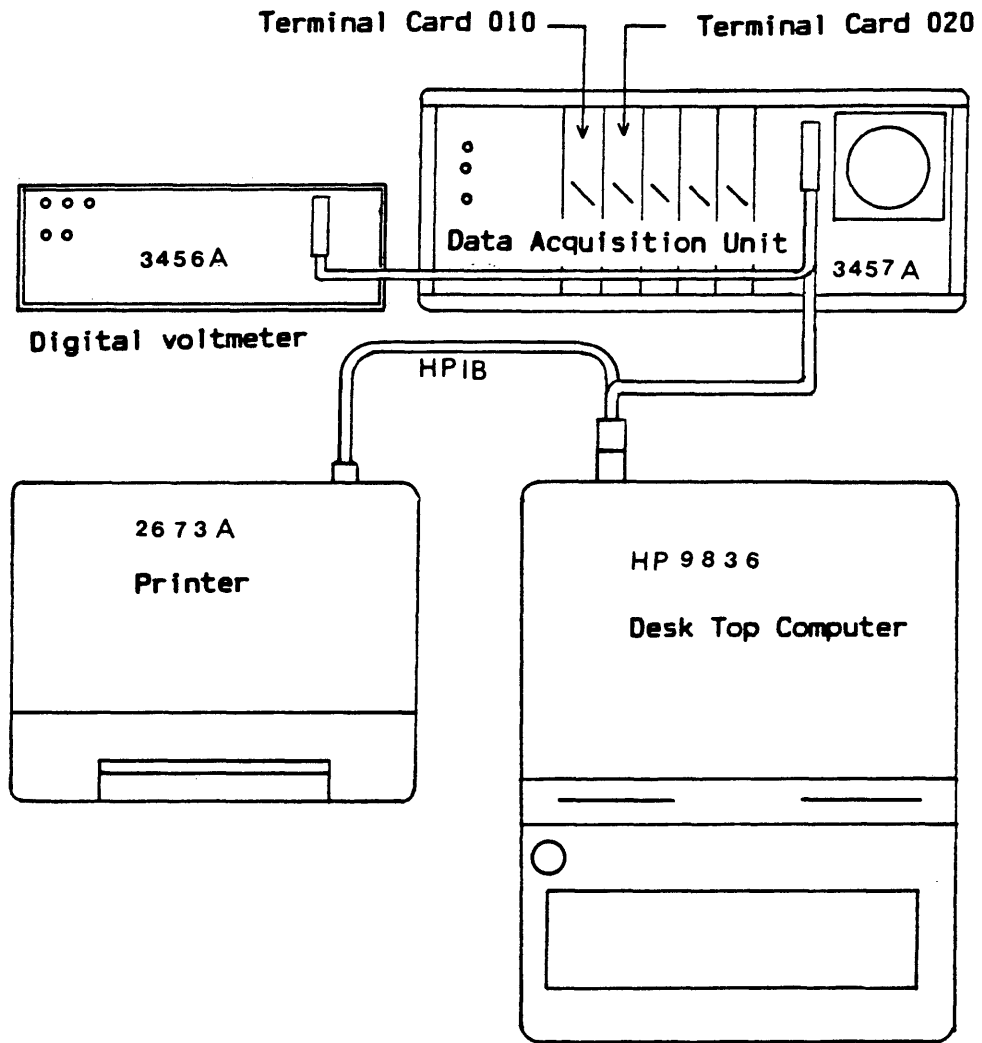


Figure 5.9. Data Acquisition/Control System Setup.

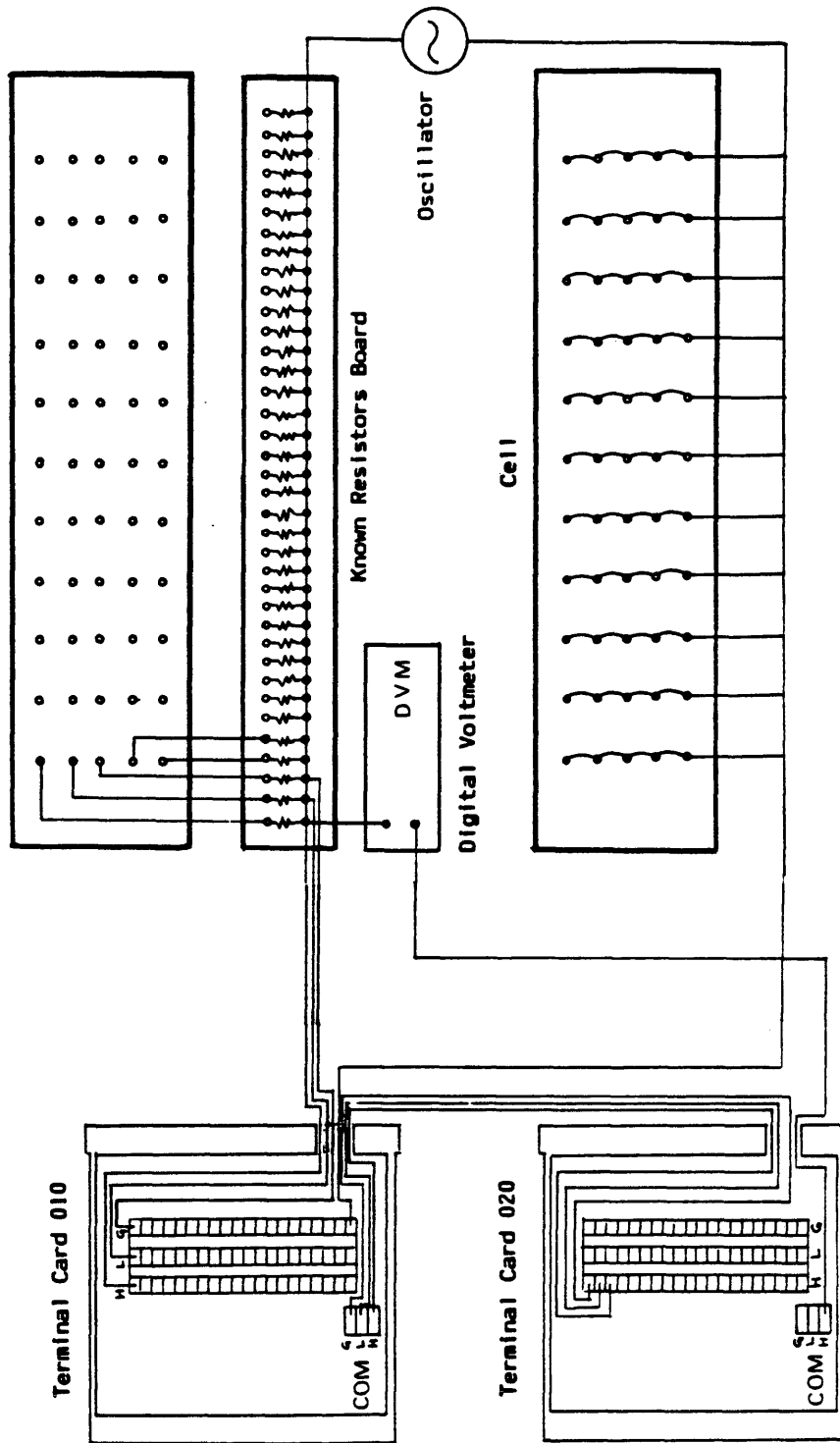


Figure 5.10. Diagram of Complete Electric Circuitry.

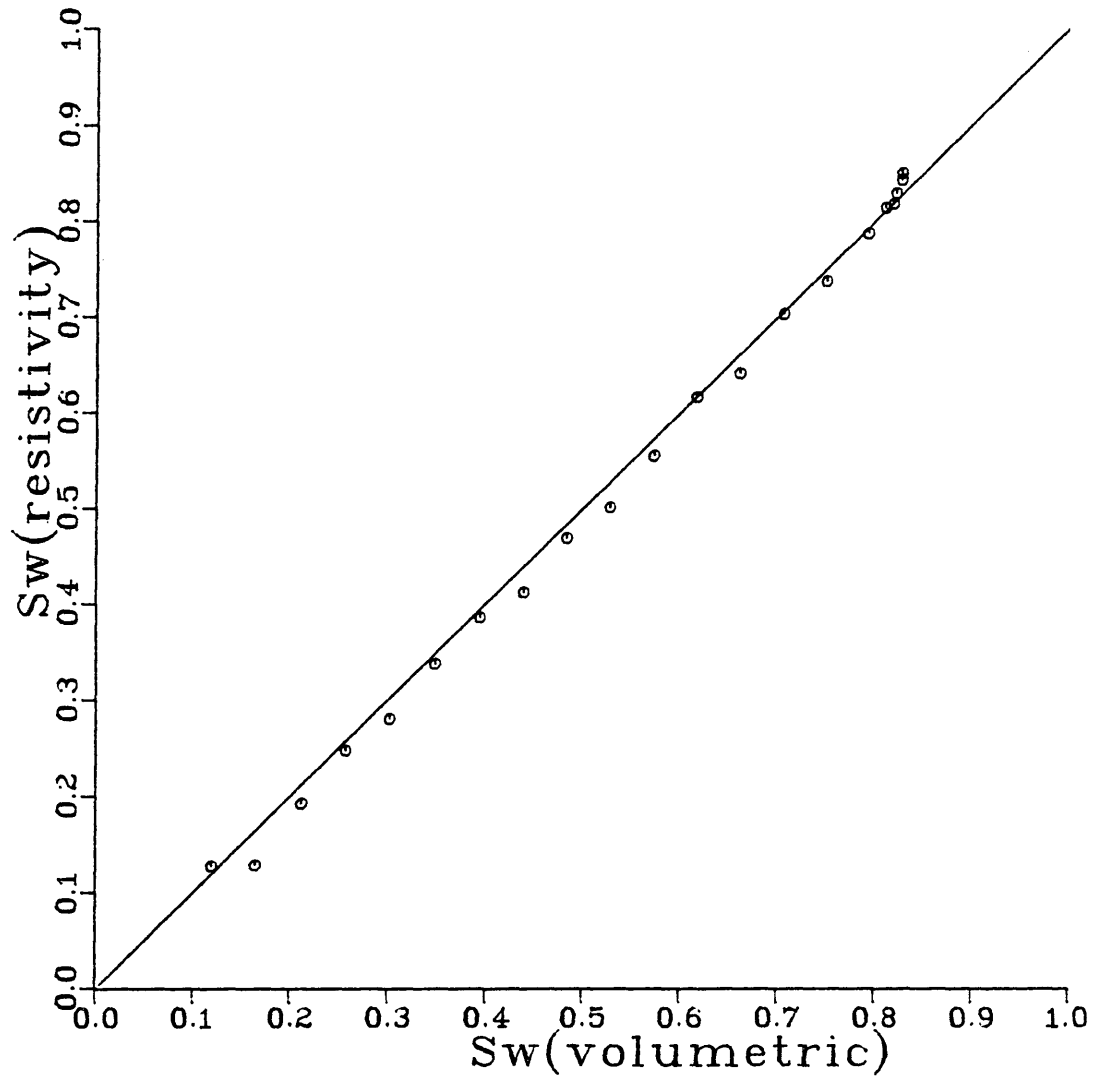


Figure 5.11. Comparison of Water Saturation Calculated from Resistivity with Water Saturation Measured Volumetrically. Run No. 1.

for water saturation determination in the remaining displacements conducted in this work.

5.5. Displacement Procedure

After uniform and satisfactory compaction is obtained, the sand pack is flooded with several pore volumes of de-aerated brine. The saturation is checked by monitoring the resistivity across the 55 pairs of electrodes until no more change in the resistivity of the 100% brine saturated sand is observed. The latest reading of resistivity is stored by the computer as R_o . Then the absolute permeability of the sand pack is determined using de-aerated brine. The pressure drop across the cell is measured with a mercury manometer (0.02 psi accuracy). Next, the cell is flooded with oil at a rate several times higher than that intended for the subsequent water or polymer flooding. Oil flooding is continued until no more water is produced and a minimum water saturation is attained. The effective permeability to oil at connate water saturation is determined at this stage. The resistivity of the cell is recorded and stored as $R_t(S_{wi})$ to be used later in Archie's equation (1942). The cell is ready to commence water or polymer flooding.

During water or polymer flooding, the flow rate, pressure drop, volumes produced, and resistivity were recorded simultaneously at each time interval.

The motion of the interface (water/oil or polymer/oil) is tracked via the 55 pairs of electrodes located on opposite sides of the cell. The breakthrough recovery is closely monitored and recorded since it

defines whether the displacement is stable or not. The flood is halted when two pore volumes are injected or when the water-oil ratio exceeded 50, whichever comes first. The effective permeability to water at residual oil saturation, $k_w(S_{or})$, is determined and the resistivity of the cell is recorded and stored as $R_t(S_{or})$. The sand is then removed from the cell using strong jets of water to ensure thorough cleaning and the cell is repacked with new sand to start another run.

CHAPTER SIX

EXPERIMENTAL RESULTS AND DISCUSSIONS6.1. Oil Flooding and the Establishment of Connate Water Saturation

As the experiments were intended to simulate a connate water bearing porous medium, initial water saturation had to be established before proceeding with the subsequent water or polymer floodings. This task was achieved by flooding the brine saturated cell with several pore volumes of oil (either kerosene or mineral oil) until no more water was produced.

It was noticed that when flooding with mineral oil, where the oil-water viscosity ratio is high, a smaller number of pore volumes of oil had to be injected in order to reach minimum water saturation, whereas when flooding with kerosene (lower oil-water viscosity ratio), about 50 pore volumes were injected to obtain minimum water saturation. However, the initial water saturation obtained in both cases showed a monotonic increase toward the outlet end of the cell, as Figure 6.1 illustrates. The initial water saturation increased from a value of 0.1 at the inlet end to about 0.19 at the outlet end. A small jump in saturation could be noticed close to the outlet end due to the end effect. A similar behavior was reported in earlier studies using microwave attenuation (Bentsen and Saeedi, 1981) and X-ray absorption techniques (Allen and Puckett, 1986).

In an attempt to explain this behavior, Parsons (1975) suggested that the part of the porous medium ahead of the water flood front is

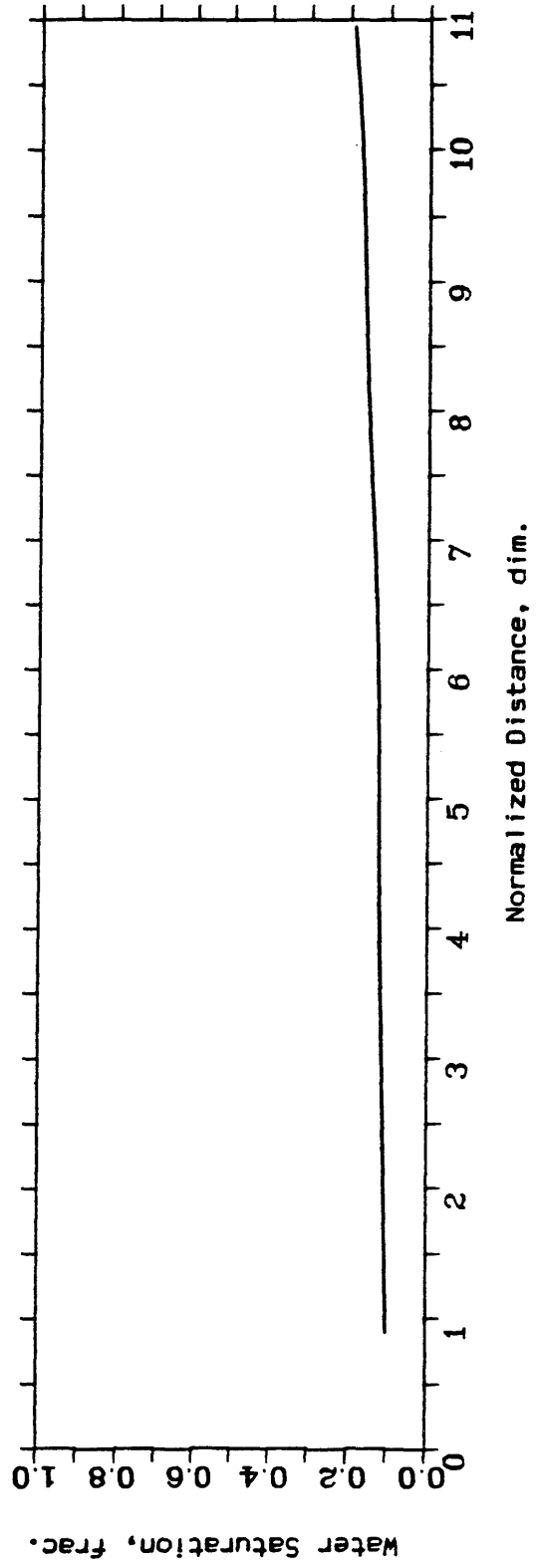


Figure 6.1. Connate Water Saturation. Run No. 1.

still experiencing the tail end of the preceding oil flood. In order to overcome this problem, the oil floods were conducted at a rate substantially higher than that planned for the subsequent water and polymer floods.

Another observation was made during oil flooding, i.e., the oil overrode the water phase, both in low and medium permeability sand packs. This is illustrated in Figures 6.2 and 6.3 representing the water saturation contours.

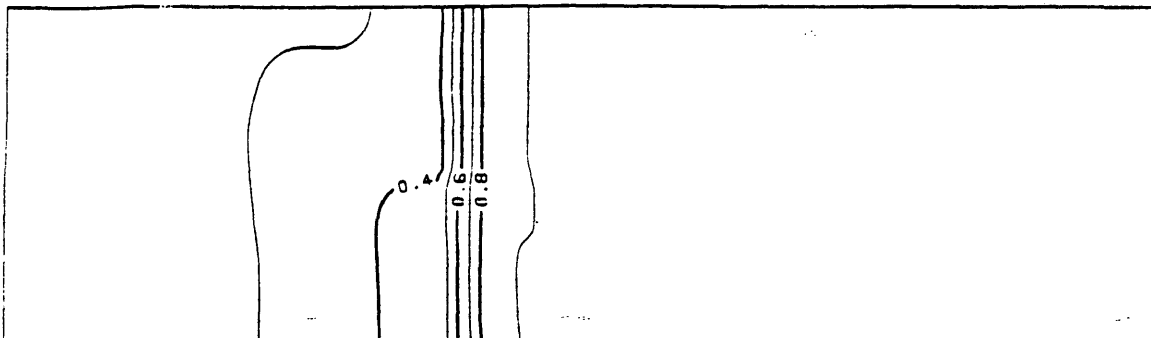
6.2. Polymer and Water Flooding

A total of 18 runs were performed in three types of porous media in terms of absolute permeability, namely, high, medium and low. Also, three different types of oil were employed to allow for various oil-water viscosity ratios.

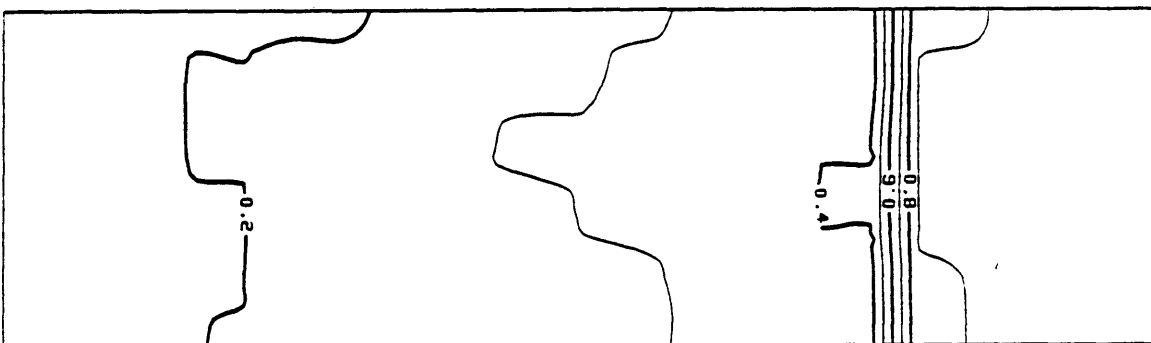
6.2.1. Low Permeability Sand Packs

An 80-100 mesh Ottawa sand was employed in runs 1 to 10 with absolute permeability in the range of 6.72 to 8.82 darcies. Polymer flooding was conducted in runs 1, 2 and 3, using kerosene as the oil phase. The viscosity ratio for these runs was 0.042, 0.184 and 0.394, respectively. The observed recovery at breakthrough was almost the same in runs 2 and 3 and slightly higher in run 1, as can be seen in Table 6.1. Figures 6.4, 6.5 and 6.6 are water saturation contours showing the motion of the displacing phase (polymer) at different time intervals. As can be seen, the polymer/oil-interface progressed uniformly during these runs with no signs of fingering or tonguing marking a stable

Time = 0.5 hr



Time = 1.0 hr

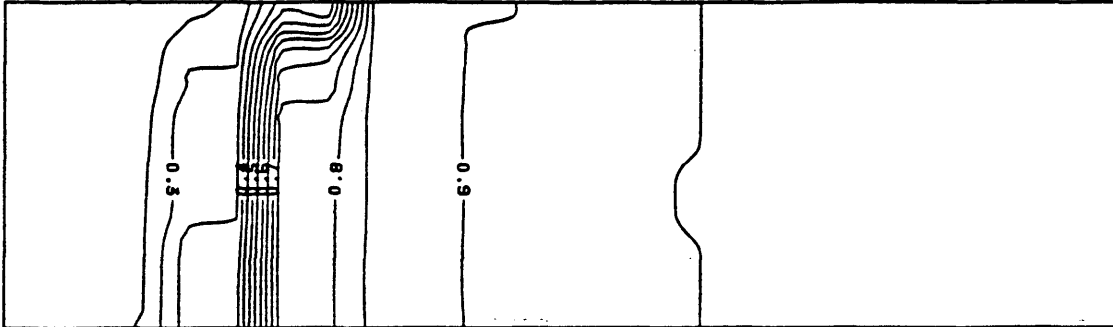


Time = 1.5 hrs

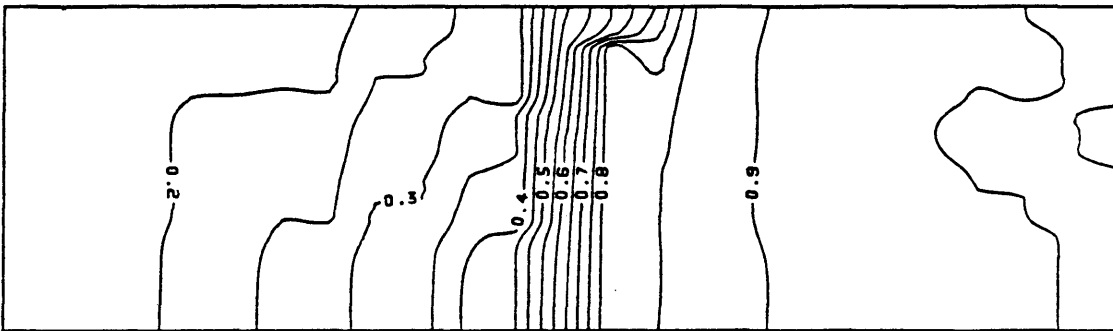


Figure 6.2. Saturation Contours of Run Number 1. Oil Flood.
Low Permeability Sand.

Time = 0.17 hr



Time = 0.25 hr



Time = 0.5 hr

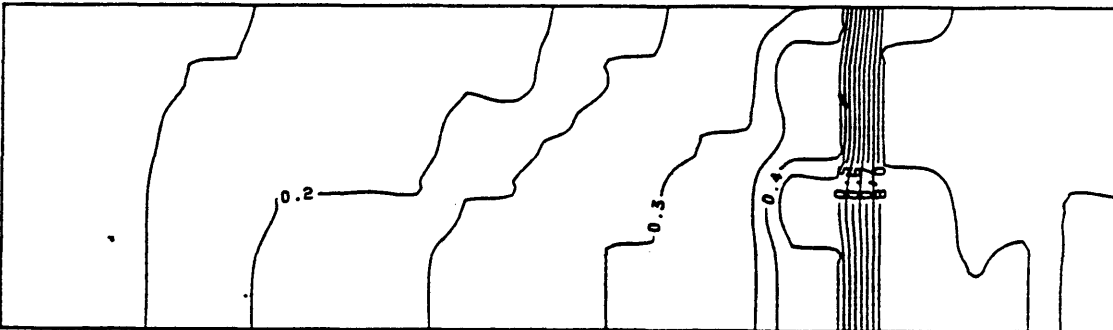


Figure 6.3. Saturation Contours of Run Number 11. Oil Flood.

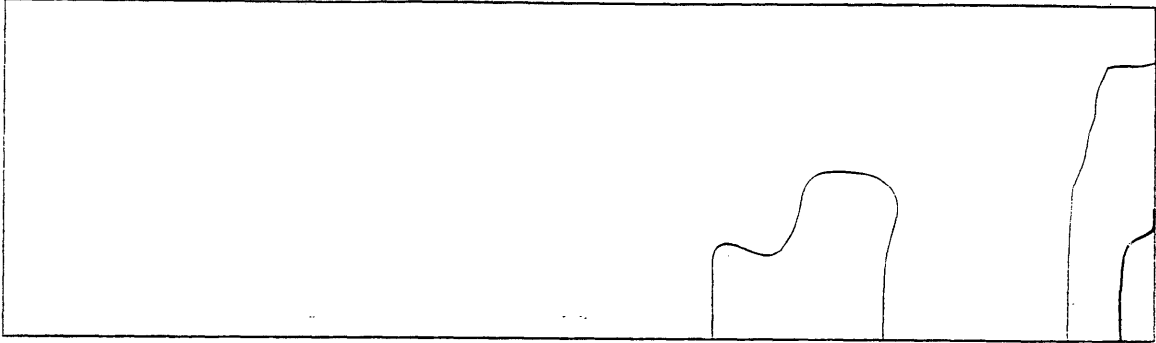
Medium Permeability Sand.

TABLE 6.1. Summary of Experimental Data. Low Permeability Sand.

Run Number	k darcy	$k_w(S_{OR})$ darcy	$k_o(S_{WI})$ darcy	ϕ %	App gm/cc	Q cc/min	μ_o / μ_w dlm.	$G \times 10^2$ dlm.	$F_s \times 10^5$ cm	Breakthrough Recovery, PV.
1	7.34	3.56	6.22	34.44	0.293	16.59	0.042	141.35	46.634	0.678
2	7.34	2.82	6.10	34.44	0.203	10.93	0.184	27.87	15.156	0.643
3	7.34	3.43	3.13	34.44	0.203	13.14	0.394	15.17	7.086	0.648
4	6.78	3.71	6.33	35.11	0.209	20.82	1.533	6.55	1.863	0.628
5	6.72	3.70	6.48	34.57	0.209	12.26	1.469	4.06	1.938	0.646
6	6.72	4.05	6.54	34.57	0.209	7.42	1.573	2.46	1.808	0.666
7	8.82	4.06	7.39	34.57	0.183	5.19	21.188	1.58	0.135	0.423
8	8.82	3.96	7.36	34.57	0.183	18.87	21.471	5.78	0.133	0.426
9	8.82	3.90	7.20	34.57	0.183	44.70	20.473	13.05	0.139	0.422
10	8.82	3.95	7.24	34.57	0.362	6.16	9.200	1.87	0.155	0.436

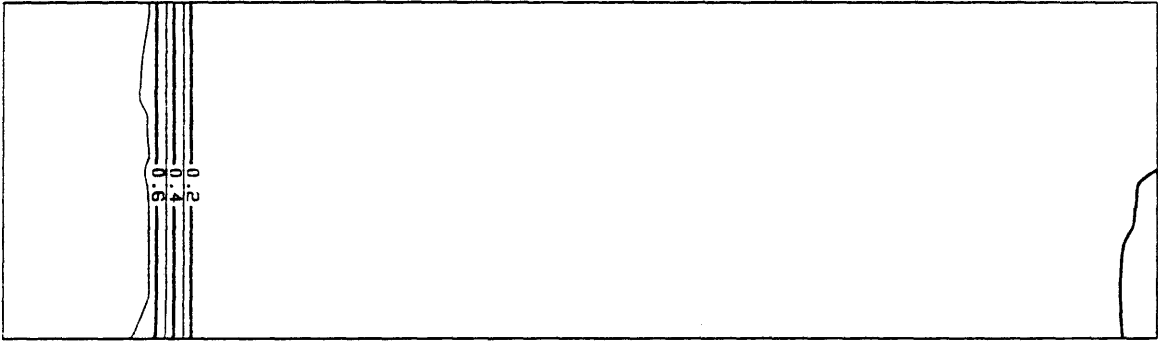
Time = 0.0 hr

Cum. Oil Produced = 0.000 PV



Time = 2.0 hrs

Cum. Oil Produced = 0.093 PV



Time = 4.0 hrs

Cum. Oil Produced = 0.184 PV

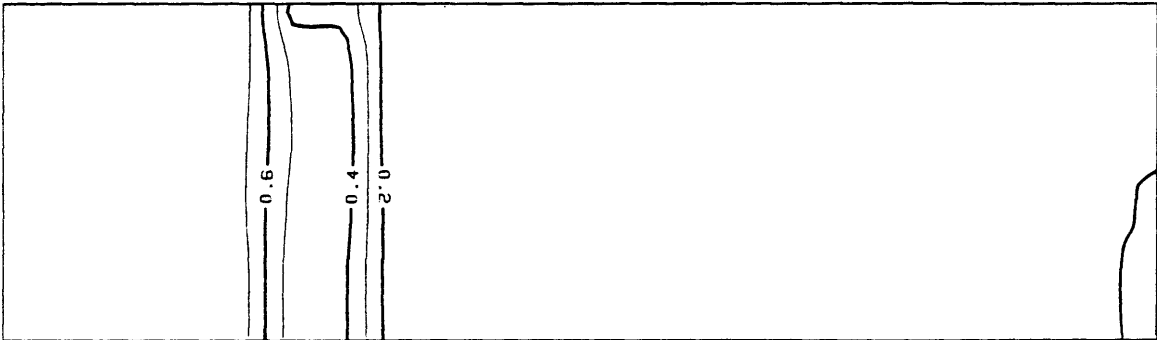
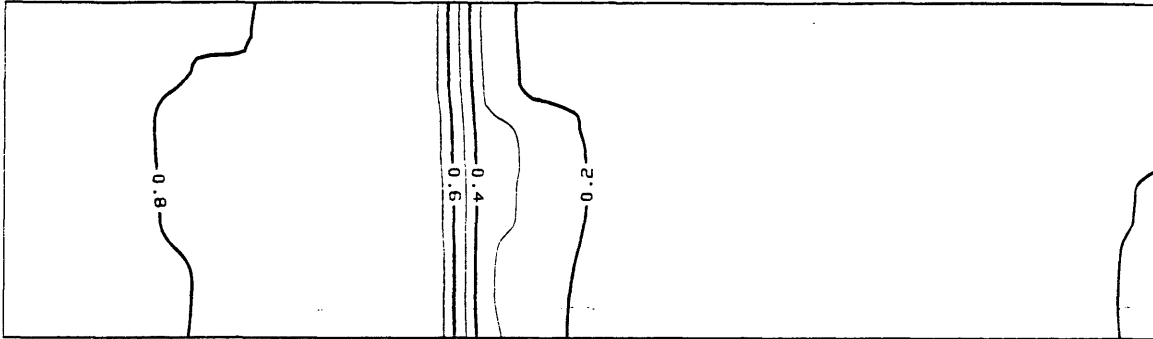


Figure 6.4. Saturation Contours of Run Number 1. Polymer Flood.
Low Permeability Sand.

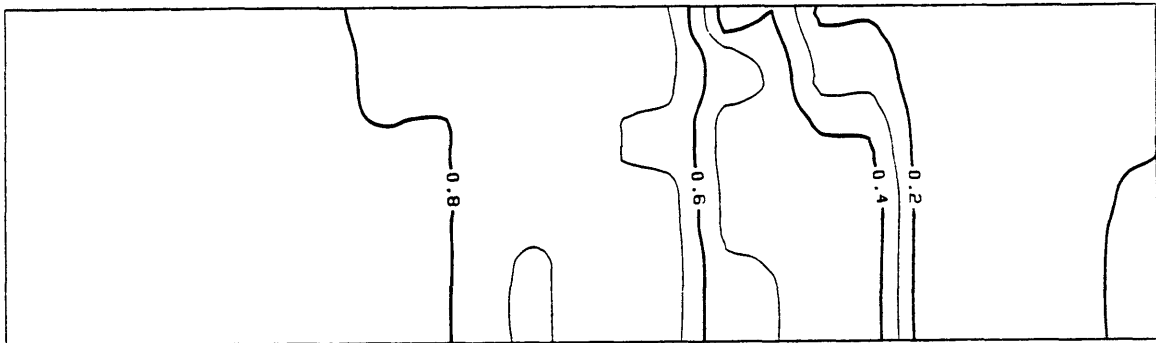
Time = 6.0 hrs

Cum. Oil Produced = 0.275 PV



Time = 10.0 hrs

Cum. Oil Produced = 0.453 PV



Time = 15.0 hrs

Cum. Oil Produced = 0.673 PV

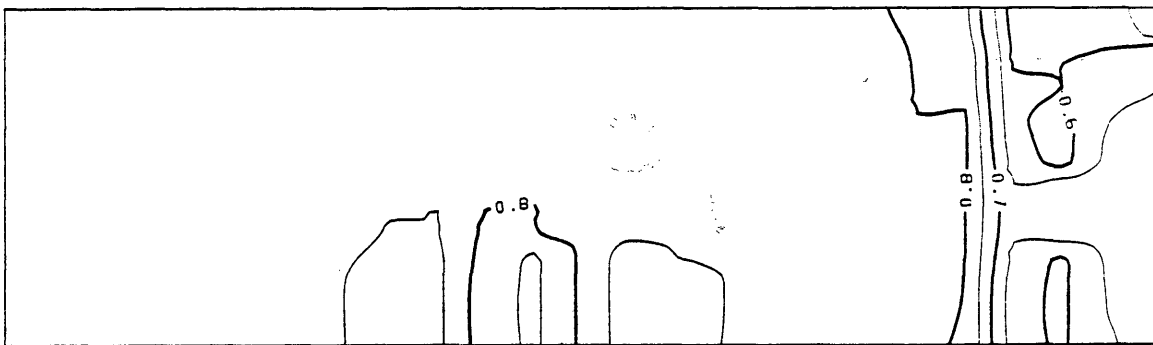
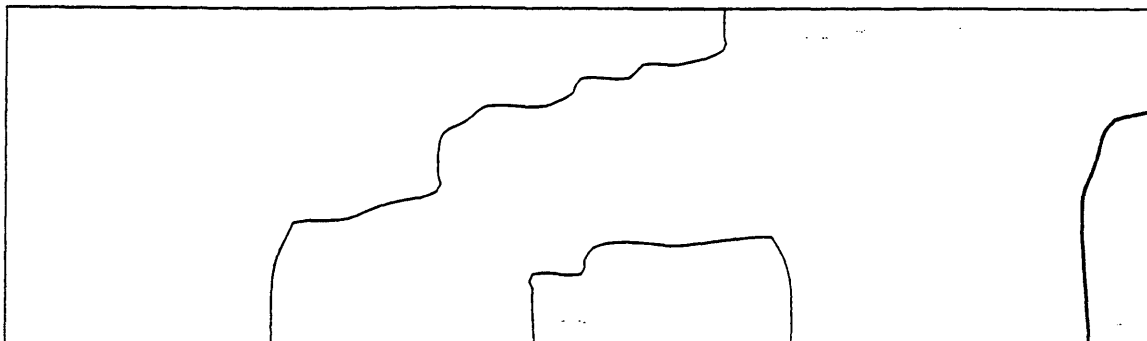


Figure 6.4. (Continued).

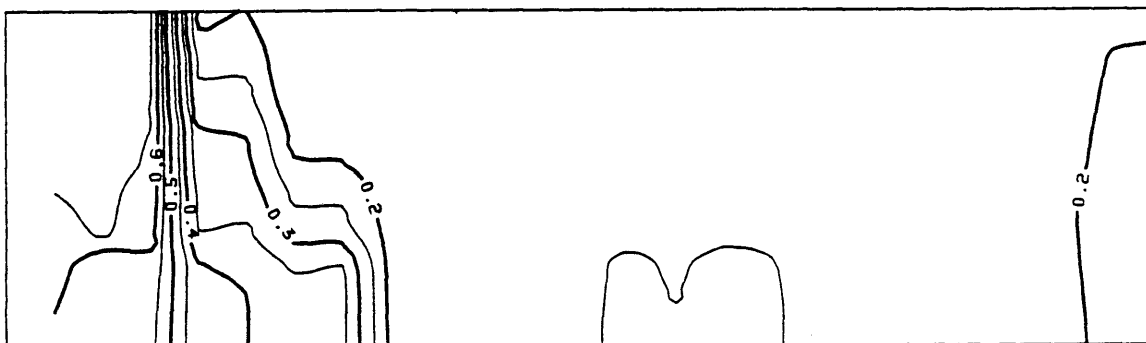
Time = 0.0 hr

Cum. Oil Produced = 0.000 PV



Time = 4.0 hrs

Cum. Oil Produced = 0.127 PV



Time = 12.0 hrs

Cum. Oil Produced = 0.330 PV

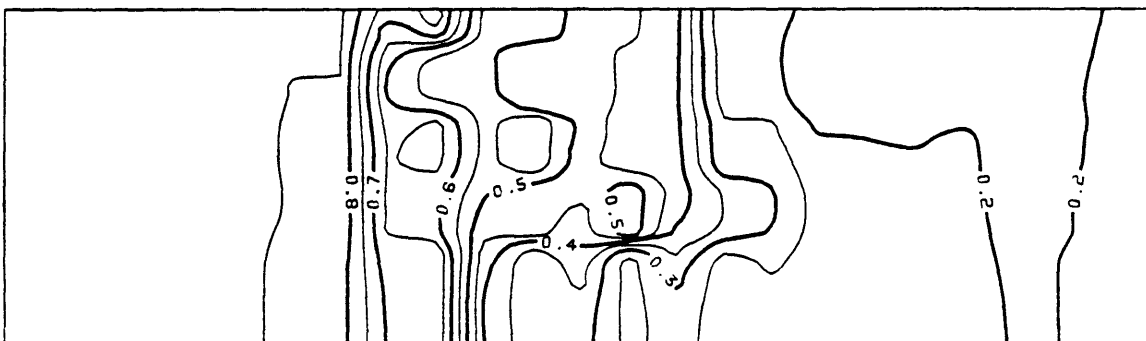
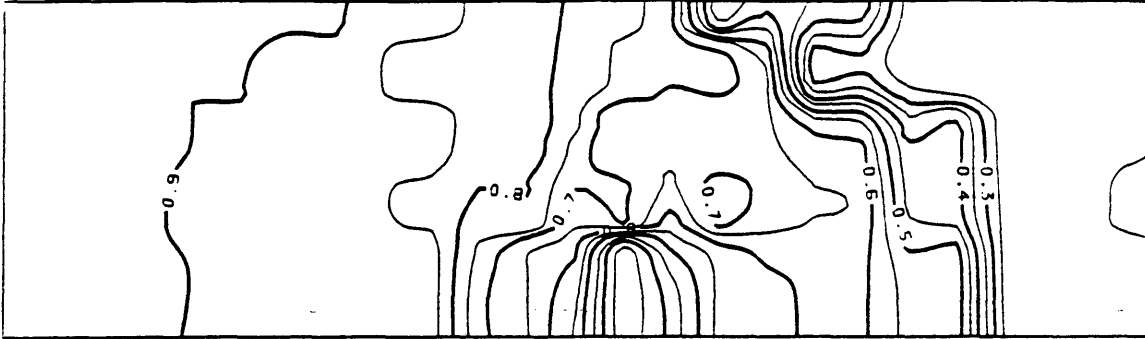


Figure 6.5. Saturation Contours of Run Number 2. Polymer Flood.
Low Permeability Sand.

Time = 16.0 hrs

Cum. O11 Produced = 0.474 PV



Time = 22.0 hrs

Cum. O11 Produced = 0.643 PV

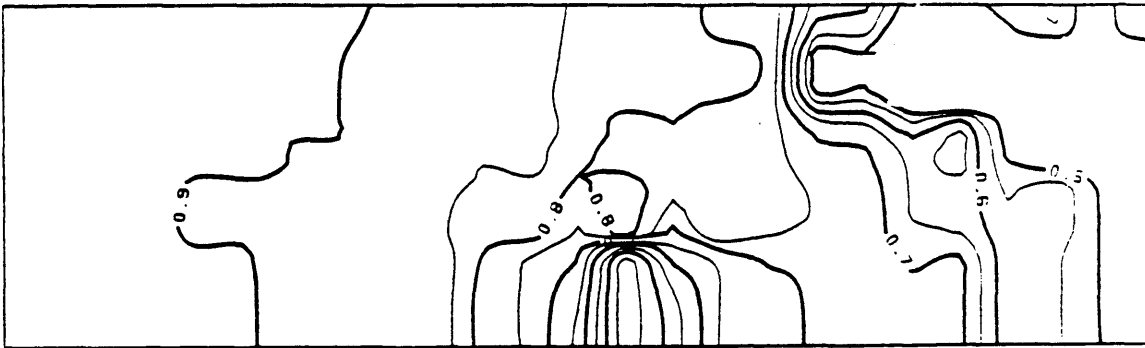
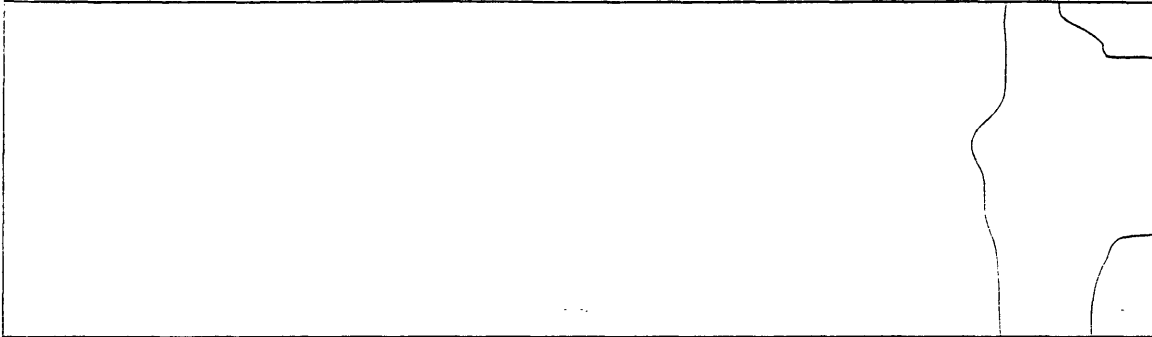


Figure 6.5. (Continued).

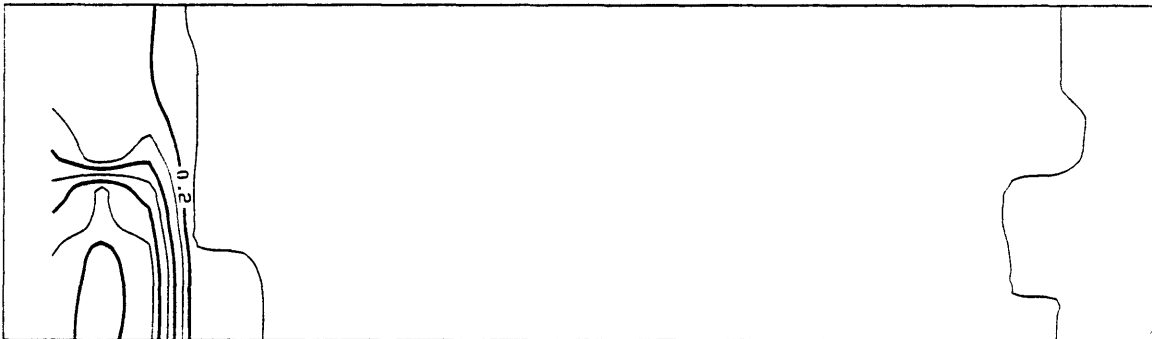
Time = 0.0 hr

Cum. Oil Produced = 0.000 PV



Time = 2.25 hrs

Cum. Oil Produced = 0.075 PV



Time = 5.50 hrs

Cum. Oil Produced = 0.167 PV

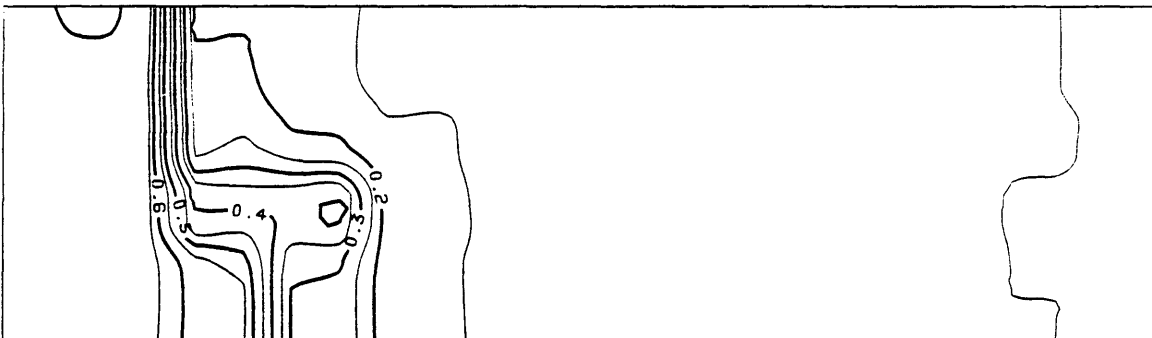
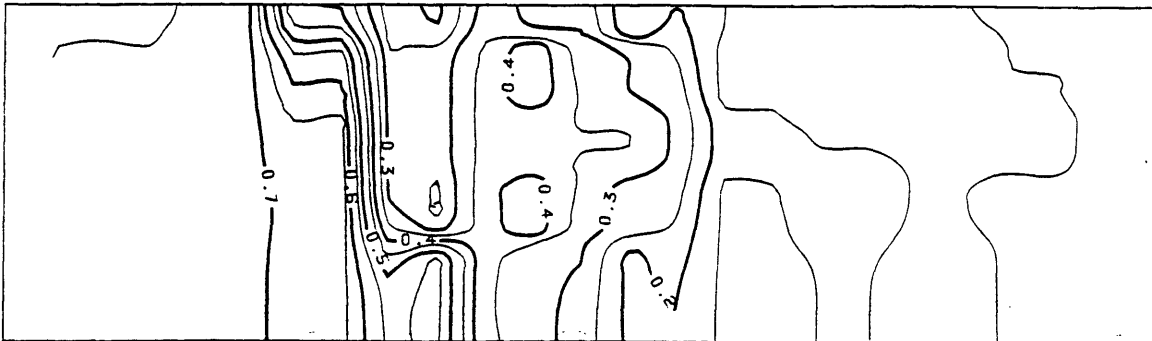


Figure 6.6. Saturation Contours of Run Number 3. Polymer Flood.
Low Permeability Sand.

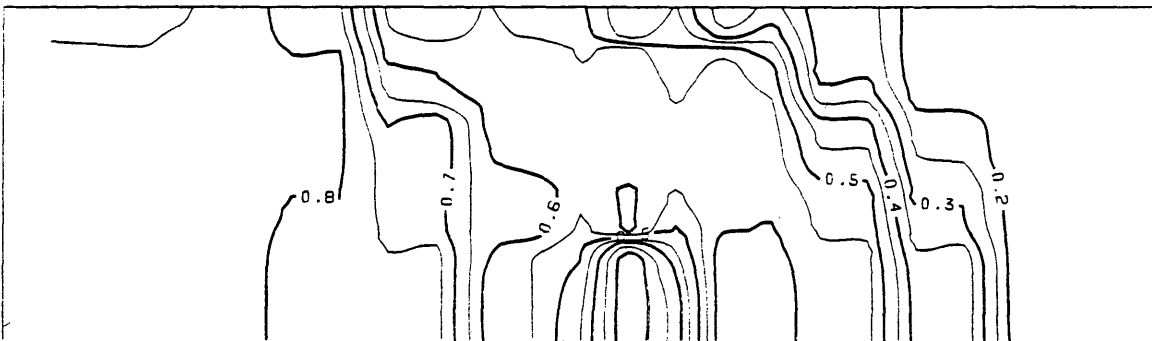
Time = 10.5 hrs

Cum. O11 Produced = 0.349 PV



Time = 14.5 hrs

Cum. O11 Produced = 0.493 PV



Time = 18.5 hrs

Cum. O11 Produced = 0.648 PV

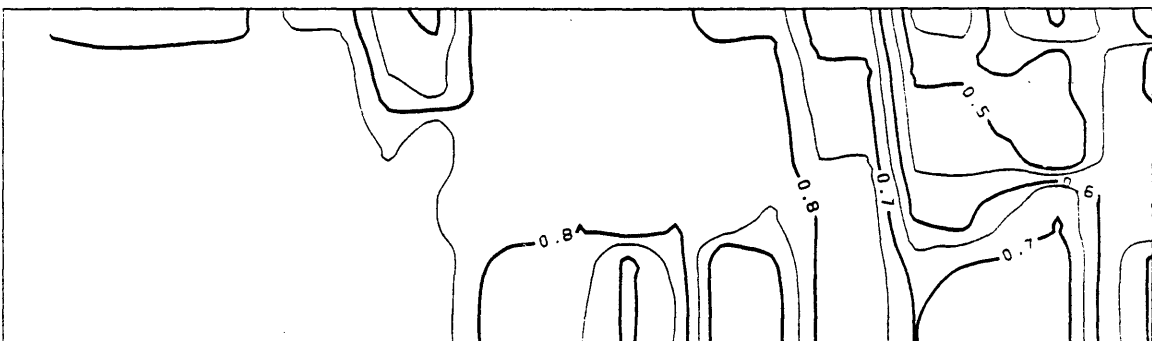


Figure 6.6. (Continued).

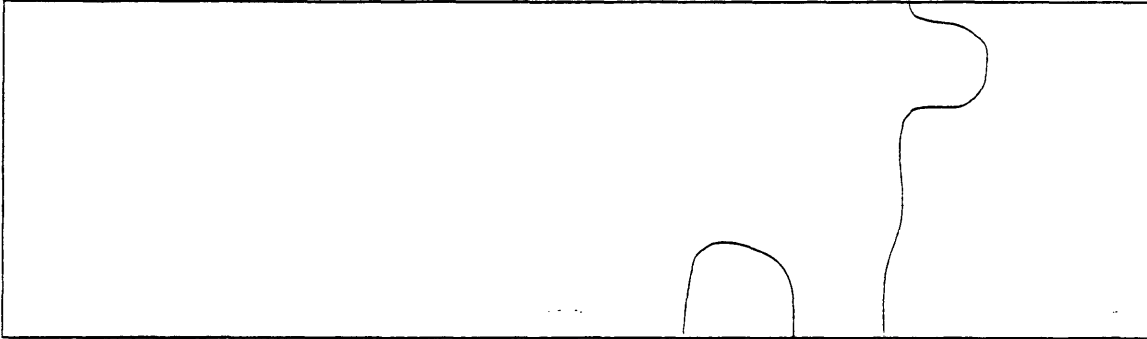
displacement.

Water flooding was performed in runs 4,5 and 6 using kerosene as the oil phase. Oil recovery at breakthrough increased about 6 percent because of a threefold reduction in the rate of injection (Table 6.1). Despite the unfavorable viscosity ratios (1.469 to 1.573), the interface remained stable and proceeded uniformly in a manner similar to that observed during polymer flooding, as Figures 6.7, 6.8 and 6.9 show. This could be attributed to the effect of capillary forces which tend to impair fluid motion in transverse direction to the bulk fluid motion, hence preventing tonguing or fingering. Added to this is the retarding effect of low permeability sand pack on gravity segregation.

In runs 7 to 10, water flooding was conducted using mineral oil as the oil phase. The viscosity ratios were 21.18, 21.47, 20.47 and 9.2, respectively. Oil recovery at breakthrough showed no sensitivity to the change in the injection rate in runs 7, 8 and 9. But, compared to the breakthrough recovery of runs 4, 5 and 6, the recovery dropped significantly because of a more unfavorable viscosity ratio. However, no fingering or tonguing could be detected from Figures 6.10, 6.11 and 6.12, which represent the saturation contours of runs 7, 8 and 9, respectively. This type of behavior allows to draw the conclusion that an immiscible displacement can be considered as unstable, based on the drop in the breakthrough oil recovery, without the expected appearance of fingering or tonguing. This makes the stability phenomena in water-wet, connate water-bearing, porous medium quite ambiguous if the observations are based only on the macroscopic behavior of the

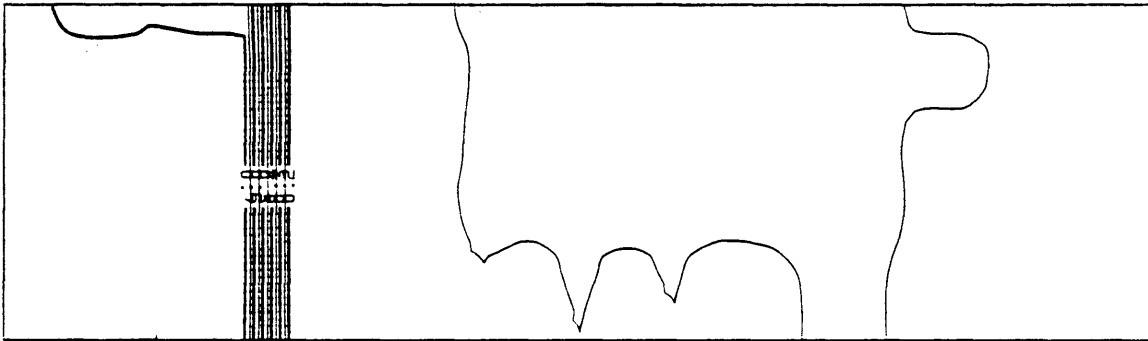
Time = 0.0 hr

Cum. Oil Produced = 0.000 PV



Time = 2.35 hrs

Cum. Oil Produced = 0.129 PV



Time = 5.35 hrs

Cum. Oil Produced = 0.296 PV



Figure 6.7. Saturation Contours of Run Number 4. Water Flood.
Low Permeability sand.

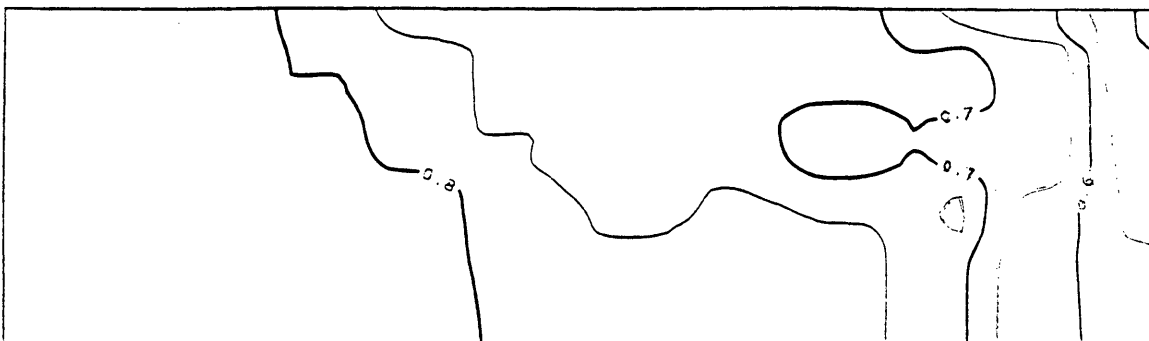
Time = 8.35 hrs

Cum. Oil Produced = 0.465 PV



Time = 10.35 hrs

Cum. Oil Produced = 0.579 PV



Time = 11.35 hrs

Cum. Oil Produced = 0.628 PV

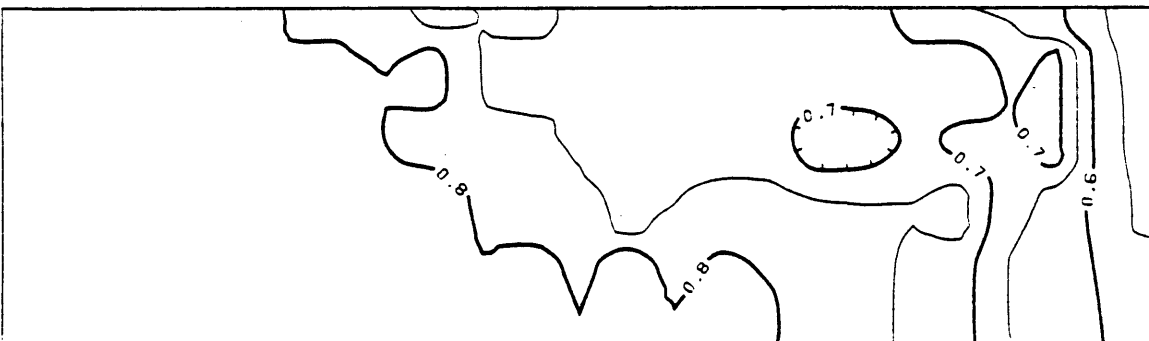
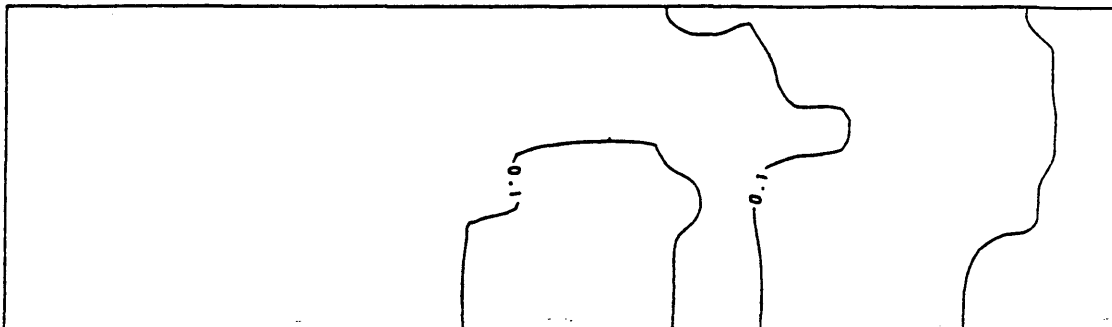


Figure 6.7. (Continued).

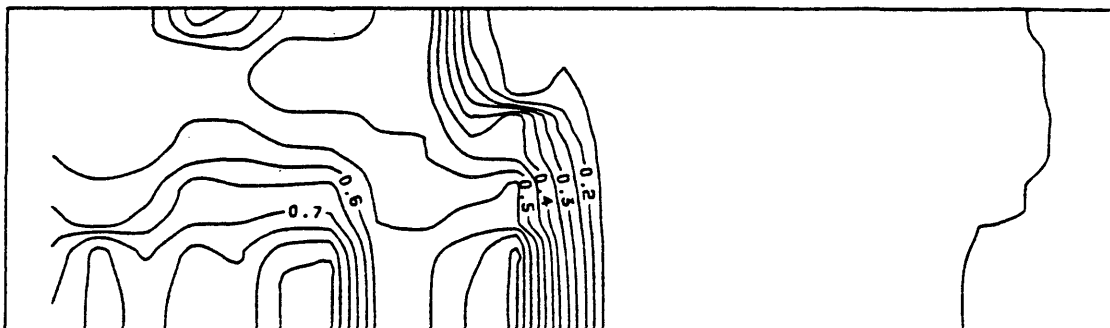
Time = 0.0 hr

Cum. Oil Produced = 0.000 PV



Time = 7.0 hrs

Cum. Oil Produced = 0.233 PV



Time = 11.0 hrs

Cum. Oil Produced = 0.313 PV

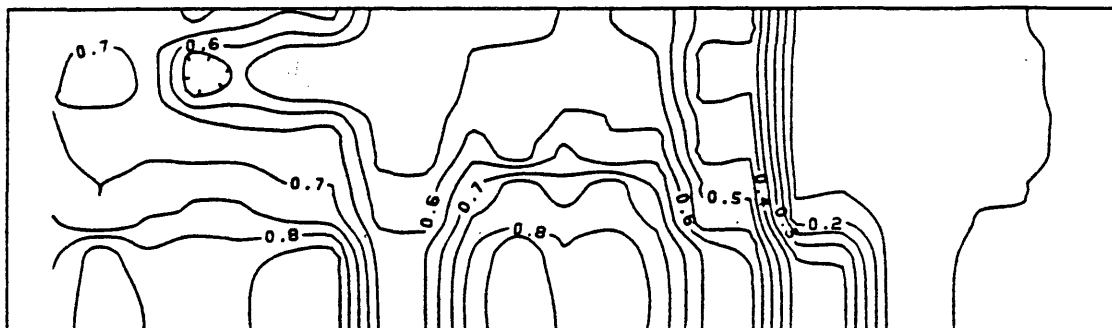
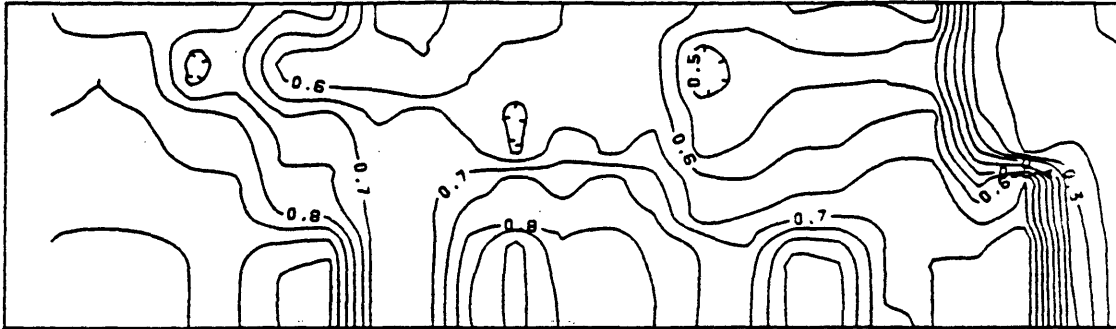


Figure 6.8. Saturation Contours of Run Number 5. Water Flood.
Low Permeability Sand.

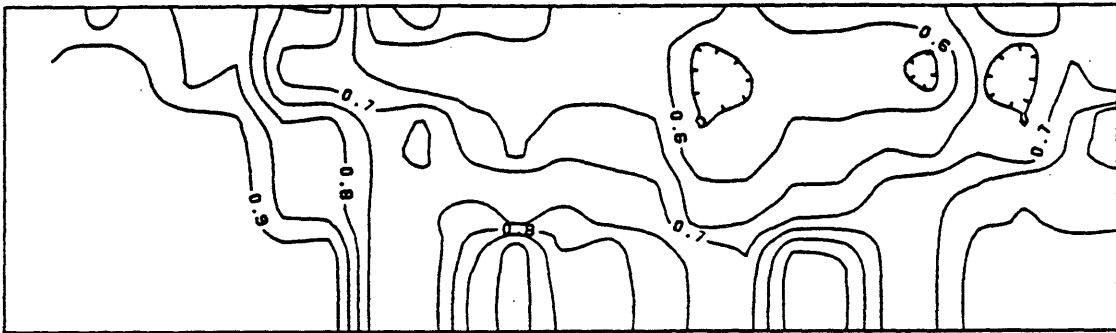
Time = 15.0 hrs

Cum. Oil Produced = 0.526 PV



Time = 18.34 hrs

Cum. Oil Produced = 0.626 PV



Time = 28.0 hrs

Cum. Oil Produced = 0.683 PV

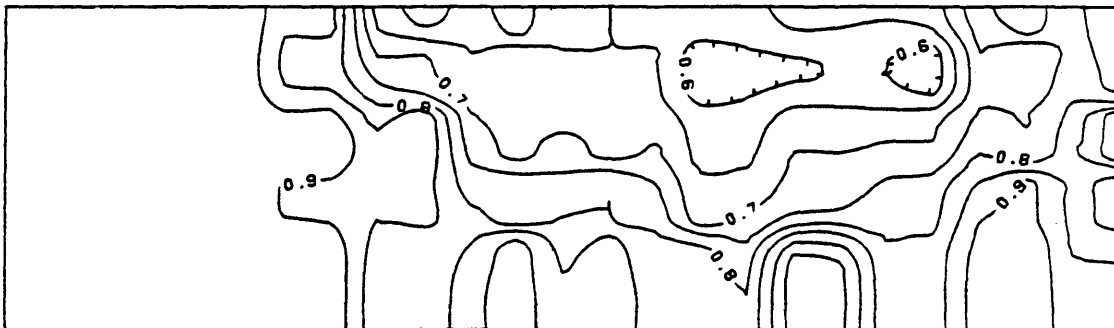


Figure 6.8. (Continued).

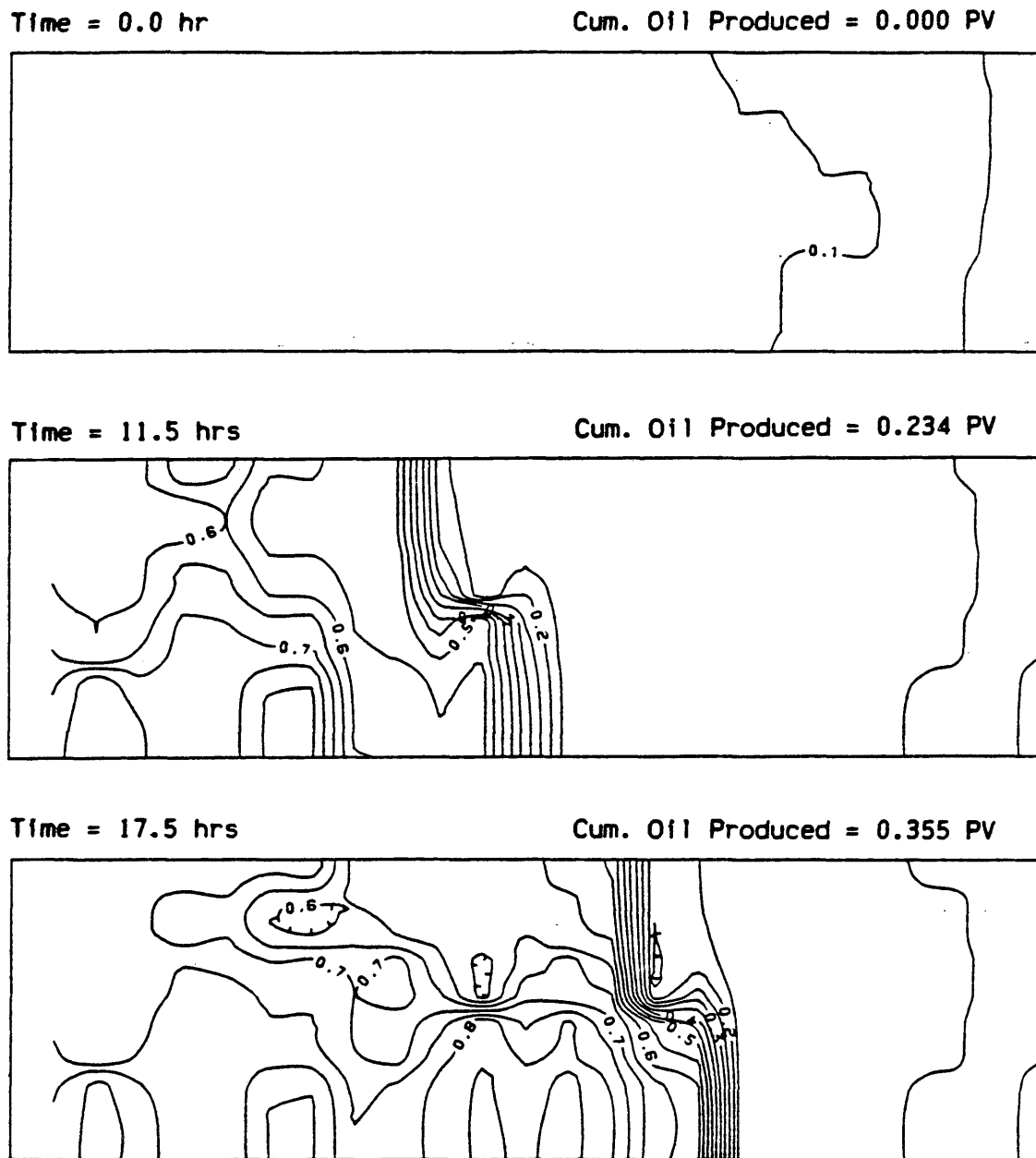
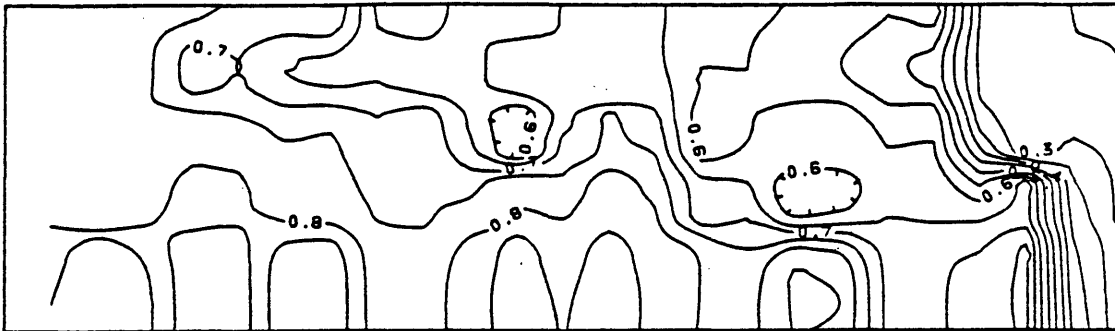


Figure 6.9. Saturation Contours of Run Number 6. Water Flood.
Low Permeability Sand.

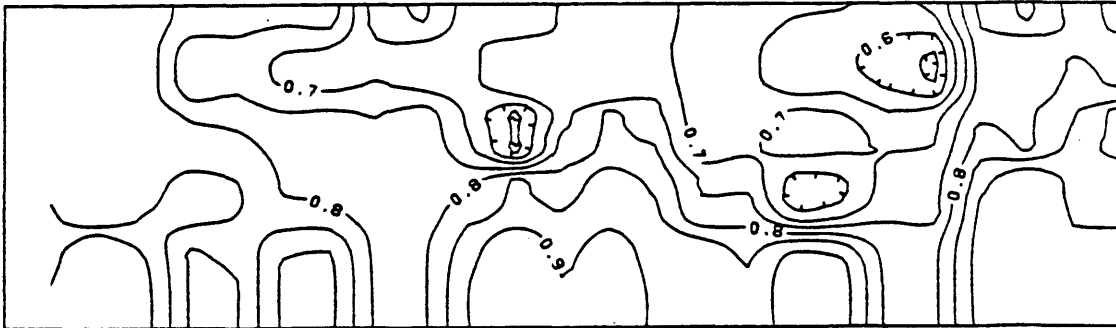
Time = 27.5 hrs

Cum. Oil Produced = 0.557 PV



Time = 33.5 hrs

Cum. Oil Produced = 0.667 PV



Time = 45.0 hrs

Cum. Oil Produced = 0.697 PV

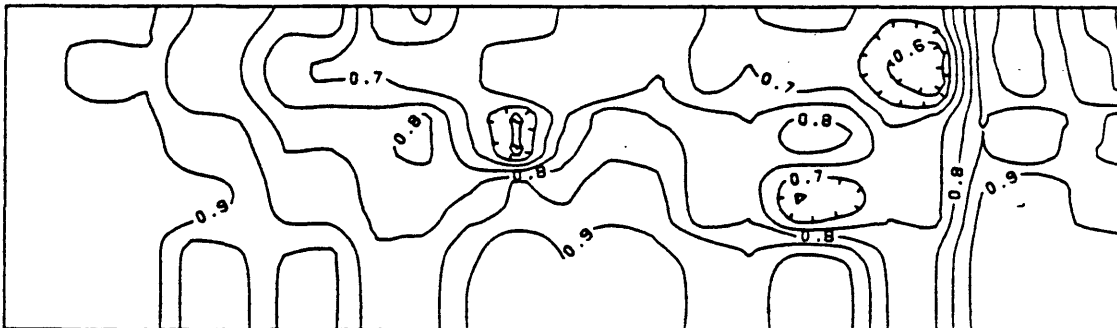


Figure 6.9. (Continued).

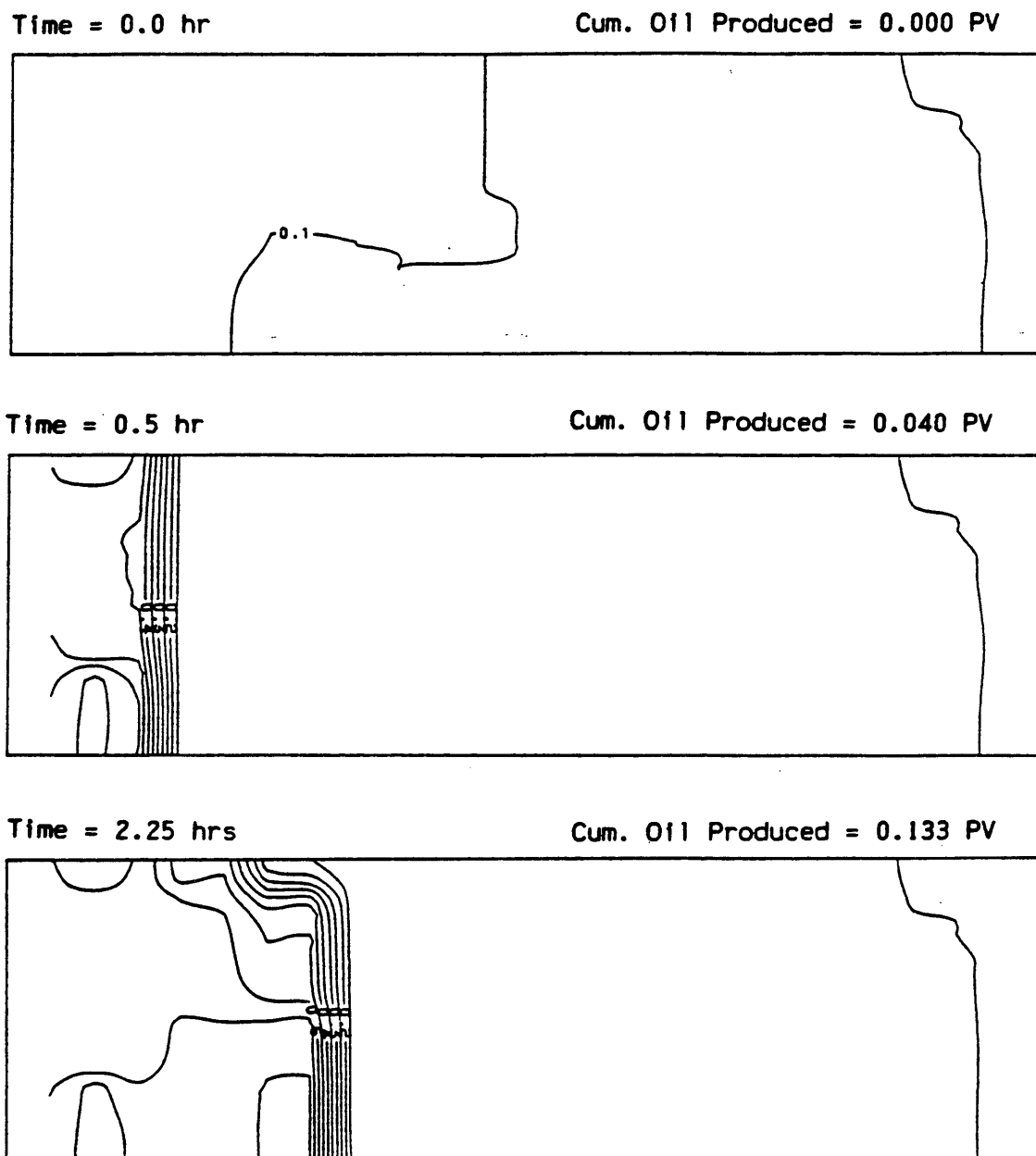
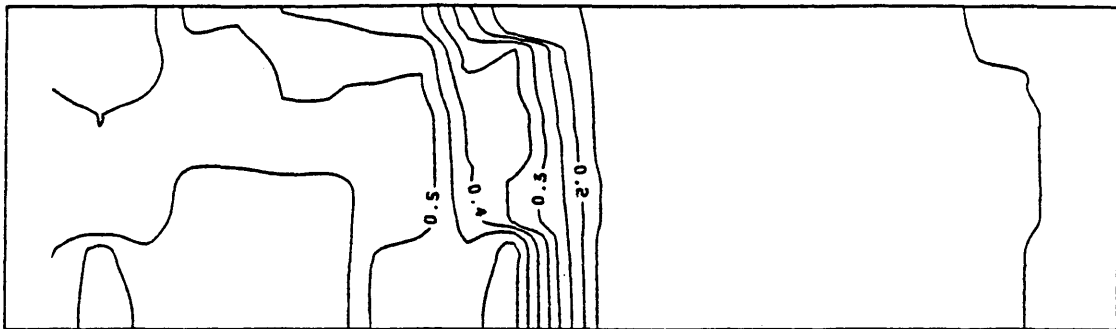


Figure 6.10. Saturation Contours of Run Number 7. Water Flood.
Low Permeability Sand.

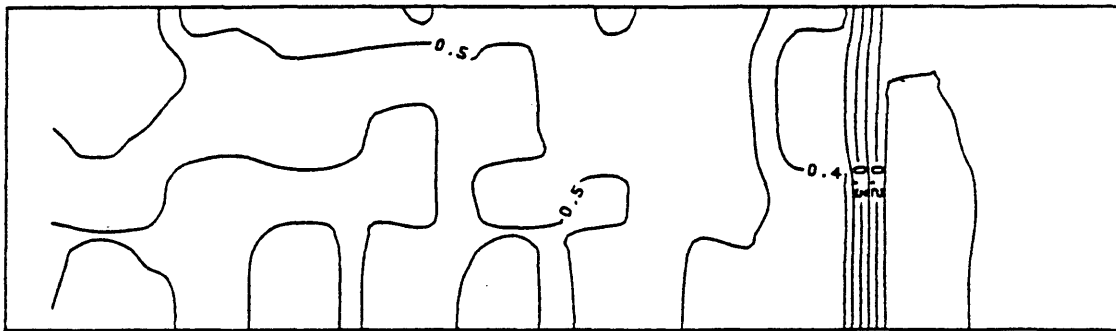
Time = 8.25 hrs

Cum. Oil Produced = 0.187 PV



Time = 19.25 hrs

Cum. Oil Produced = 0.295 PV



Time = 30.25 hrs

Cum. Oil Produced = 0.413 PV

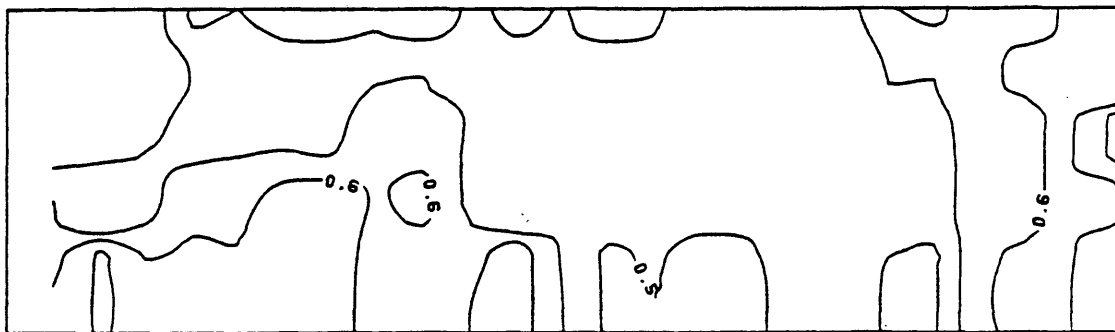


Figure 6.10. (Continued).

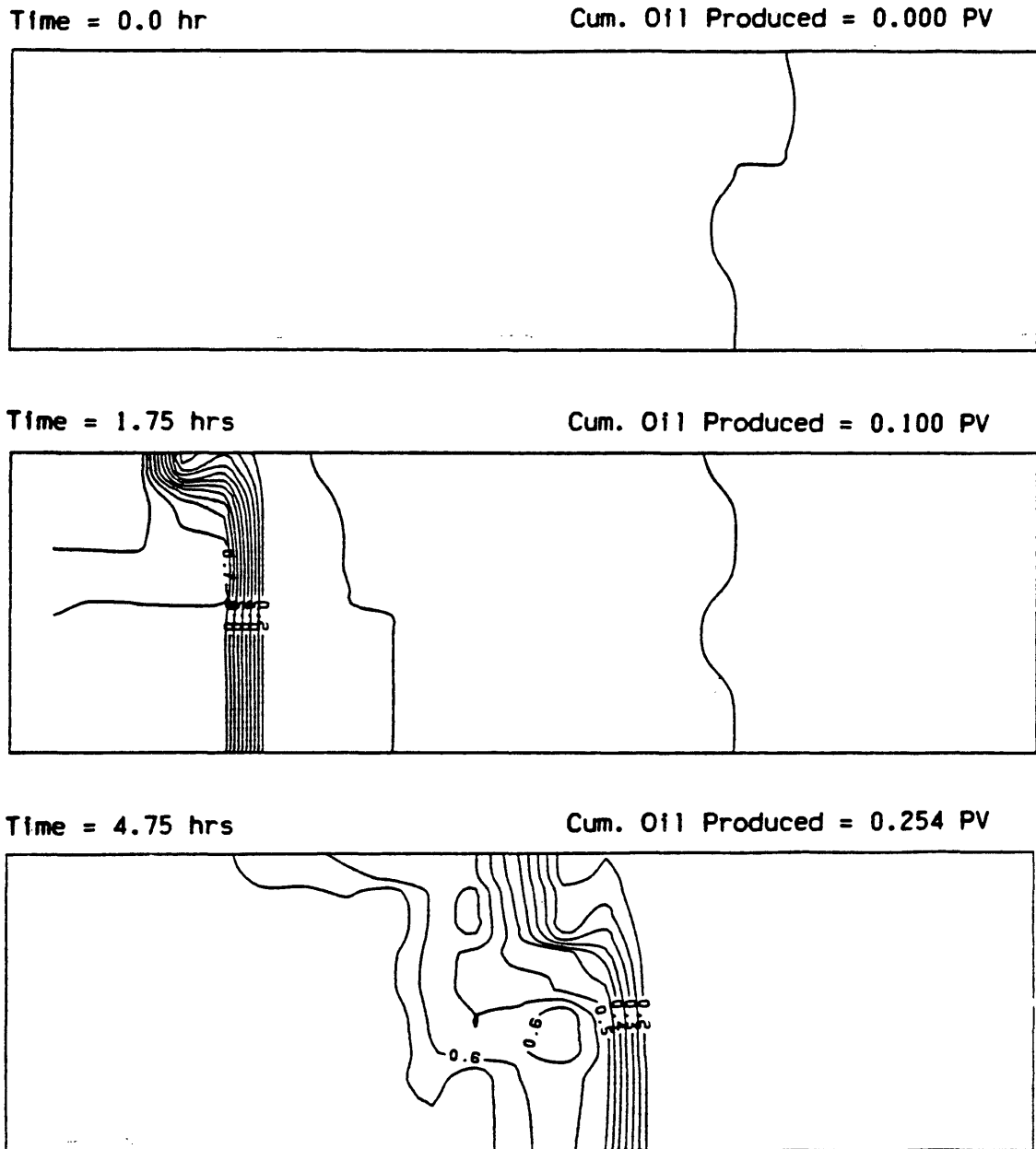


Figure 6.11. Saturation Contours of Run Number 8. Water Flood.
Low Permeability Sand.

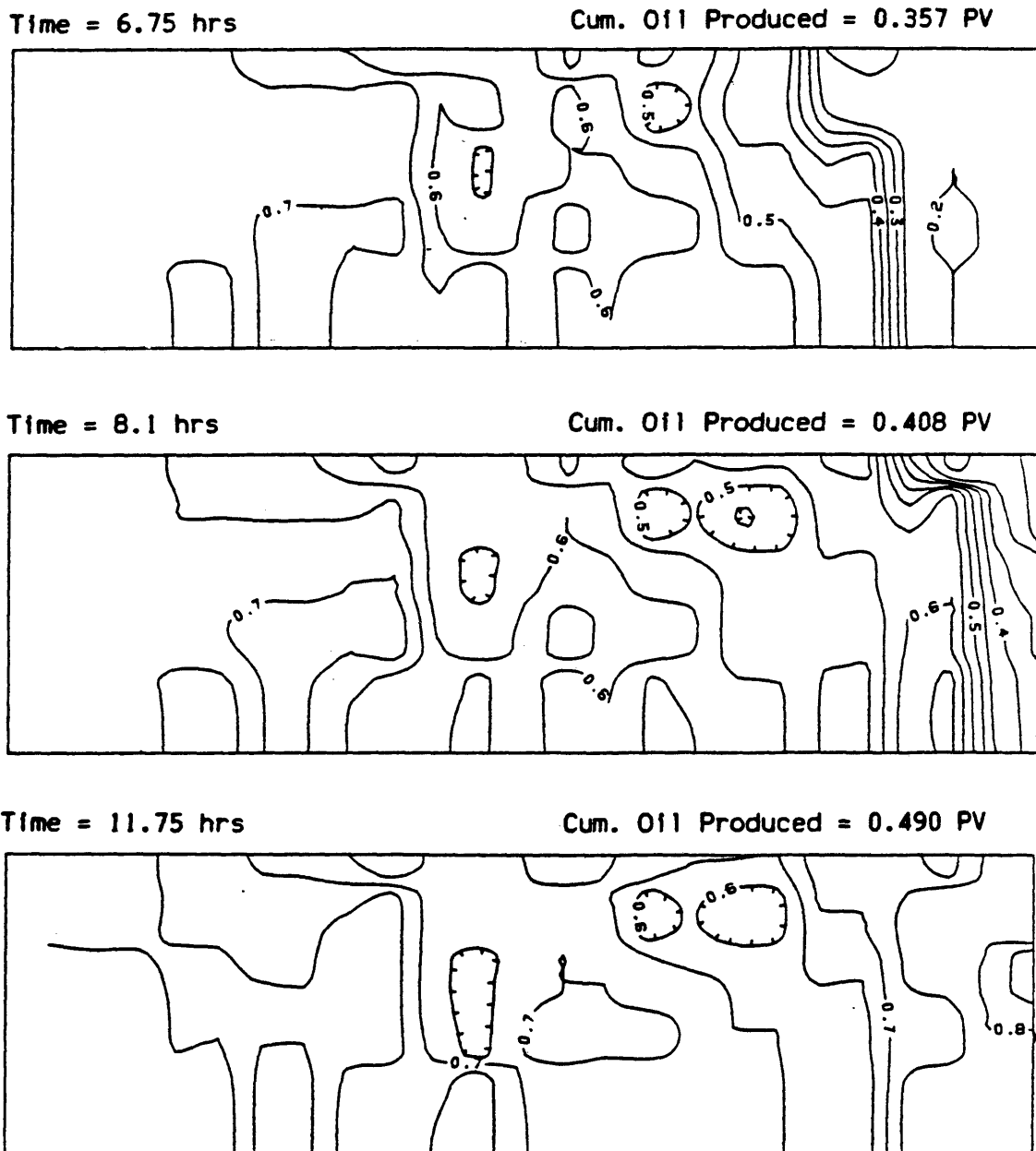


Figure 6.11. (Continued).

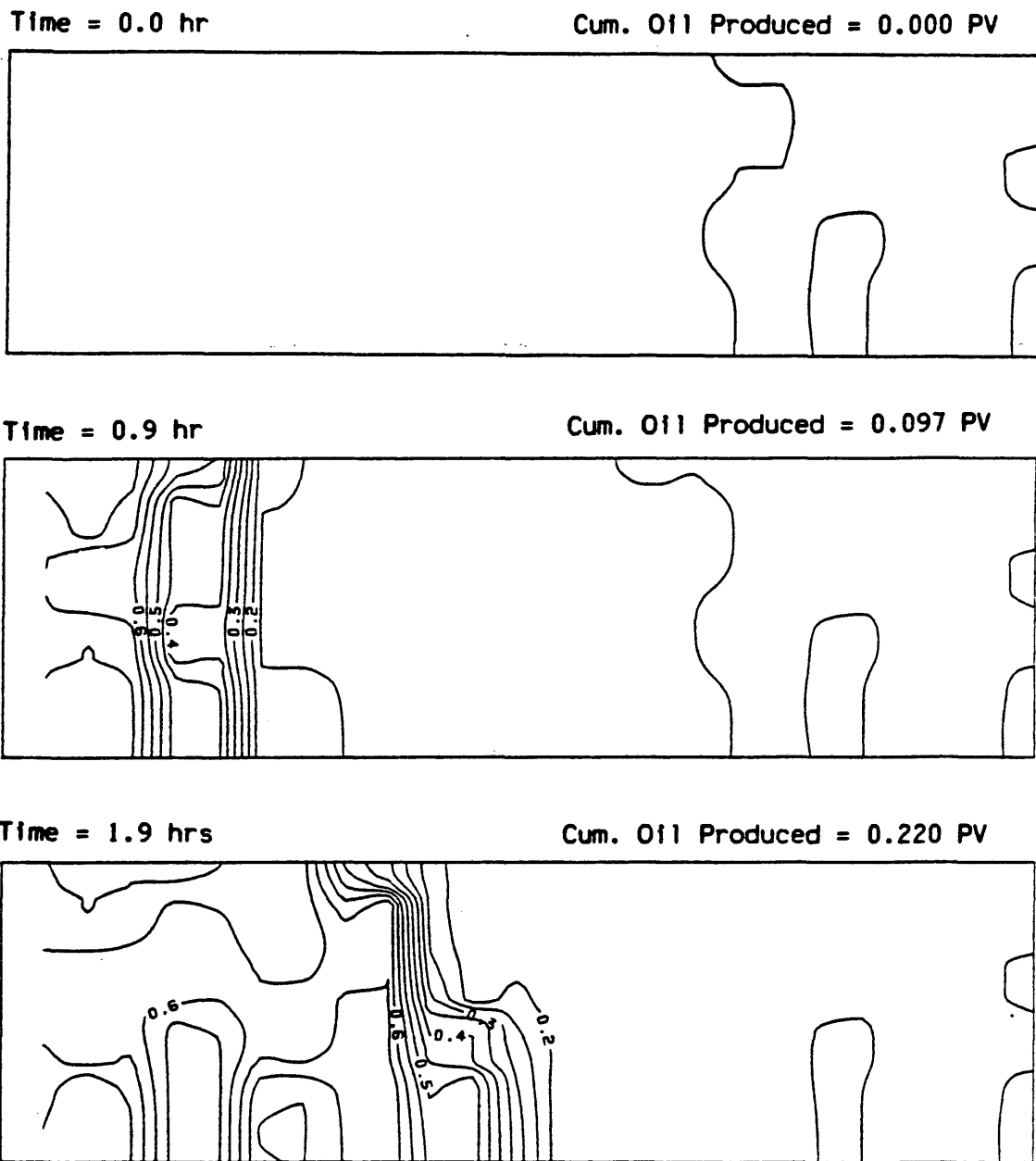
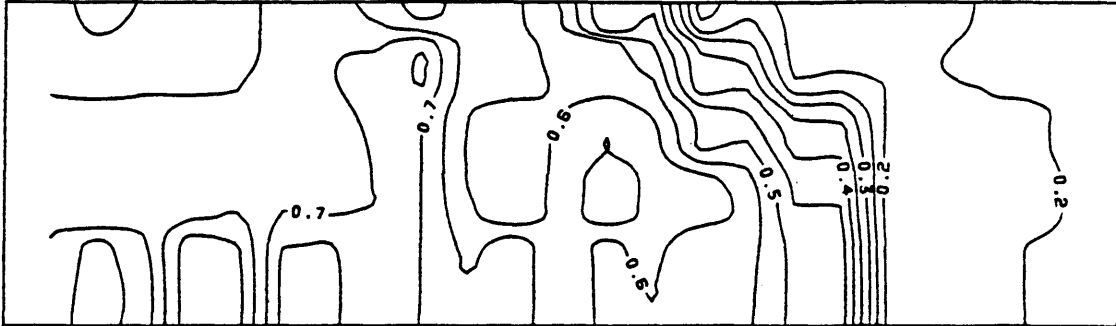


Figure 6.12. Saturation Contours of Run Number 9. Water Flood.
Low Permeability Sand.

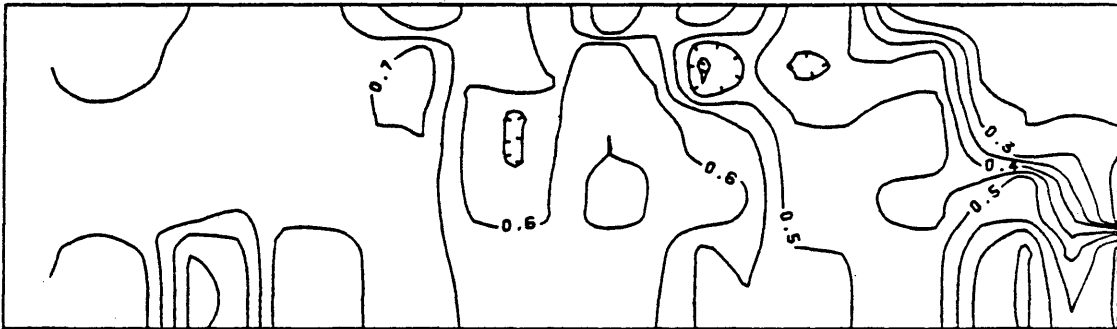
Time = 2.9 hrs

Cum. Oil Produced = 0.341 PV



Time = 3.57 hrs

Cum. Oil Produced = 0.422 PV



Time = 7.15 hrs

Cum. Oil Produced = 0.571 PV

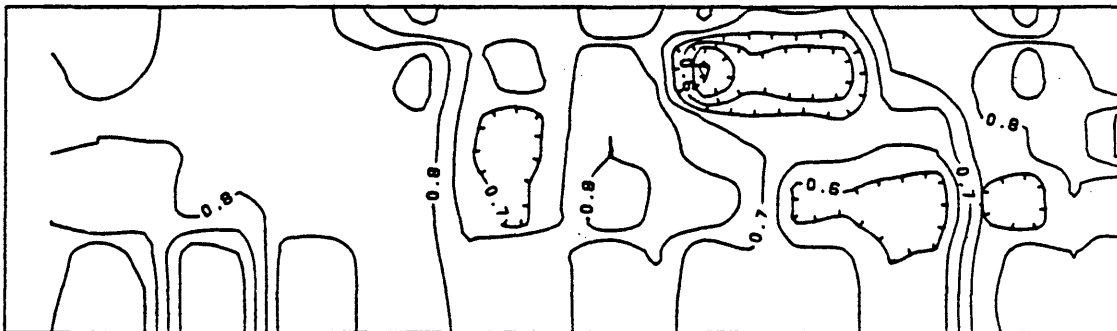


Figure 6.12. (Continued).

interface.

On a microscopic scale, the drop in the breakthrough recovery could be explained if the porous medium is approximated by a bundle of tubes. At low injection rates, the displacing phase preferentially displaces the more viscous oil phase from the larger diameter tubes, i.e., tubes with lower resistance to flow, leaving behind the oil in small diameter tubes.

In run 10, the water gravity and viscosity were increased above those used in runs 7, 8 and 9. Figure 6.13 shows a short gravity tongue denoting a slight instability in the displacement. The appearance of this tongue could be attributed to the increase in the gravity forces compared to the capillary forces. However, oil recovery at breakthrough slightly increased over that of runs 7, 8 and 9 because of the reduction in the viscosity ratio by a factor of two.

6.2.2. Medium Permeability Sand Packs

Runs 11 to 14 were conducted in medium permeability sand packs using 20-40 mesh Ottawa sand. In Figures 6.14, 6.15 and 6.17 the water saturation contours of these runs are shown. In these figures clear gravity tongues underrun the oil phase causing instability of these displacements. In runs 11, 12 and 13, kerosene was used as the oil phase. The oil recovery at breakthrough of runs 11 to 13 showed no sensitivity to the rate of injection, as is presented in Table 6.2. However, breakthrough recovery dropped below that obtained from runs 4 to 6 conducted in low permeability sand packs using the same viscosity ratios. In run 14, mineral oil was used as the oil phase (viscosity

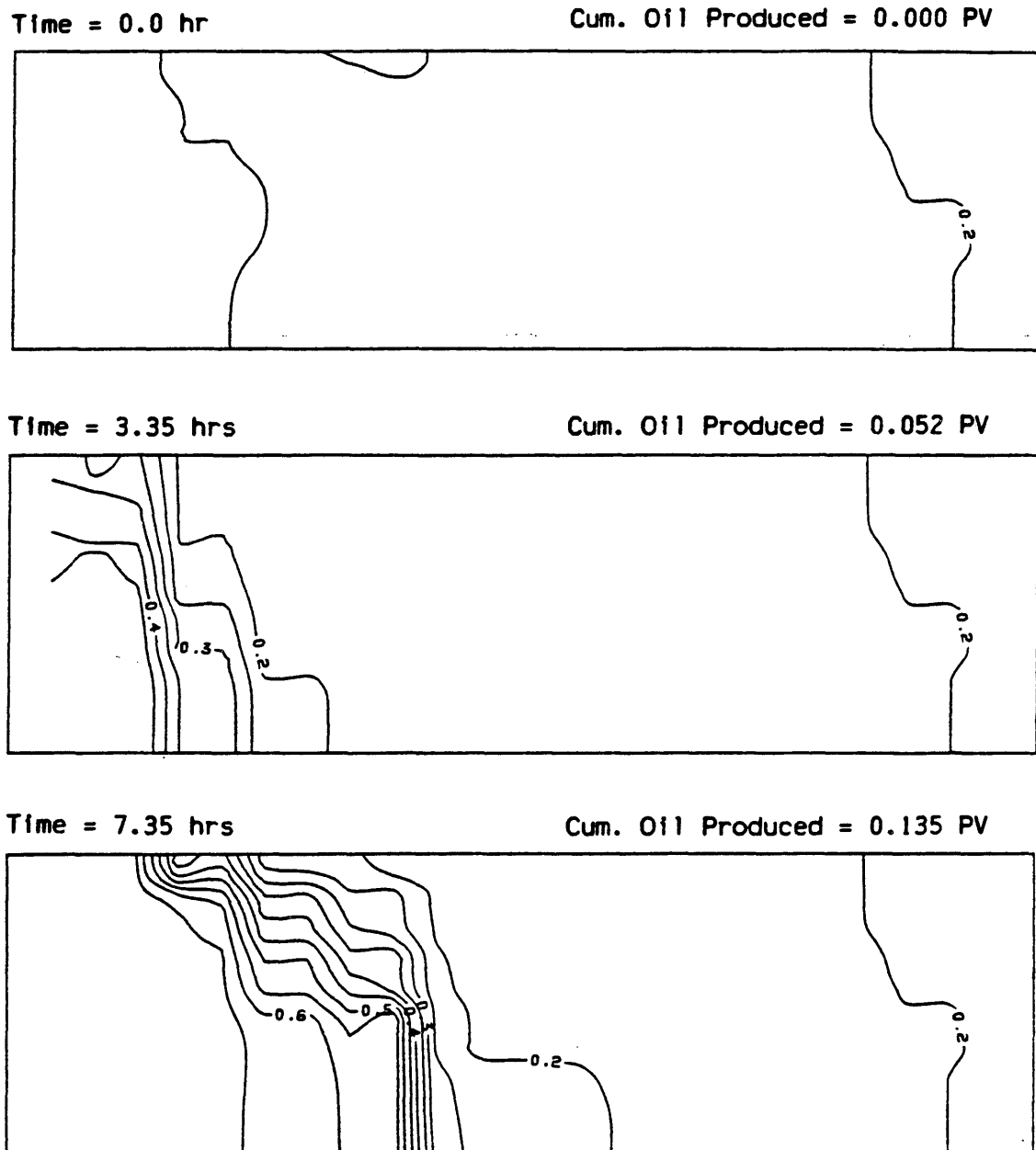
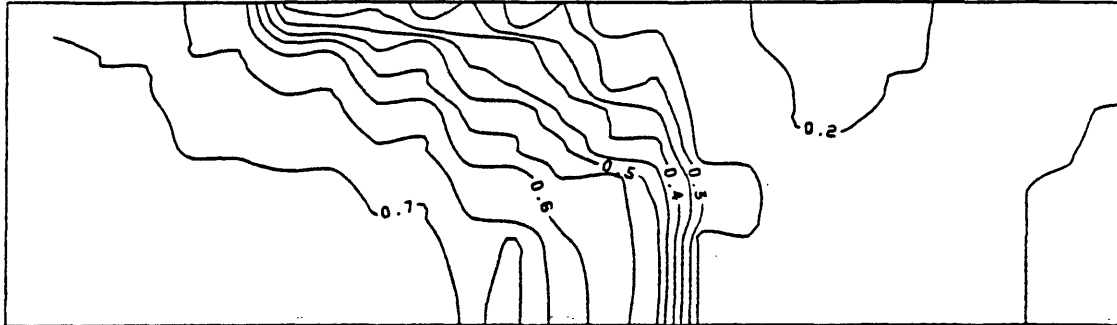


Figure 6.13. Saturation Contours of Run Number 10. Water Flood.
Low Permeability Sand.

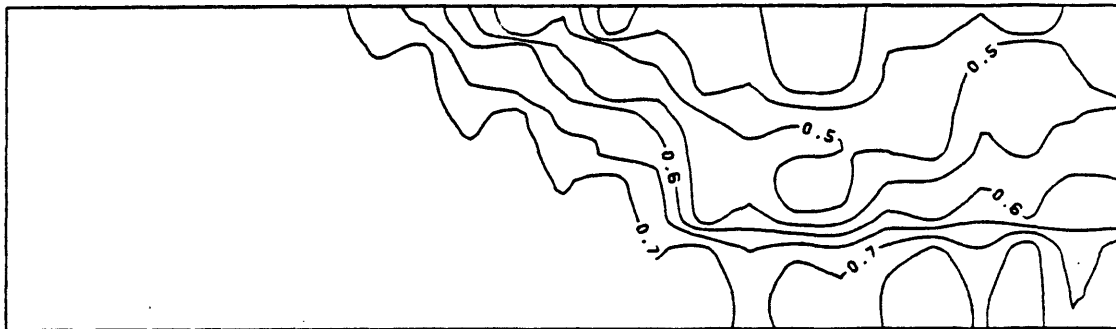
Time = 13.35 hrs

Cum. Oil Produced = 0.222 PV



Time = 24.85 hrs

Cum. Oil Produced = 0.419 PV



Time = 25.35 hrs

Cum. Oil Produced = 0.436 PV

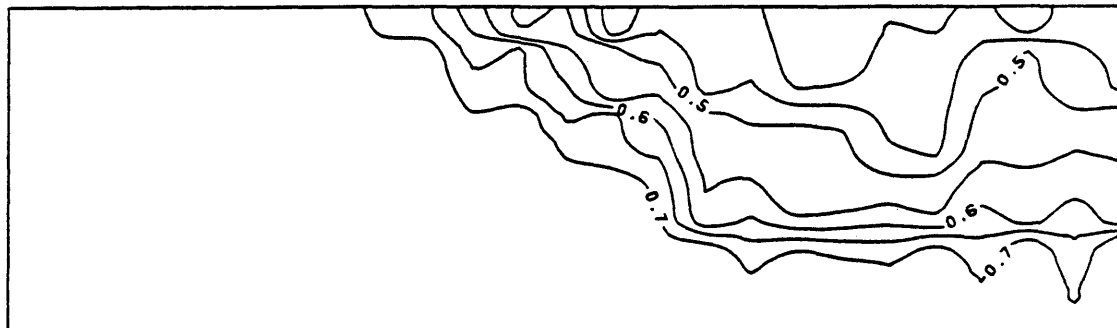


Figure 6.13. (Continued).

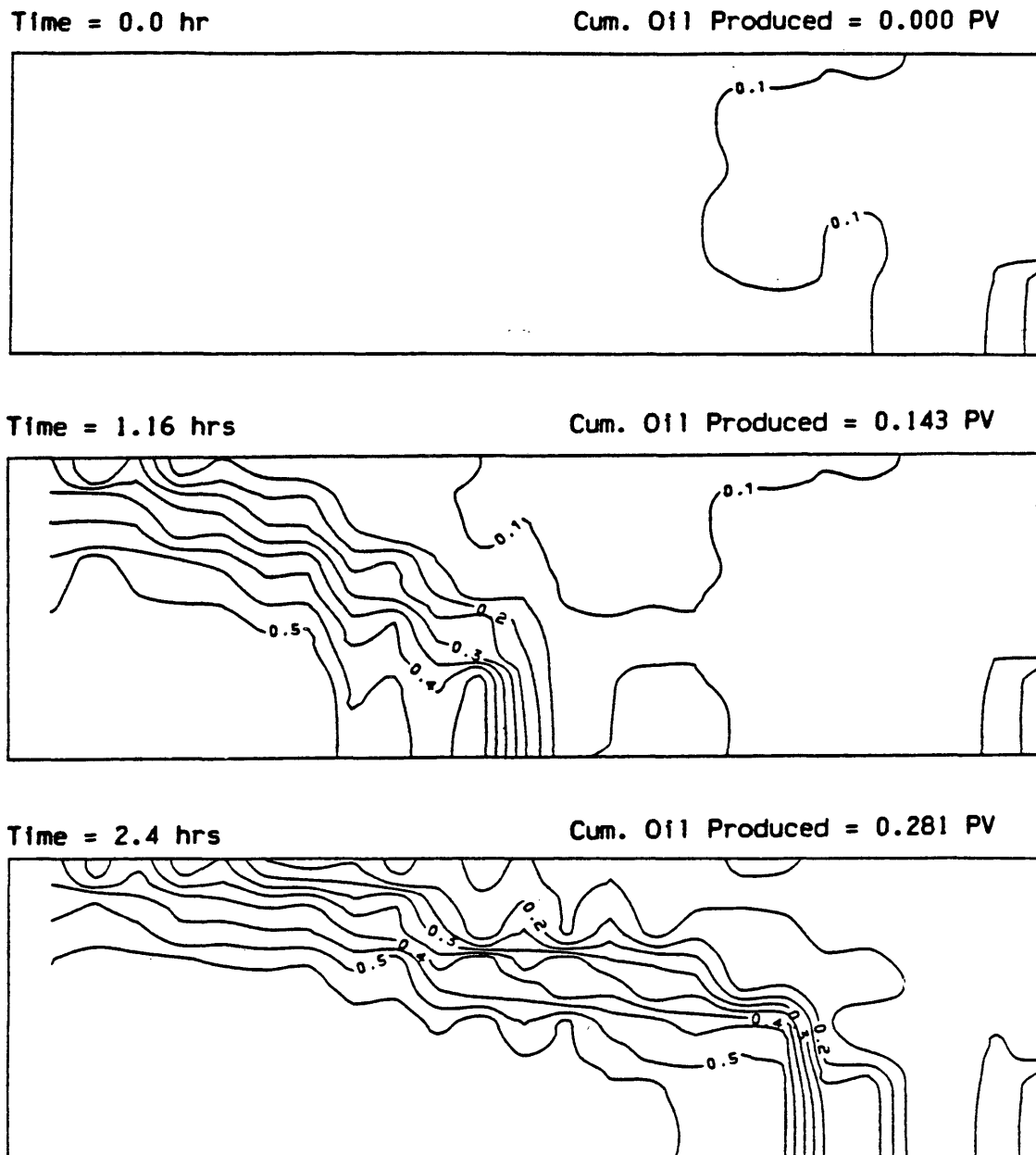
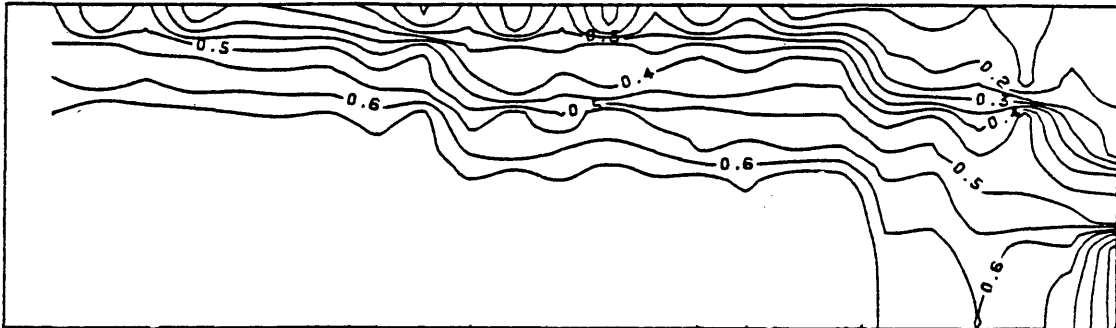


Figure 6.14. Saturation Contours of Run Number 11. Water Flood.
Medium Permeability Sand.

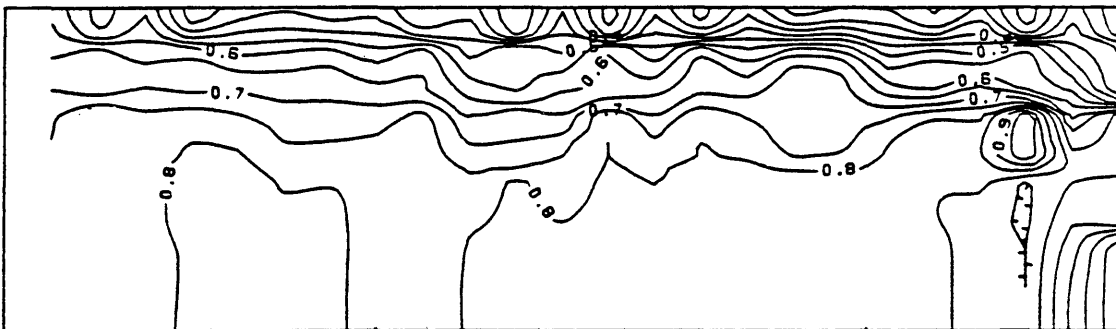
Time = 3.66 hrs

Cum. Oil Produced = 0.417 PV



Time = 5.0 hrs

Cum. Oil Produced = 0.559 PV



Time = 11.15 hrs

Cum. Oil Produced = 0.675 PV



Figure 6.14. (Continued).

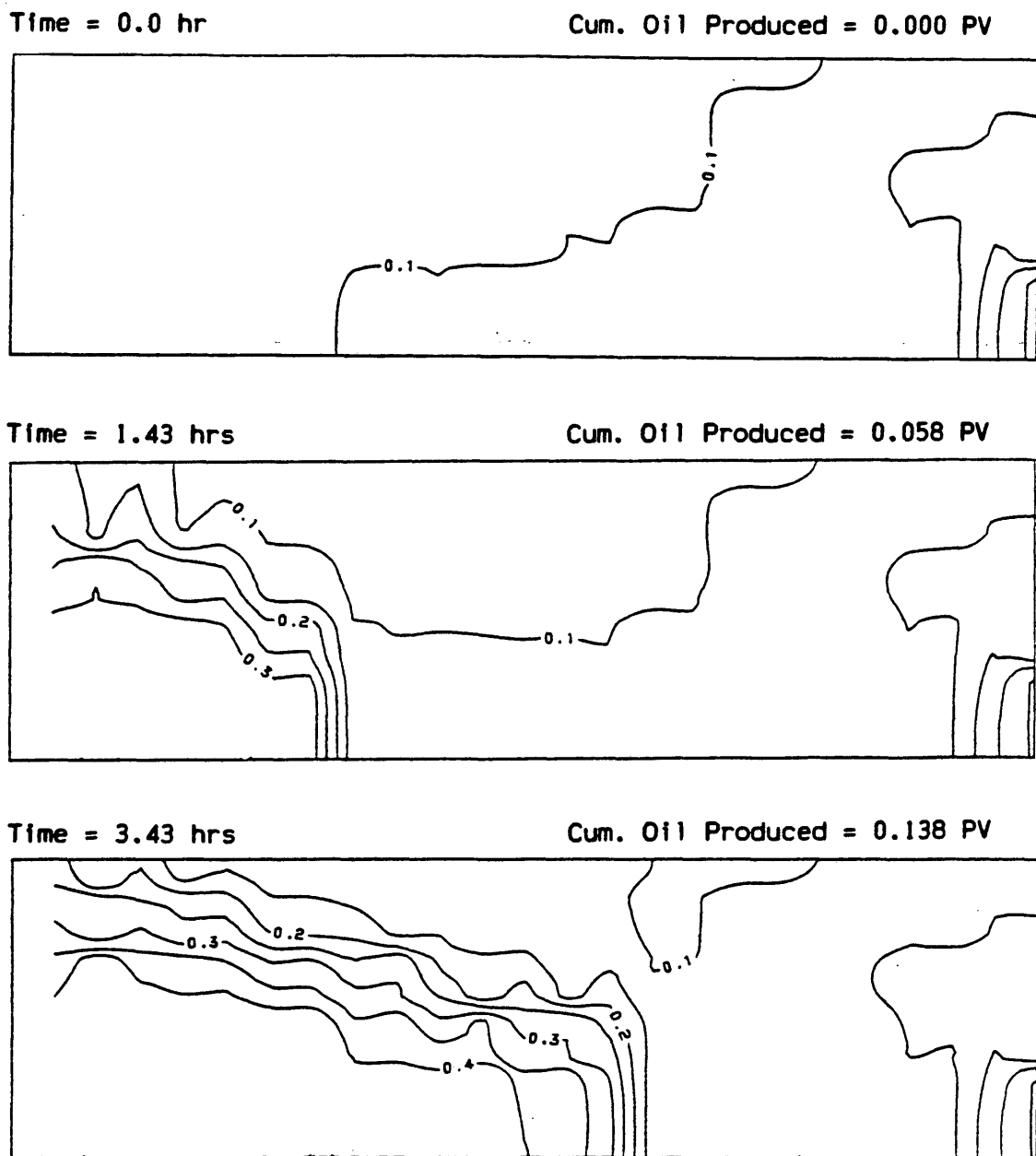
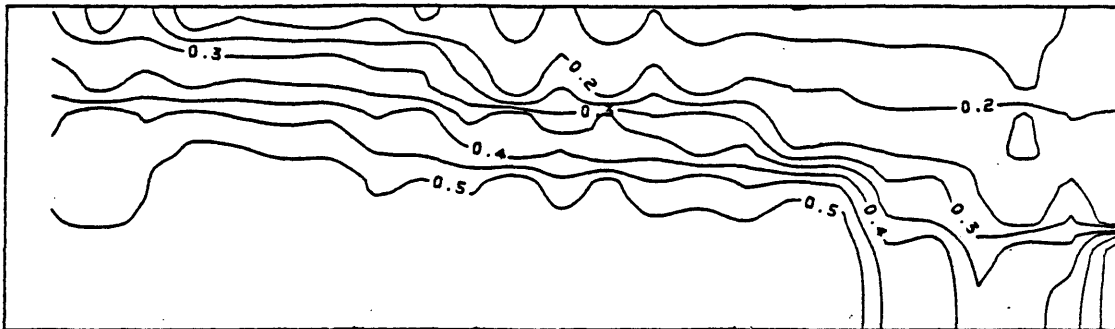


Figure 6.15. Saturation Contours of Run Number 12. Water Flood.
Medium Permeability Sand.

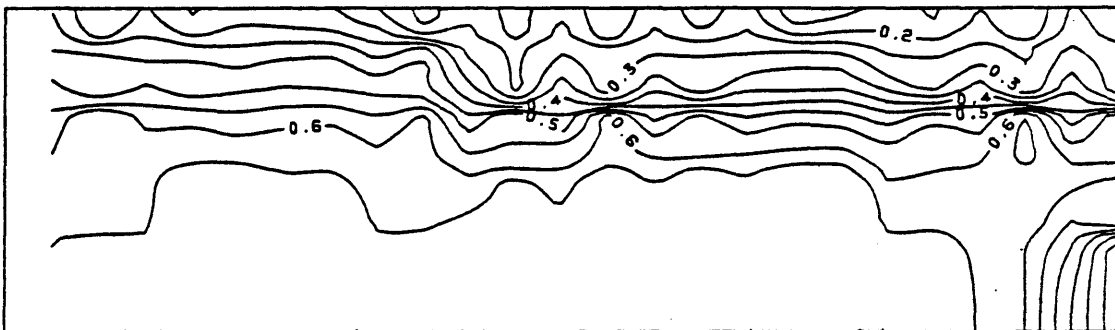
Time = 6.43 hrs

Cum. Oil Produced = 0.257 PV



Time = 10.85 hrs

Cum. Oil Produced = 0.427 PV



Time = 14.0 hrs

Cum. Oil produced = 0.554 PV

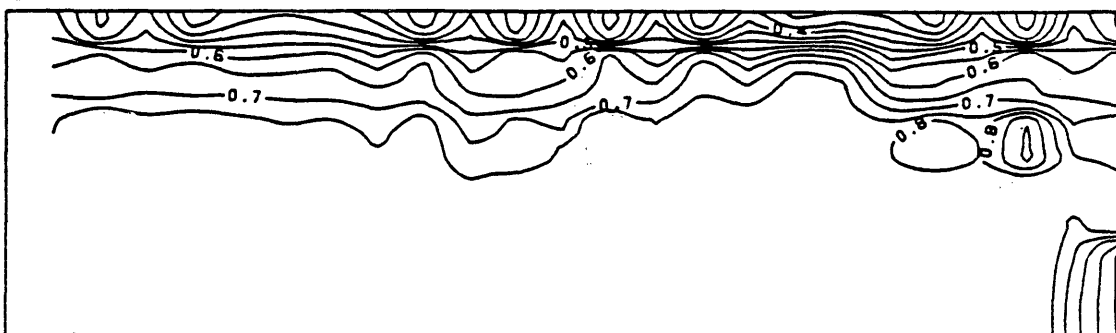
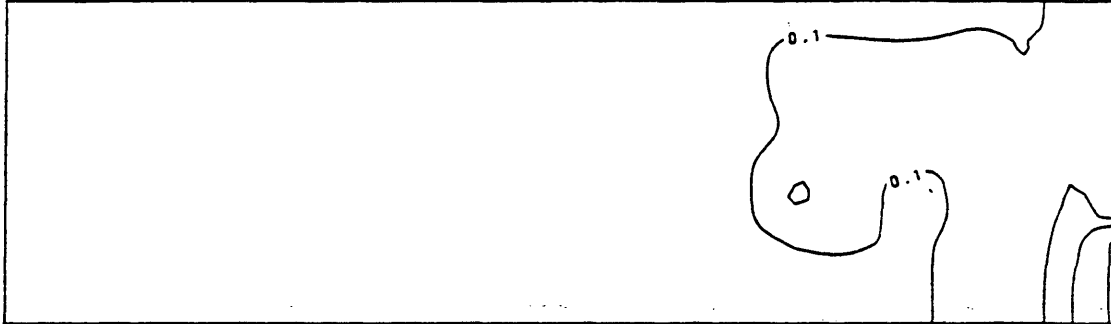


Figure 6.15. (Continued).

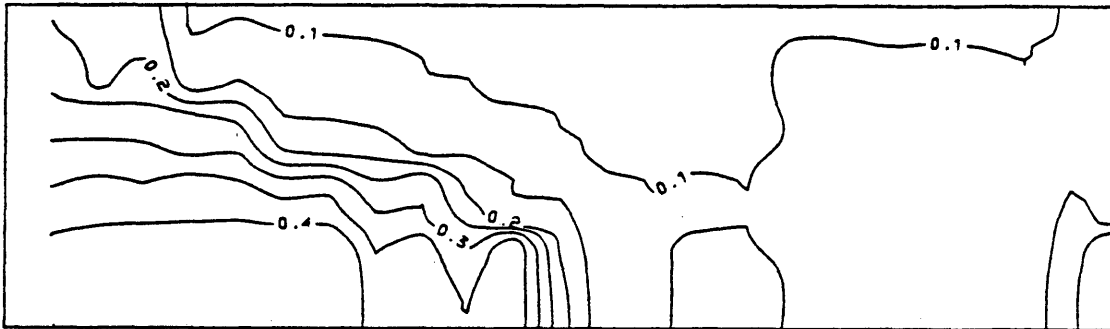
Time = 0.0 hr

Cum. Oil Produced = 0.000 PV



Time = 5.75 hrs

Cum. Oil Produced = 0.089 PV



Time = 11.58 hrs

Cum. Oil Produced = 0.170 PV

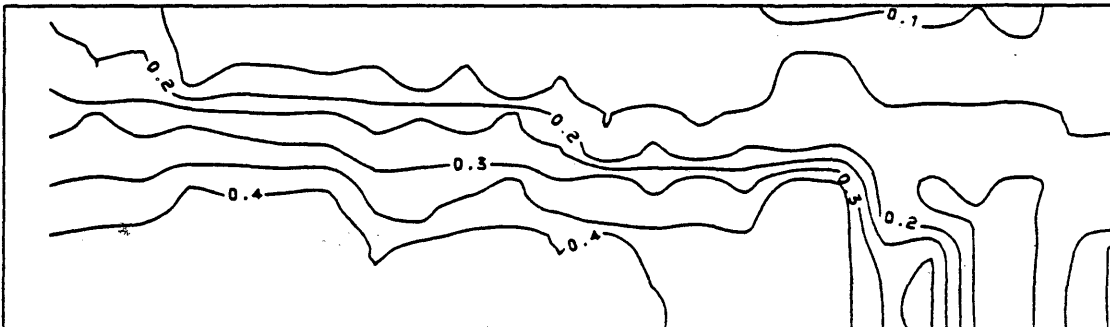
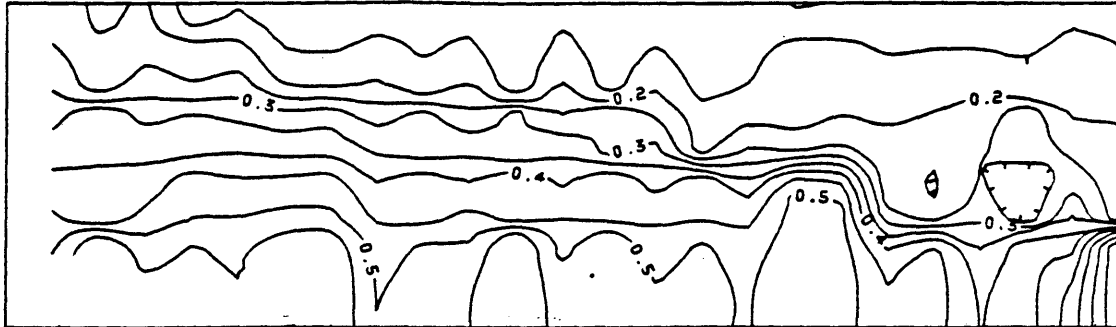


Figure 6.16. Saturation Contours of Run Number 13. Water Flood.
Medium Permeability Sand.

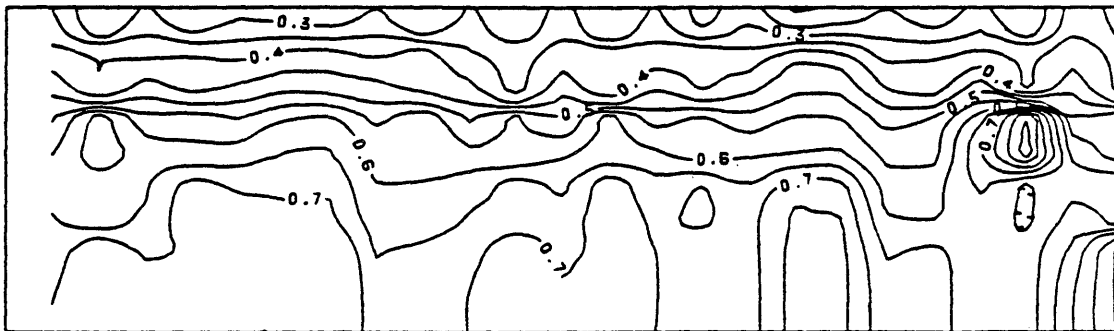
Time = 16.75 hrs

Cum. Oil Produced = 0.237 PV



Time = 25.85 hrs

Cum. Oil Produced = 0.418 PV



Time = 35.25 hrs

Cum. Oil Produced = 0.565 PV

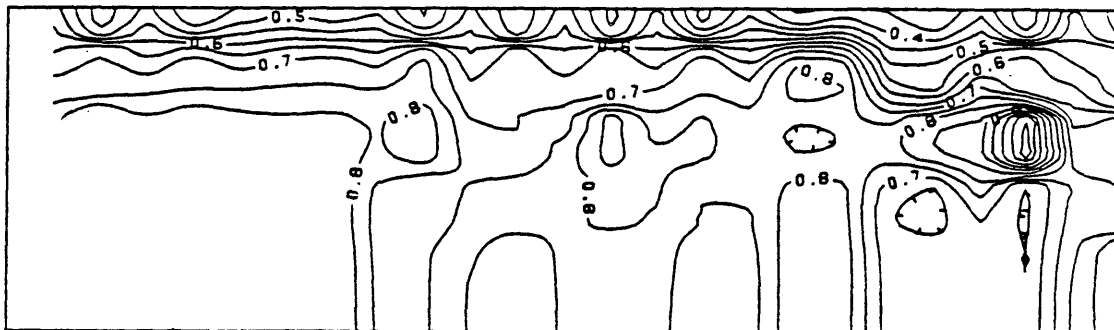


Figure 6.16. (Continued).

TABLE 6.2. Summary of Experimental Data. Medium and High Permeability Sands.

Run Number	k darcy	$k_w(S_{or})$ darcy	$k_o(S_{wf})$ darcy	ϕ %	$\Delta\rho_g$ gm/cc	Q cc/min	ν_o / ν_w dlm.	G x 10 ² dlm.	$F_s \times 10^5$ cm	Breakthrough Recovery, PV.
11	67.83	24.20	52.23	34.77	0.209	42.40	1.466	1.38	0.613	0.559
12	67.83	2.15	38.00	34.77	0.209	14.76	1.481	0.47	0.606	0.554
13	67.83	0.69	33.87	34.77	0.209	6.04	1.481	0.20	0.606	0.565
14	67.83	5.81	35.15	34.77	0.183	15.36	19.222	0.56	0.053	0.367
15	106.00	4.10	37.30	34.93	0.209	17.28	1.460	0.38	0.494	0.547
16	106.00	13.04	37.34	34.93	0.209	60.78	1.505	1.24	0.478	0.494
17	106.00	3.42	82.50	34.93	0.189	12.97	11.702	0.30	0.069	0.390
18	106.00	4.99	103.73	34.93	0.189	59.48	12.118	1.46	0.066	0.317

ratio 19.22). Instability manifested itself also as a gravity tongue underrunning the oil phase, as Figure 6.17 indicates.

It is obvious that increasing the sand pack permeability has altered the stability condition of the displacement. Gravity tongues developed in all runs at all rates of injection and viscosity ratios used. This is because the reduction in the capillary forces caused by the increase in the sand permeability gives more role to the gravity forces to induce tonguing.

6.2.3. High Permeability Sand Packs

In runs 15, 16, 17 and 18, 10-20 mesh Ottawa sand having an absolute permeability of 106 darcies was used. The gravity effect on these runs was more profound because of the large reduction in the capillary forces. In runs 15 and 16 kerosene was used as the oil phase. Breakthrough recovery dropped below that of medium permeability sand packs. Breakthrough recovery dropped as the rate of injection increased. This is also reported in runs 17 and 18 where mineral oil represented the oil phase. Figures 6.18 through 6.21 show gravity tongues penetrating the oil zone, causing a reduction in the breakthrough oil recovery.

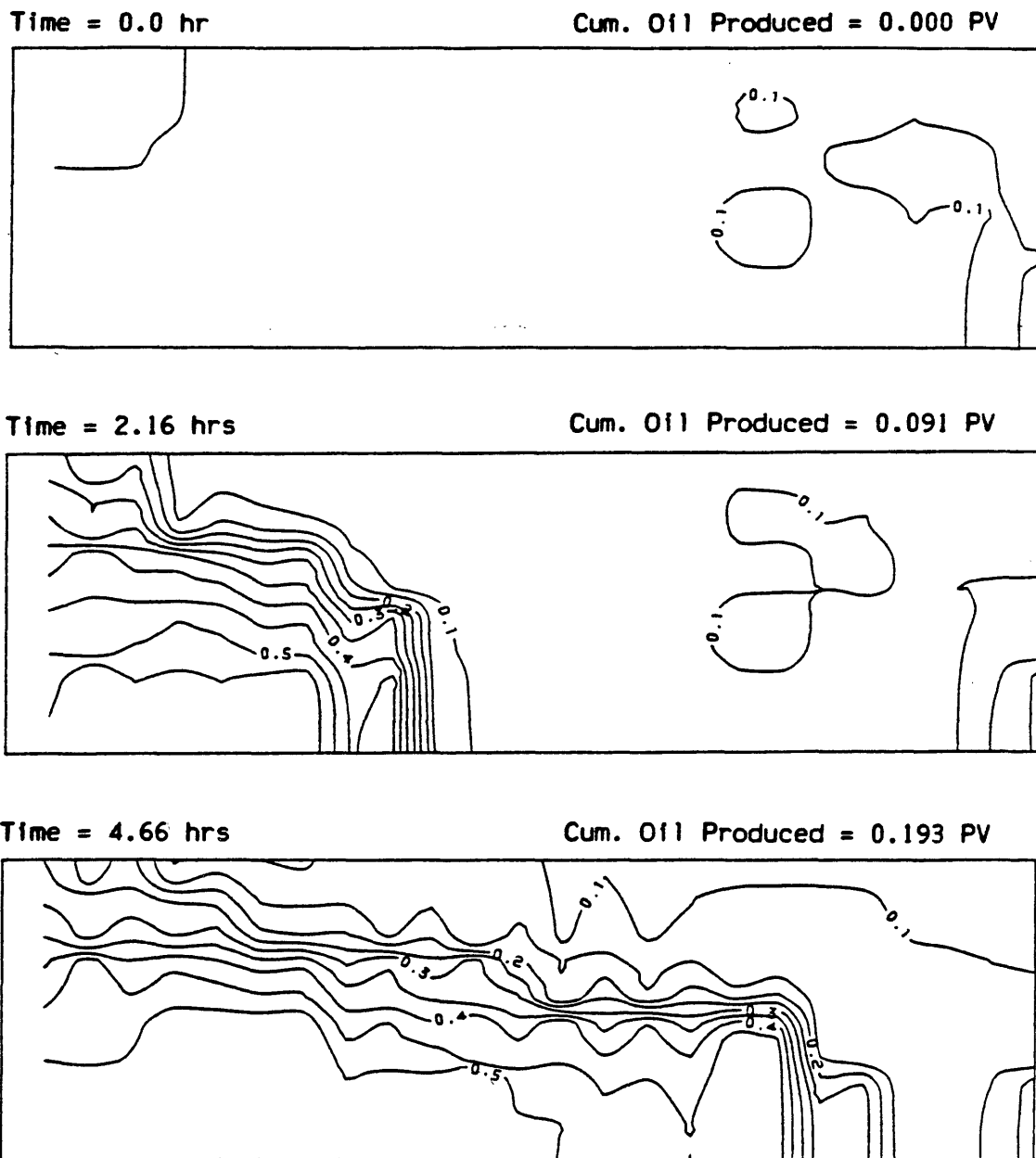
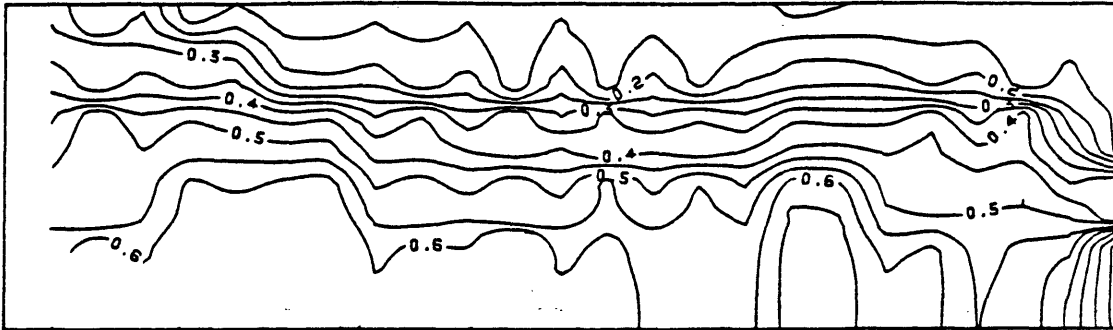


Figure 6.17. Saturation Contours of Run Number 14. Water Flood.
Medium Permeability Sand.

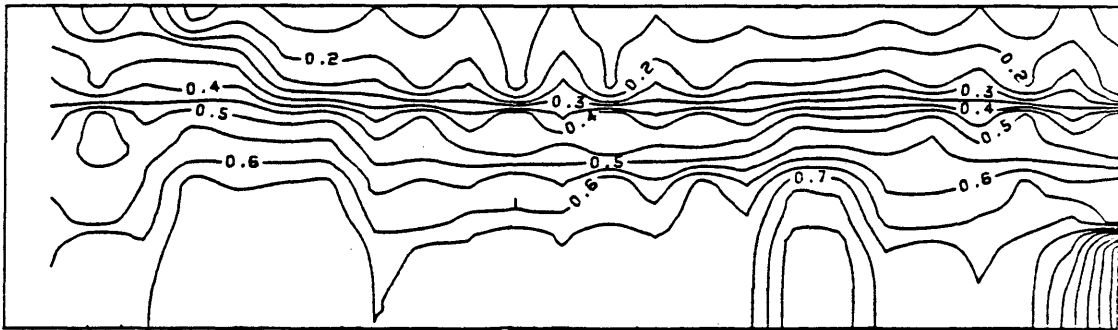
Time = 7.16 hrs

Cum. Oil Produced = 0.291 PV



Time = 9.15 hrs

Cum. Oil Produced = 0.367 PV



Time = 26.15 hrs

Cum. Oil Produced = 0.578 PV

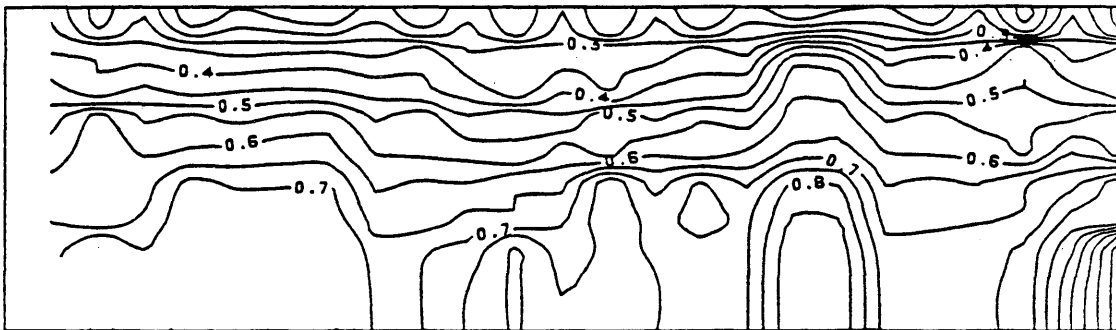


Figure 6.17. (Continued).

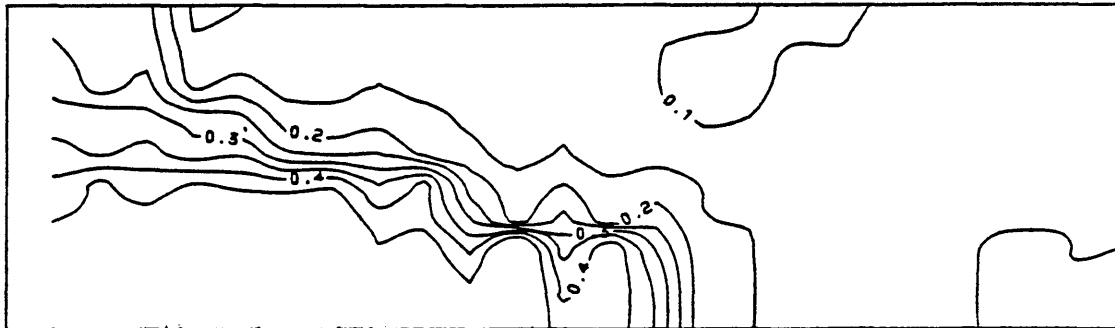
Time = 0.0 hr

Cum. Oil Produced = 0.000 PV



Time = 2.5 hrs

Cum. Oil Produced = 0.138 PV



Time = 4.5 hrs

Cum. Oil Produced = 0.237 PV

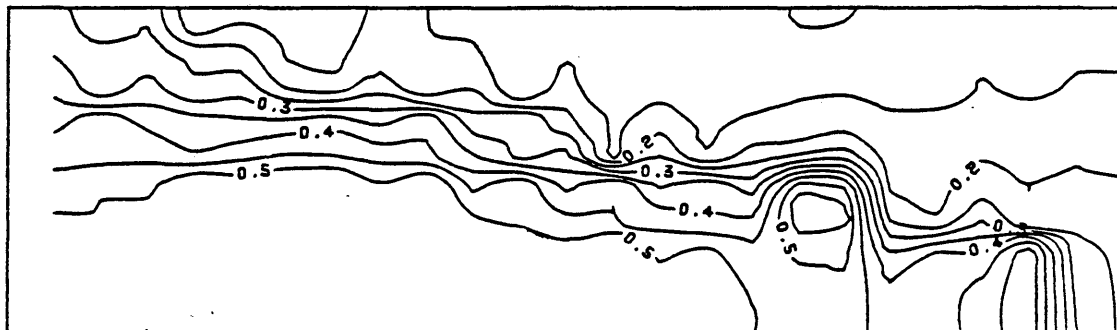
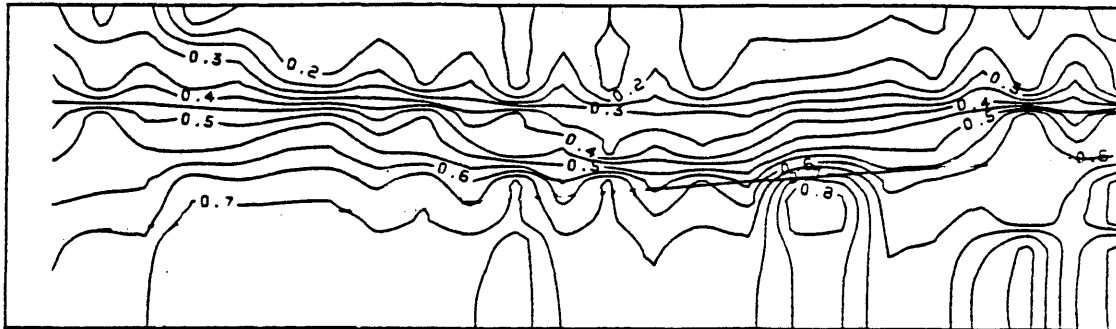


Figure 6.18. Saturation Contours of Run Number 15. Water Flood.
High Permeability Sand.

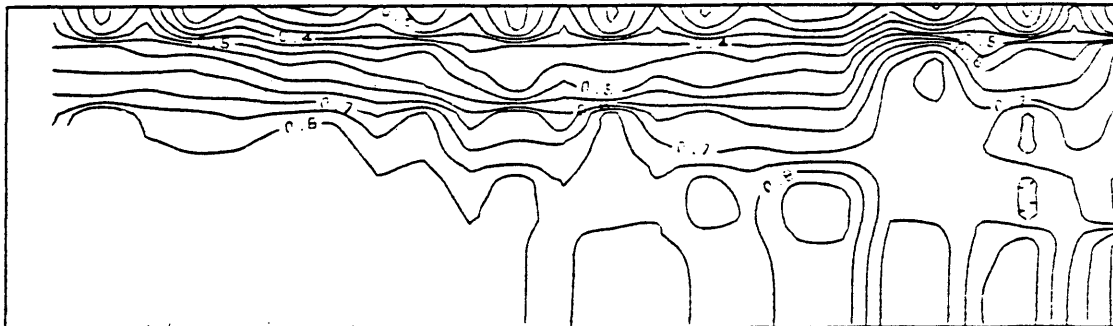
Time = 7.35 hrs

Cum. Oil Produced = 0.365 PV



Time = 12.27 hrs

Cum. Oil Produced = 0.548 PV



Time = 21.0 hrs

Cum. Oil Produced = 0.626 PV



Figure 6.18. (Continued).

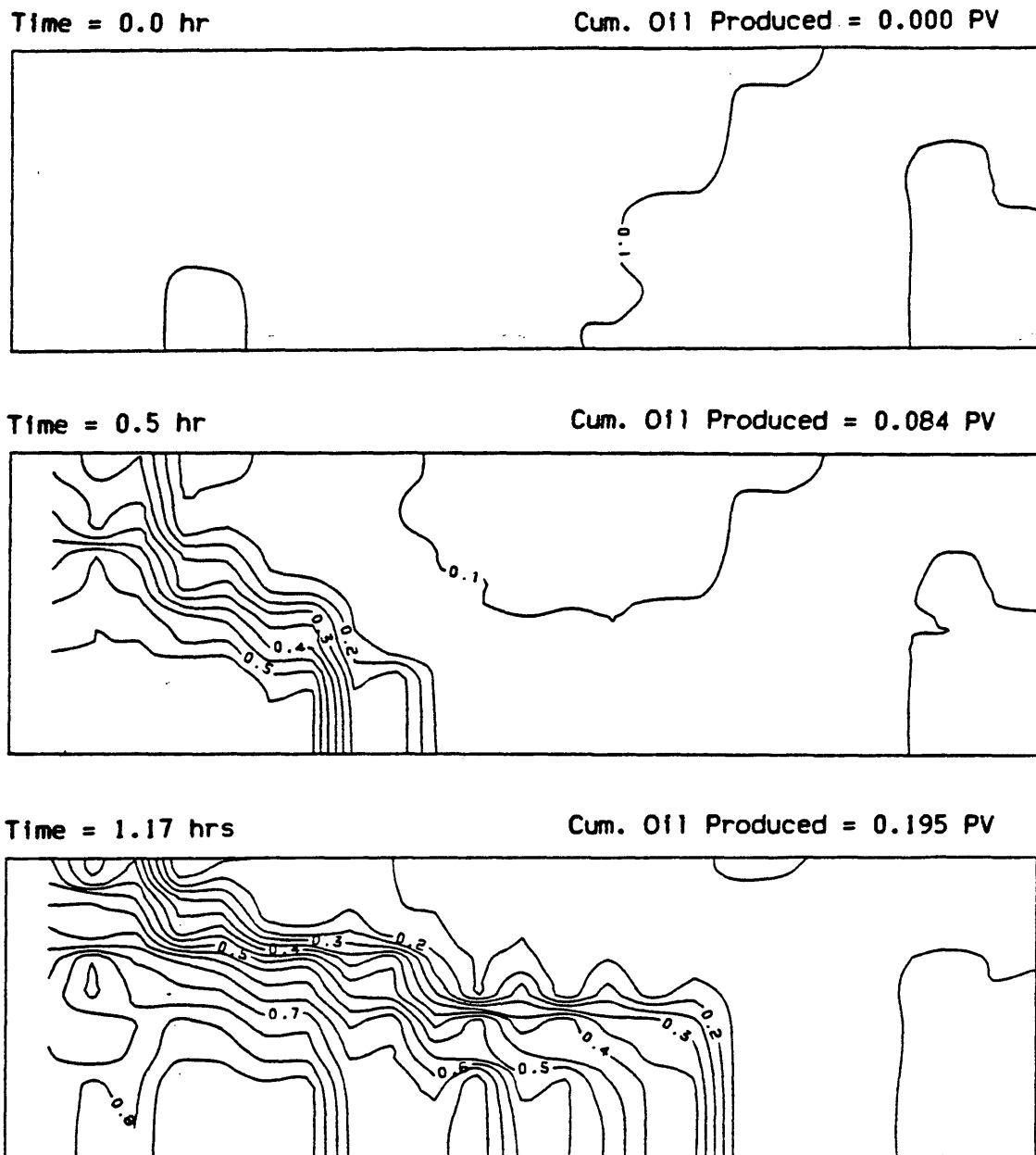
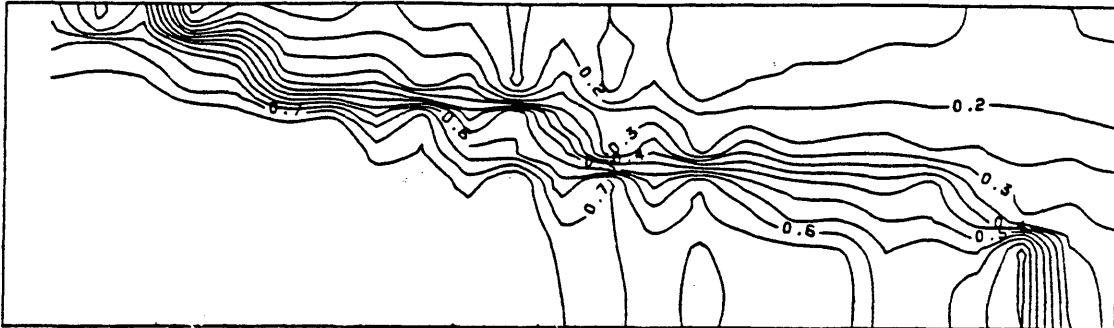


Figure 6.19. Saturation Contours of Run Number 16. Water Flood.
High Permeability Sand.

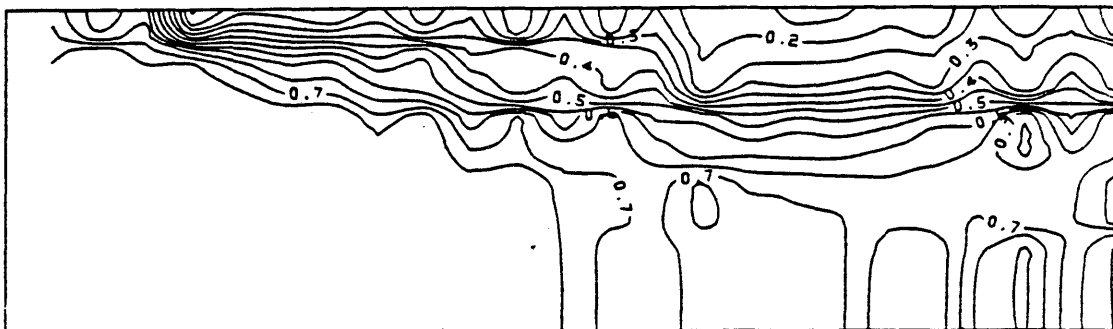
Time = 2.17 hrs

Cum. Oil Produced = 0.359 PV



Time = 3.0 hrs

Cum. Oil Produced = 0.493 PV



Time = 5.67 hrs

Cum. Oil Produced = 0.629 PV

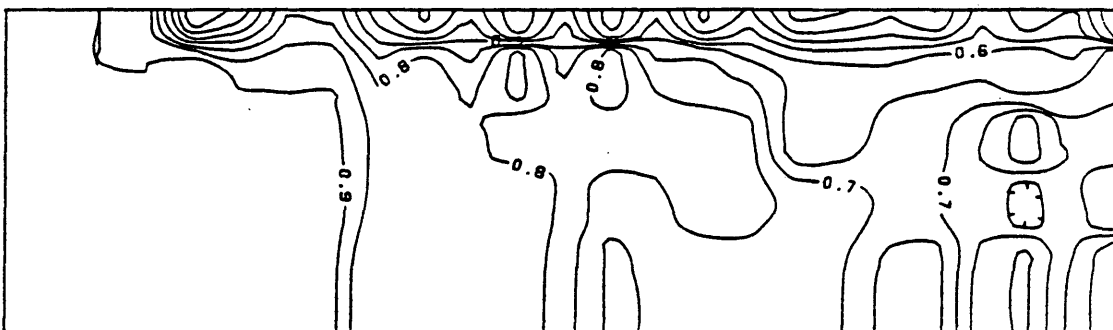
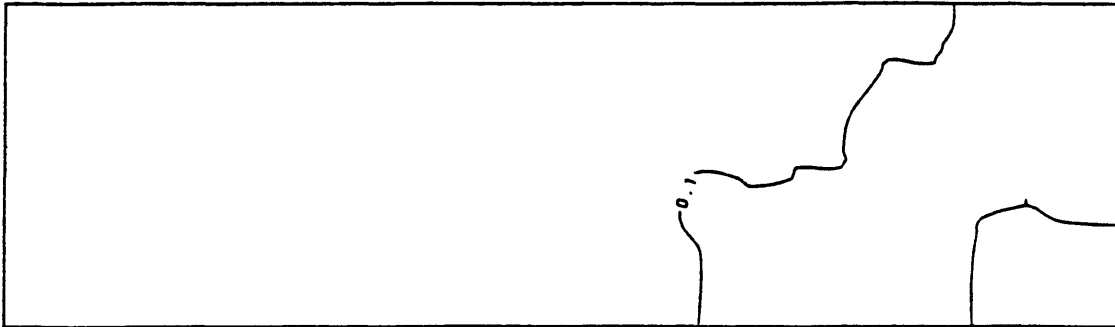


Figure 6.19. (Continued).

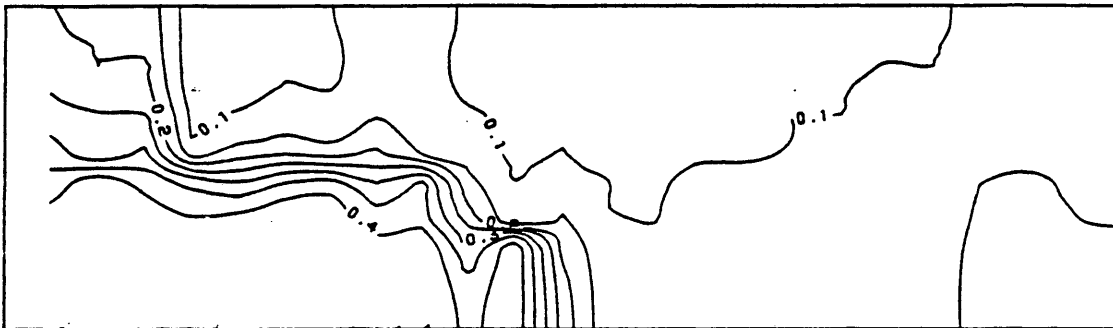
Time = 0.0 hr

Cum. Oil Produced = 0.000 PV



Time = 2.28 hrs

Cum. Oil Produced = 0.082 PV



Time = 4.28 hrs

Cum. Oil Produced = 0.151 PV

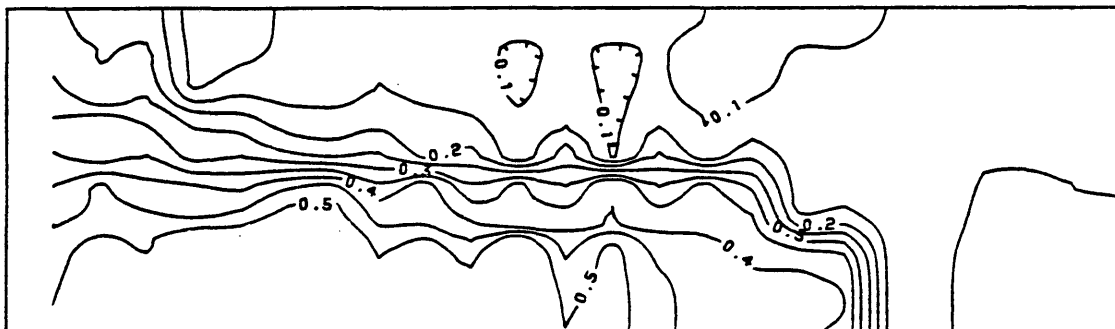


Figure 6.20. Saturation Contours of Run Number 17. Water Flood.
High Permeability Sand.

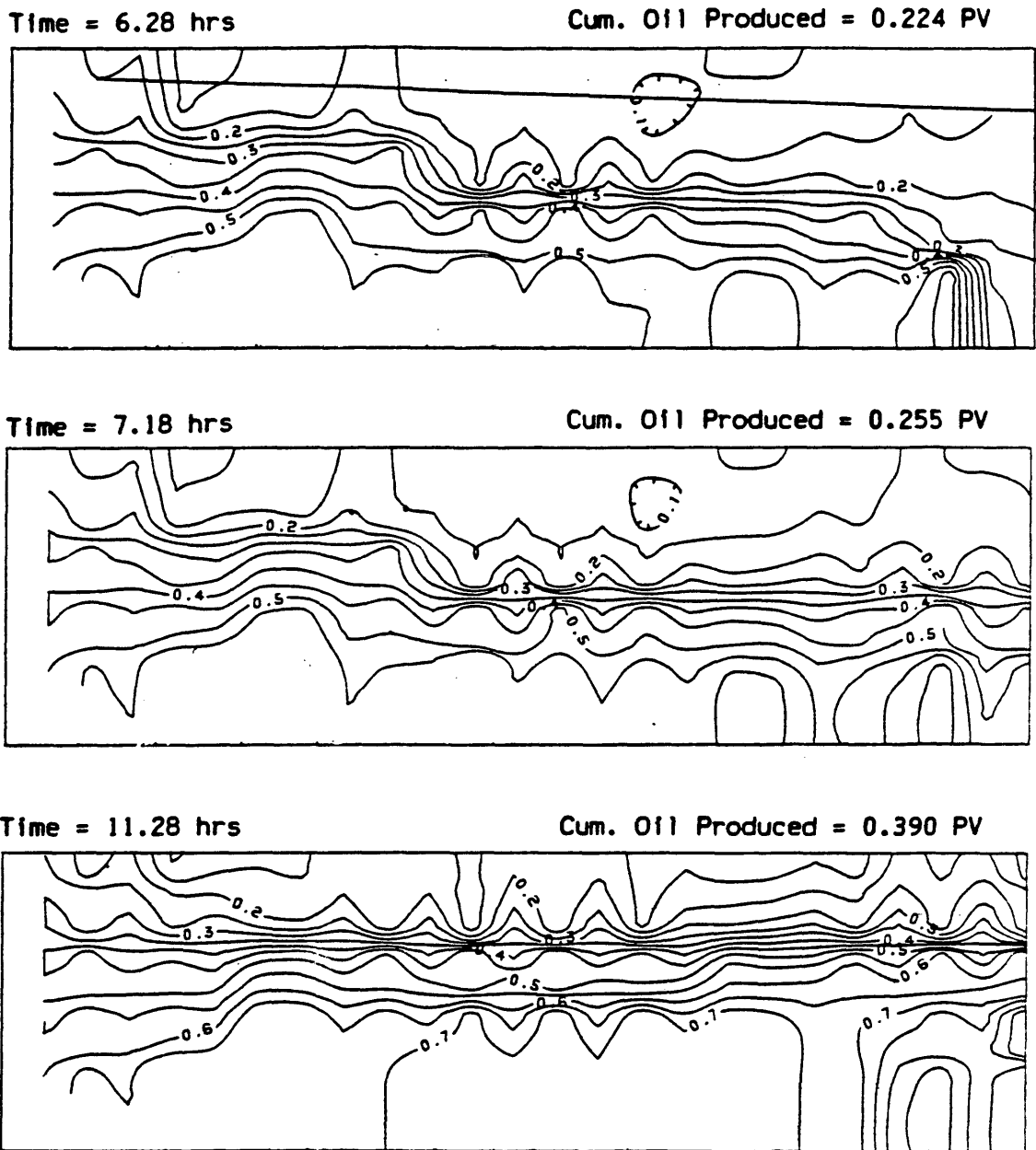


Figure 6.20. (Continued).

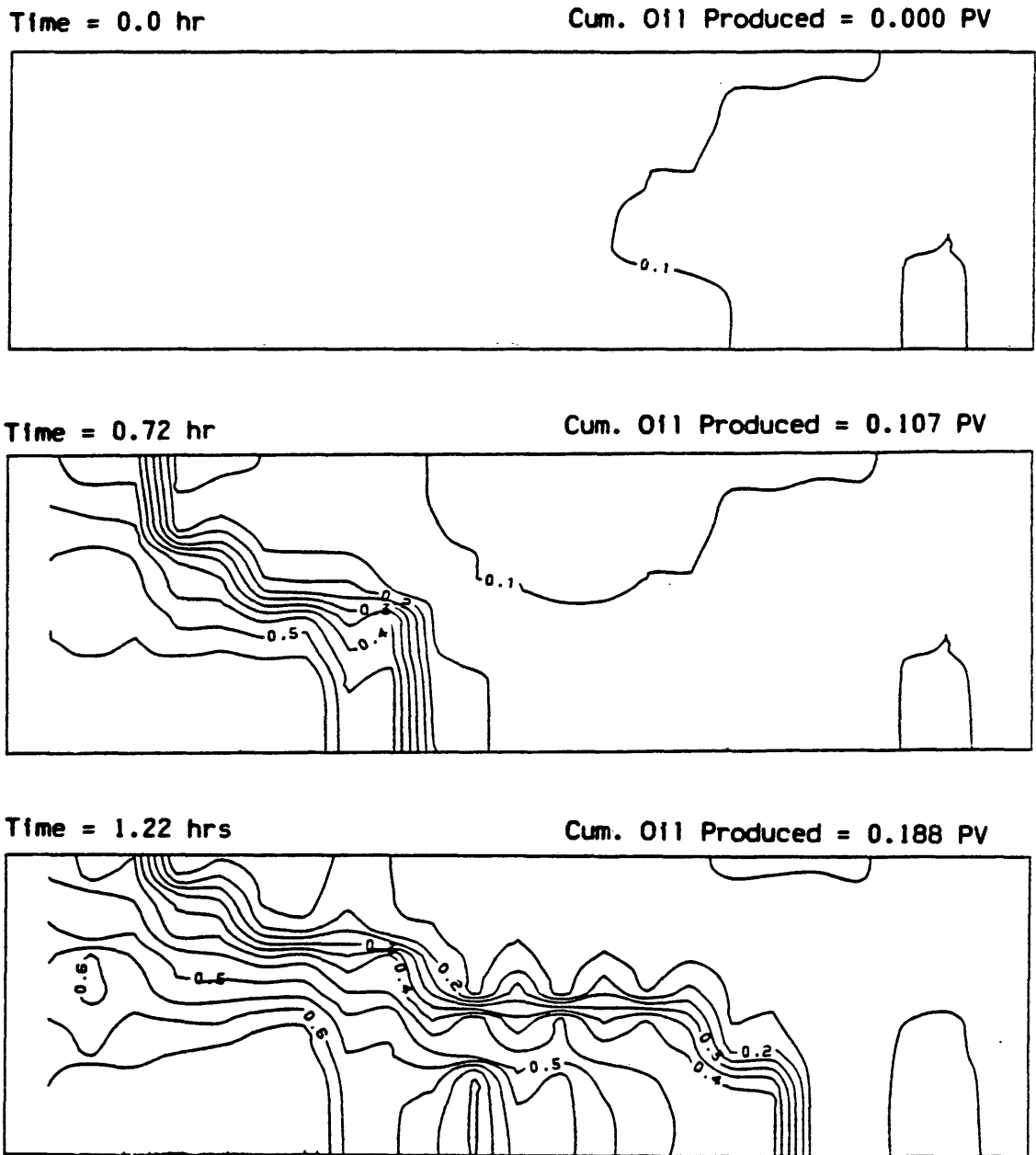


Figure 6.21. Saturation Contours of Run Number 18. Water Flood.
High Permeability Sand.

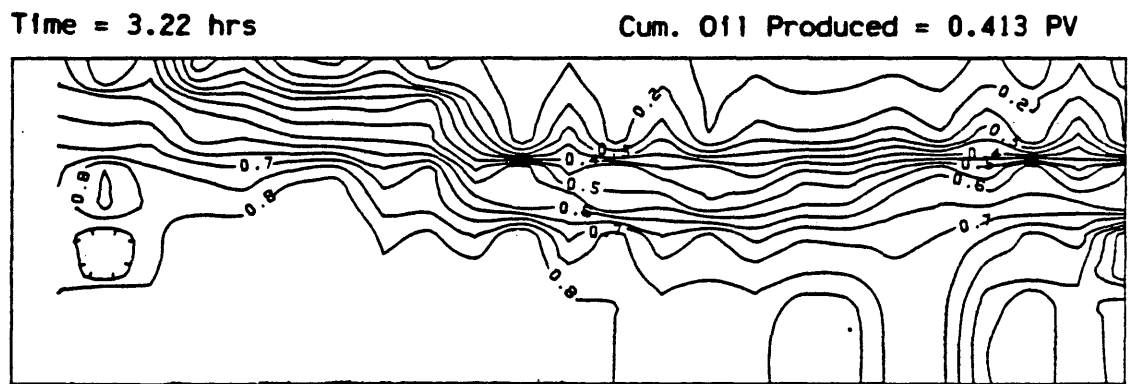
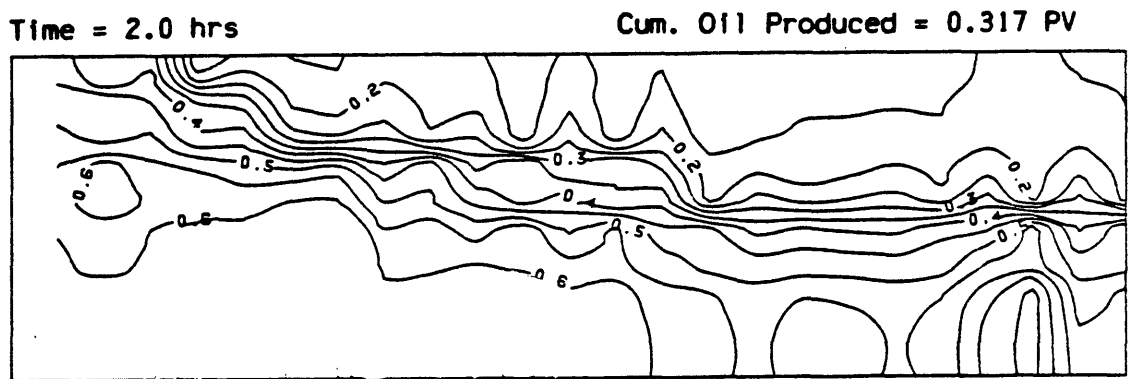
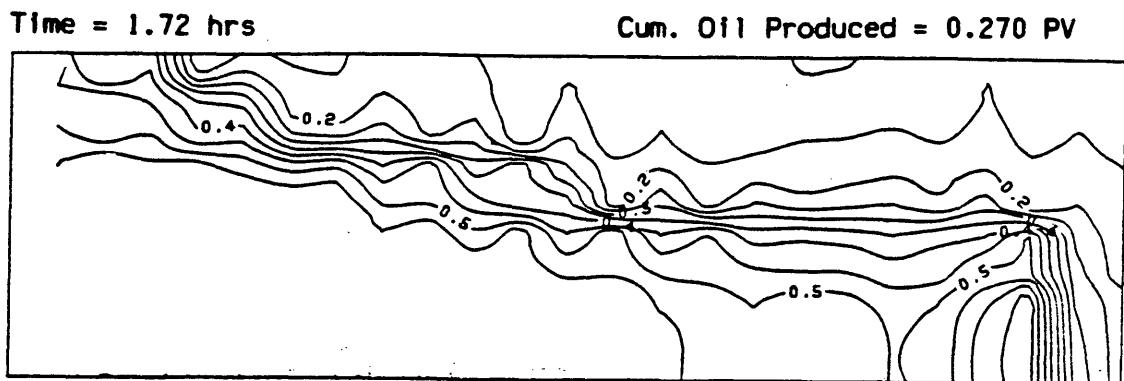


Figure 6.21. (Continued).

6.3. The Boundaries of Stability

Since instability causes premature breakthrough of the displacing phase, the two dimensionless stability number resulting from inspectional analysis discussed in Chapter Four was correlated with the oil recovery at breakthrough. Figure 6.22 shows that the displacement is unstable below certain critical value of F_s . The value that delineates the boundaries of stability during immiscible displacement was found to be

$$F_s = \frac{\sigma \sqrt{\phi/k}}{\Delta\rho g M} > 1.83 \times 10^5 \quad (6.1)$$

Results of experiments conducted by Allam (1979) and Peggs (1973) on the same system are plotted in Figure 6.23. The recovery at breakthrough also dropped at a certain value of F_s showing unstable displacement. However, instability took place at a value of F_s close to 1.83×10^5 .

Accordingly, one should design the flood in such a way that F_s is kept above the critical value shown above in order to maximize the displacement efficiency.

In Figure 6.24 the oil-water viscosity ratio is plotted against the oil recovery at breakthrough. As can be seen, no clear-cut correlation is visible, where at the same viscosity ratio different values of recovery at breakthrough were obtained. Figure 6.25 shows the plot of the factor G , which represents the ratio of viscous to gravity forces, versus breakthrough oil recovery. Also no correlation can be

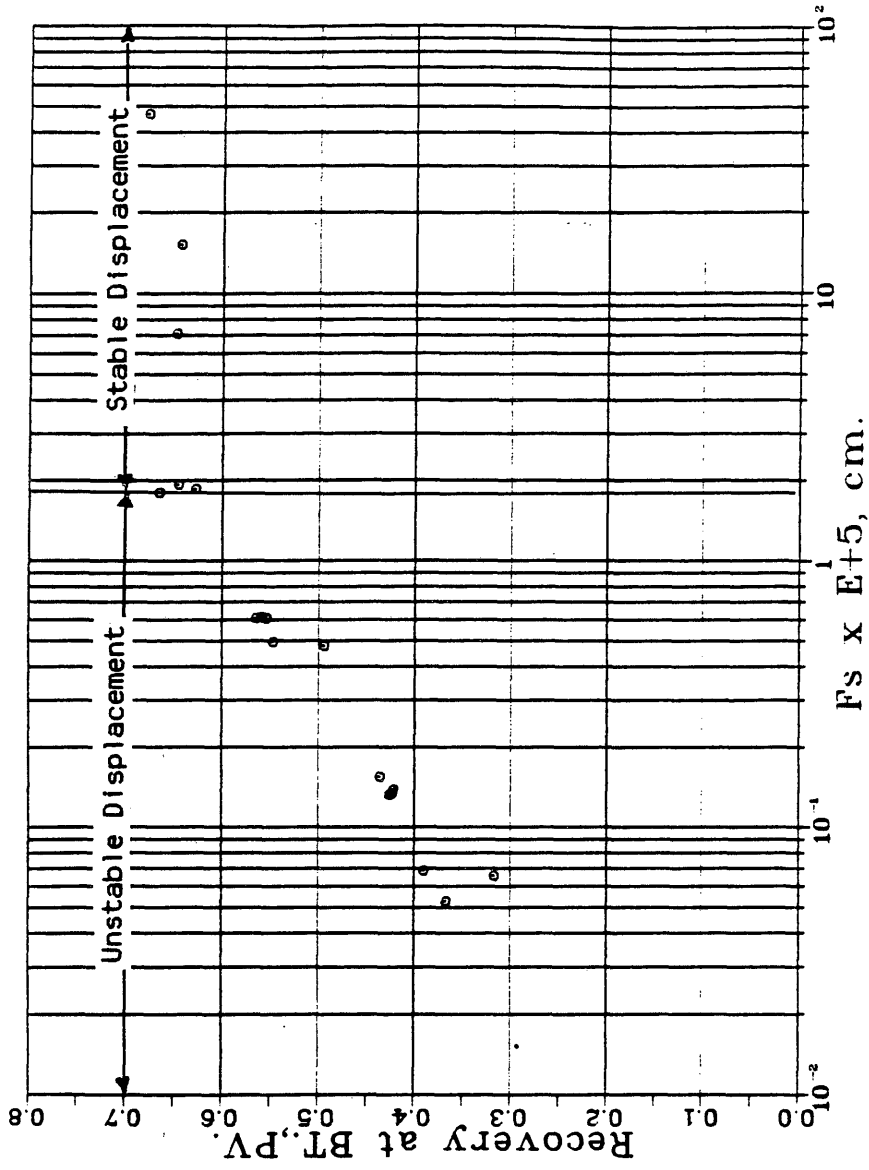


Figure 6.22. Boundaries of Stability as Defined by the Stability Factor, F_s.

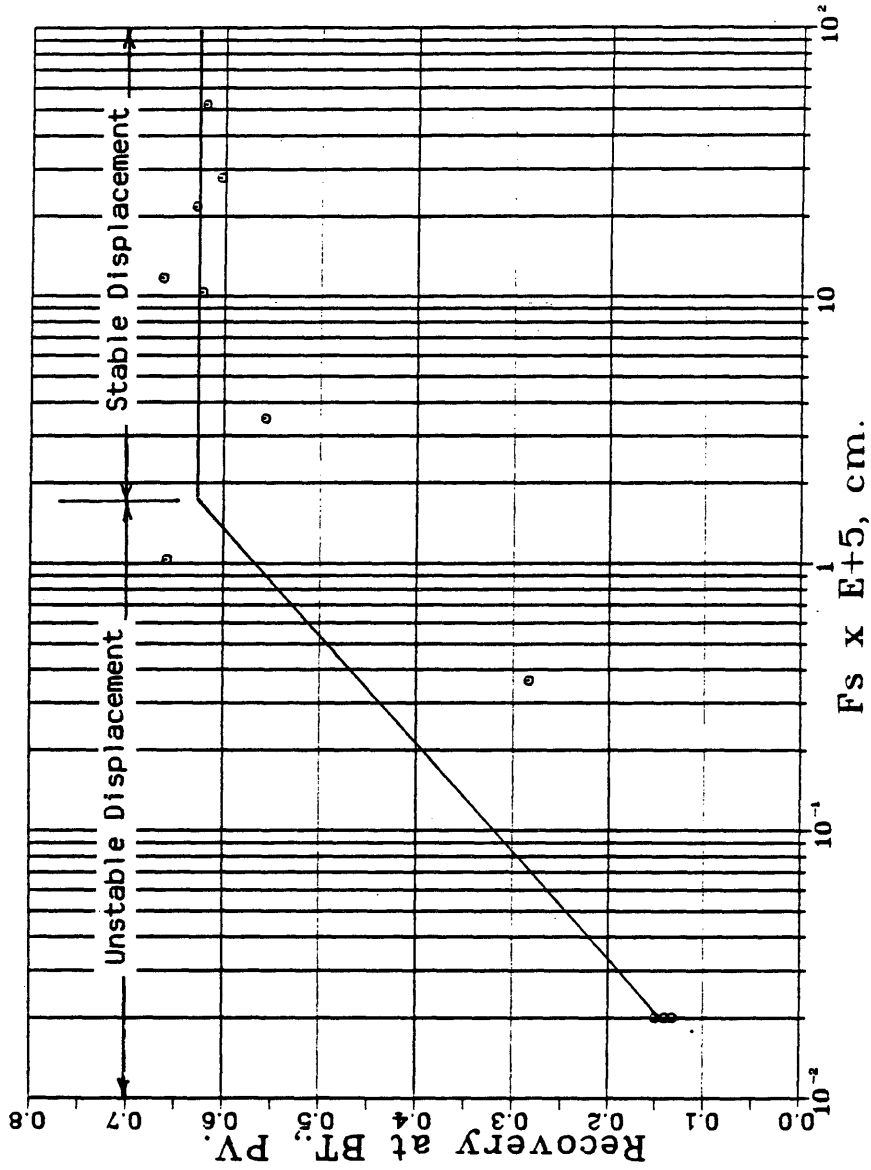


Figure 6.23. Correlation of the Stability Factor F_s with the Breakthrough Oil Recovery. Data from Allam (1979) and Peggs (1973).

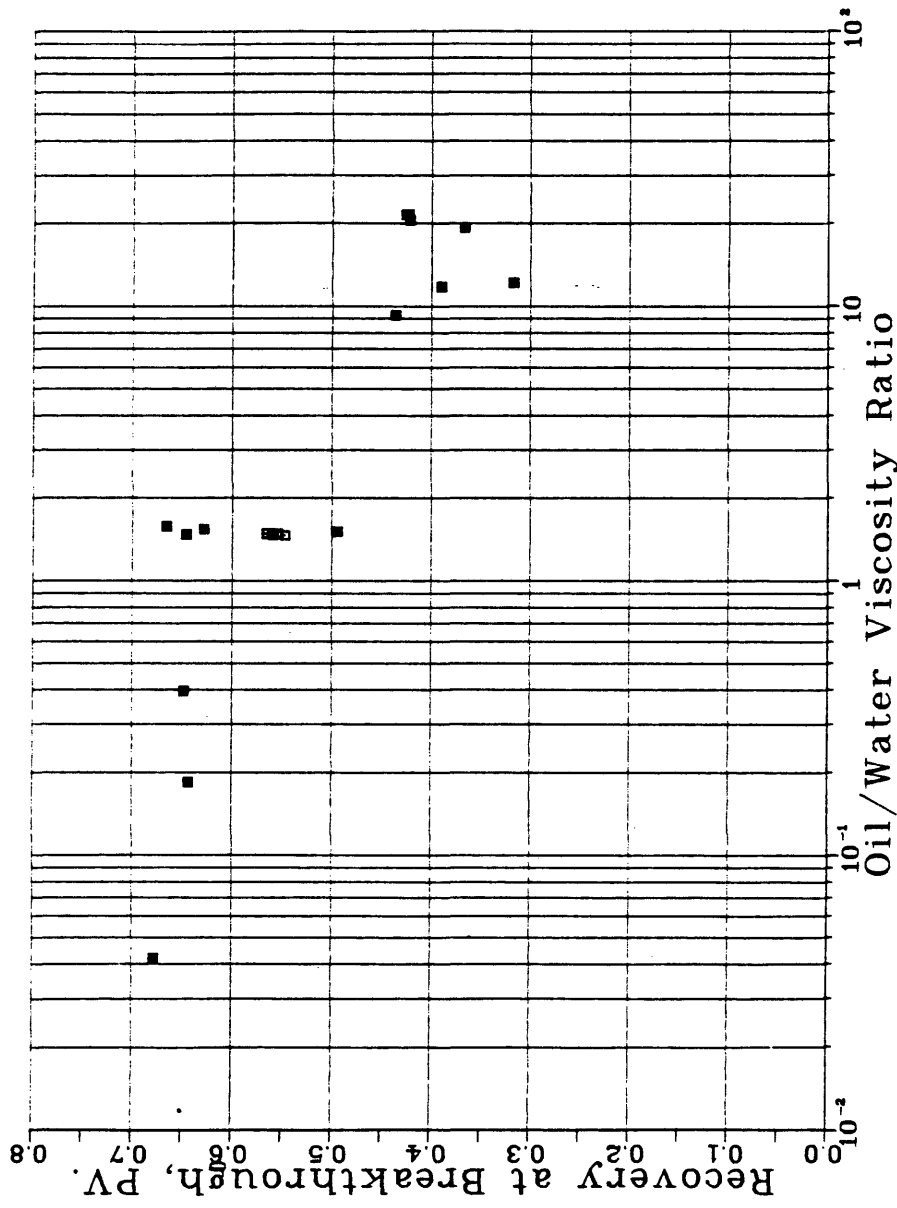


Figure 6.24. Effect of Viscosity Ratio on Breakthrough Oil Recovery.

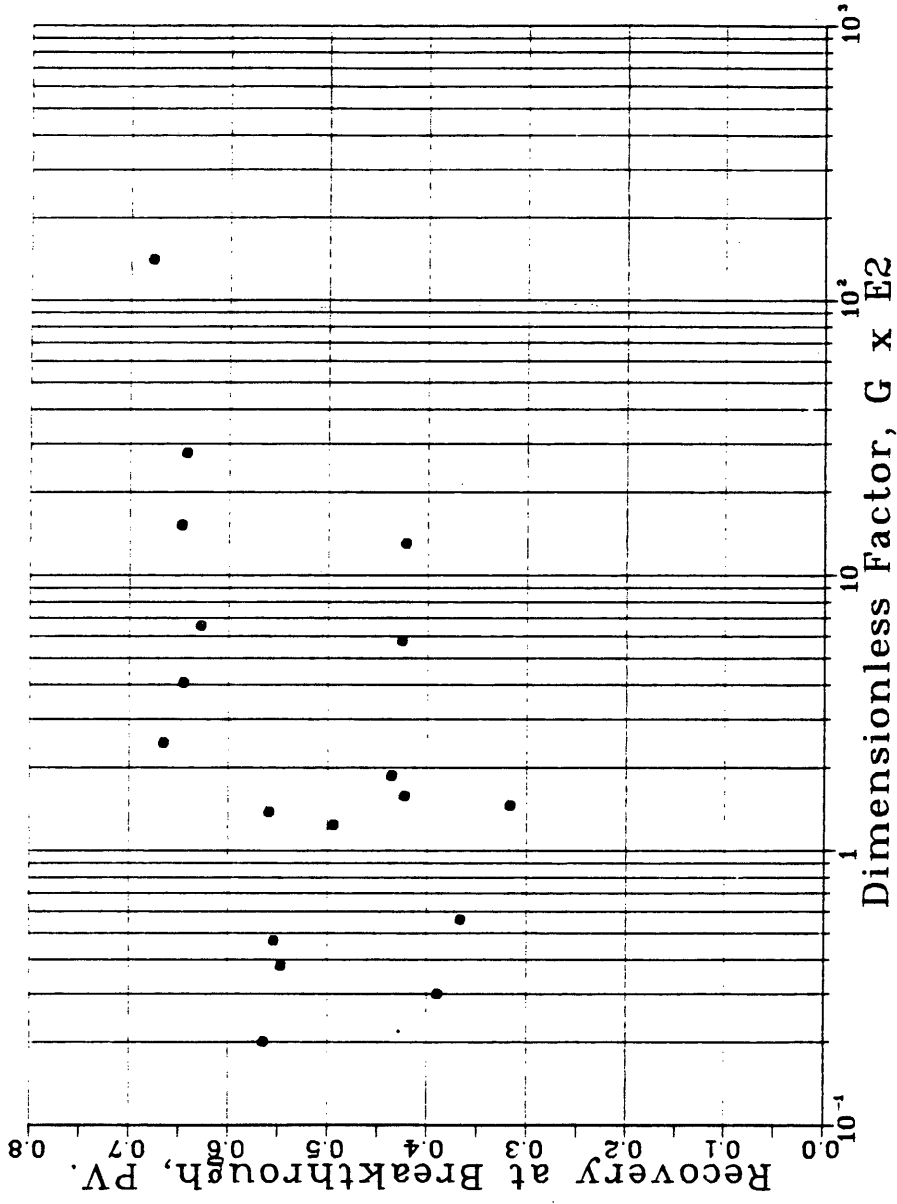


Figure 6.25. Correlation of Dimensionless Factor G with Breakthrough

'011 Recovery.

cited. This could be attributed to the fact that the viscous forces were neutralized when the system was designed to have a value of the scaling coefficient $LV\mu_w$, proposed by Rapoport and Leas (1953), larger than the critical value of 1.5 for all the runs conducted in this work.

CONCLUSIONS AND RECOMMENDATIONS

Conclusions

1. The displacement is stable if the stability number F_s is greater than the critical value of 1.83×10^5 .
2. No correlation could be obtained between the breakthrough recovery and the dimensionless groups representing oil-water viscosity ratio or viscous to gravity forces ratio.
3. The rate of injection has little or no effect on oil recovery at breakthrough if the model is scaled according to the scaling coefficient $LV\mu_w$ introduced by Rapoport and Leas (1953).
4. An adverse mobility or viscosity ratio is by no means a sufficient condition for instability. Other parameters, such as gravity forces, capillary forces, viscous resistance and system geometry play a major role in the stability of immiscible displacement in porous media.
5. The only manifestation of instability observed during immiscible displacements conducted in water-wet, connate water-bearing, porous media was gravity tonguing. No viscous fingering could be observed despite the condition of an adverse viscosity ratio.
6. At large values of oil-water viscosity ratio, instability may take place on a microscopic scale, i.e., the displacing phase sweeps the oil preferentially from channels with less resistance to flow, bypassing considerable amounts of oil in channels with higher

resistance to flow.

7. In all oil floods conducted in this work, the oil overran the water in the form of a gravity tongue.
8. In a stable displacement, water and polymer flooding yield close values of oil recovery at breakthrough under similar flow conditions and properties of porous medium.

Recommendations

1. This work could be extended to include consolidated porous medium if certain modifications were applied to the cell and the flow system.
2. Similar experiments could be performed on the same apparatus using different arrangements of sand-fluid systems.
3. A similar work could be conducted on cylindrical cores.
4. It is of a great importance to devote a study to investigate the monotonic increase in water saturation toward the outlet end of the core sample after an oil flood.

REFERENCES CITED

1. Allam, F.M., (1979), "The Behavior of the Interface Between Two Immiscible Fluids of Unequal Mobilities During Displacement in Porous Media", CSM, Thesis T-2208.
2. Allen, F.R., and Puckett, D.A., (1986), "Theoretical and Experimental Studies of Rate-Dependent Two-Phase Immiscible Flow", SPE Production Engineering, Jan., 62.
3. Archie, G.E., (1942), "Electrical Resistivity Log as an Aid in Determining Some Reservoir Characteristics", Trans. AIME, 146, 54.
4. Bentsen, R.G., (1978), "Conditions Under Which the Capillary Term May Be Neglected", J. Can. Pet. Tech., Oct.-Dec., 25.
5. Bentsen, R.G., and Saeedi, J., (1981), "Liquid-Liquid Immiscible Displacement in Unconsolidated Porous Media", J. Can. Pet. Tech., Jan.-Mar., 93.
6. Buckley, S.E., and Leverett, M.C., (1942), "Mechanics of Fluid Displacement in Sands", Trans. AIME, 146, 107.
7. Chuoke, R.L., van Meurs, P., and van der Poel, C., (1959), "The Instability of Liquid-Liquid Displacements in Permeable Media", Trans. AIME, 216, 188.
8. Craig, F.F. Jr., (1980), "The Reservoir Engineering Aspects of Waterflooding", Monograph Vol. 3, AIME, 24.
9. Craig, F.F. Jr., Sanderlin, J.L., Moore, D.W., and Geffen, T.M., (1957), "A Laboratory Study of Gravity Segregation in Frontal

- Drives", Trans. AIME, 210, 275.
10. Croes, G.A., and Schwarz, N., (1955), "Dimensionally Scaled Experiments and the Water-Drive Process", Trans. AIME, 204, 35.
 11. Dietz, D.N., (1953), "A Theoretical Approach to the Problem of Encroaching and By-Passing Edge Water", Proc. Koninkl. Ned. Akad. Wetenschap, B56.
 12. Engelbert, W.F., and Klinkenberg, L.J., (1951), "Laboratory Experiments on the Displacement of Water from Packs of Granular Material", Proc. 3rd World Pet. Cong., 544.
 13. Fayers, F.J., and Sheldon, J.W., (1959), "The Effect of Capillary Pressure and Gravity on Two-Phase Fluid Flow in a Porous Medium", Trans. AIME, 216, 147.
 14. Geertsma, J., Croes, G.A., and Schwarz, N., (1956), "Theory of Dimensionally Scaled Models of Petroleum Reservoirs", Trans. AIME, 207, 118.
 15. George, P.D., Bentsen, R.G., and Flock, D.L., (1982), "A Multi-Dimensional Approach to Scaled Immiscible Fluid Displacement", J. Can. Pet. Tech., July-Aug, 49.
 16. Hagoort, J., (1974), "Displacement Stability of Water-Wet Connate-Water-Bearing Reservoirs", SPE J., Feb., 63.
 17. Hawthorne, R.G., (1960), "Two-Phase Flow in Two-Dimensional Systems-Effect of Rate, Viscosity and Density on Fluid Displacement in Porous Media", Trans. AIME, 219, 81.
 18. Hovanessian, S.A., and Fayers, F.J., (1961), "Linear Water Flood with Gravity and Capillary Effects", SPE J., Mar., 32.

19. Leverett, M.C., (1939), "Flow of Oil-Water Mixtures through Unconsolidated Sands", Trans. AIME, 132, 149.
20. Leverett, M.C., (1941), "The Capillary Behavior in Porous Solids", Trans. AIME, 142, 152.
21. Leverett, M.C., Lewis, W.B., and True, M.E., (1942), "Dimensional-Model Studies of Oil-field Behavior", Trans. AIME, 146, 175.
22. Lewis, D.J., (1951), "The Instability of Liquid Surface When Accelerated in a Direction Perpendicular to Their Planes. II", Proc. Roy. Soc. A, 202, 81.
23. McWilliams, M.H., (1962), "Investigation of the Scaling Factor $LV\mu_w$ in the Recovery of Oil", Agric. and Mech. Coll. of Texas, M.Sc. Thesis.
24. Parsons, R.W., (1975), "Microwave Attenuation - A New Tool for Monitoring Saturations in Laboratory Flooding Experiments", Trans. AIME, 259, 302-309.
25. Peggs, J.K., (1973), "Physical Comparison of the Buckley-Leverett and Dietz Frontal Advance Theories for a Linear, Horizontal Waterflood", CSM, Thesis T-1583.
26. Perkins, T.K., and Johnston, O.C., (1969), "A Study of Immiscible Fingering in Linear Models", SPE J., Mar., 39.
27. Peters, E.J., and Flock, D.L., (1981), "The Onset of Instability During Two-Phase Immiscible Displacement in Porous Media", SPE J., Apr., 249.
28. Rachford, H.H. Jr., (1964), "Instability in Water Flooding Oil

- from Water-Wet Porous Media Containing Connate Water", SPE J., June, 133.
29. Rapoport, L.A., (1955), "Scaling Laws for Use in Design and Operation of Water-Oil Flow Models", Trans. AIME, 204, 143.
 30. Rapoport, L.A., and Leas, W.J., (1953), "Properties of Linear Waterfloods", Trans. AIME, 198, 139.
 31. Richardson, J.G., and Perkins, F.M. Jr., (1957), "A Laboratory Investigation of the Effect of Rate on Recovery of Oil by Water Flooding", Trans. AIME, 210, 114.
 32. Saffman, P.G., and Taylor, G., (1958), "The Penetration of a Fluid into a Porous Medium or Hele-Shaw Cell Containing a More Viscous Liquid", Proc. Roy. Soc., 245, 312.
 33. Van Meurs, P., (1957), "The Use of Transparent Three-Dimensional Models for Studying the Mechanism of Flow Processes in Oil Reservoirs", Trans. AIME, 210, 295.
 34. Van Meurs, P., and van der Poel, C., (1958), "A Theoretical Description of Water-Drive Processes Involving Viscous Fingering", Trans. AIME, 213, 103.
 35. Welge, H.J., (1952), "A Simplified Method for Computing Oil Recovery by Gas or Water Drive", Trans. AIME, 195, 91.

APPENDIX A

TABLE A1. RUN NO. 1. POLYMER FLOOD

TIME HRS.	CUM PV INJECTED	CUM PV PRODUCED	INJ RATE CC/MIN	INJ RATE CUFT/DAY	PRESS DROP PSIG
0.00	0.000	0.000	17.32	0.881	1.00
2.00	0.093	0.093	17.04	0.867	3.25
4.00	0.184	0.184	16.83	0.856	6.00
6.00	0.275	0.275	16.80	0.854	8.70
10.00	0.453	0.453	16.66	0.847	12.80
15.00	0.673	0.673	16.05	0.816	17.20
POROSITY				34.44 %	
AVERAGE Swi				12.02 %	
AVERAGE Sor				17.17 %	
ABSOLUTE PERMEABILITY				7.34 darcies	
Ko(Swi)				6.22 darcies	
Kw(Sor)				3.56 darcies	
VISCOSITY OF WATER				1.03 cp	
VISCOSITY OF POLYMER				37.80 cp	
VISCOSITY OF OIL				1.57 cp	
MOBILITY RATIO				0.024	

TABLE A2. RUN NO. 2. POLYMER FLOOD.

TIME HRS.	CUM PV INJECTED	CUM PV PRODUCED	INJ RATE CC/MIN	INJ RATE CUFT/DAY	PRESS DROP PSIG
0.00	0.000	0.000	9.98	0.508	0.55
4.00	0.127	0.127	10.37	0.527	0.75
8.00	0.243	0.243	10.72	0.545	1.30
12.00	0.330	0.330	10.79	0.549	1.55
16.00	0.474	0.474	10.64	0.541	2.20
22.00	0.643	0.643	10.62	0.540	2.80
POROSITY				34.44 %	
AVERAGE Swi				12.78 %	
AVERAGE Sor				21.10 %	
ABSOLUTE PERMEABILITY				7.34 darcies	
Ko(Swi)				6.10 darcies	
Kw(Sor)				2.82 darcies	
VISCOSITY OF WATER				0.99 cp	
VISCOSITY OF POLYMER				7.87 cp	
VISCOSITY OF OIL				1.45 cp	
MOBILITY RATIO				0.085	

TABLE A3. RUN NO. 3. POLYMER FLOOD.

TIME HRS.	CUM PV INJECTED	CUM PV PRODUCED	INJ RATE CC/MIN	INJ RATE CUFT/DAY	PRESS DROP PSIG
0.00	0.000	0.000	15.73	0.800	0.80
2.25	0.075	0.075	11.75	0.597	0.65
5.50	0.167	0.167	11.76	0.598	0.65
10.50	0.349	0.349	11.39	0.579	0.82
14.50	0.493	0.493	13.30	0.676	1.20
18.50	0.648	0.648	13.27	0.675	1.50
POROSITY				34.44 %	
AVERAGE S_{wi}				13.81 %	
AVERAGE S_{or}				19.77 %	
ABSOLUTE PERMEABILITY				7.34 darcies	
$K_o(S_{wi})$				3.13 darcies	
$K_w(S_{or})$				3.43 darcies	
VISCOSITY OF WATER				0.96 cp	
VISCOSITY OF POLYMER				3.55 cp	
VISCOSITY OF OIL				1.40 cp	
MOBILITY RATIO				0.432	

TABLE A4. RUN NO. 4. WATER FLOOD.

TIME HRS.	CUM PV INJECTED	CUM PV PRODUCED	INJ RATE CC/MIN	INJ RATE CUFT/DAY	PRESS DROP PSIG
0.00	0.000	0.000	18.66	0.949	0.40
2.35	0.129	0.129	20.92	1.064	0.40
5.35	0.296	0.296	21.08	1.072	0.40
8.35	0.465	0.465	21.58	1.098	0.40
10.35	0.579	0.579	21.33	1.085	0.40
11.35	0.628	0.628	20.09	1.022	0.70
POROSITY				35.11 %	
AVERAGE Swi				13.23 %	
AVERAGE Sor				18.37 %	
ABSOLUTE PERMEABILITY				6.78 darcies	
Ko(Swi)				6.33 darcies	
Kw(Sor)				3.71 darcies	
VISCOSITY OF WATER				0.92 cp	
VISCOSITY OF OIL				1.41 cp	
MOBILITY RATIO				0.898	

TABLE A5. RUN NO. 5. WATER FLOOD.

TIME HRS.	CUM PV INJECTED	CUM PV PRODUCED	INJ RATE CC/MIN	INJ RATE CUFT/DAY	PRESS DROP PSIG
0.00	0.000	0.000	13.14	0.668	0.35
7.00	0.233	0.233	12.32	0.627	0.35
11.00	0.313	0.313	12.73	0.627	0.35
15.00	0.526	0.526	12.73	0.647	0.35
18.34	0.626	0.626	10.91	0.555	0.35
28.00	0.939	0.683	16.88	0.859	0.55
POROSITY				34.57 %	
AVERAGE S_{wi}				11.49 %	
AVERAGE S_{or}				18.81 %	
ABSOLUTE PERMEABILITY				6.72 darcies	
$K_o(S_{wi})$				6.48 darcies	
$K_w(S_{or})$				3.70 darcies	
VISCOSITY OF WATER				0.96 cp	
VISCOSITY OF OIL				1.41 cp	
MOBILITY RATIO				0.839	

TABLE A6. RUN NO. 6. WATER FLOOD.

TIME HRS.	CUM PV INJECTED	CUM PV PRODUCED	INJ RATE CC/MIN	INJ RATE CUFT/DAY	PRESS DROP PSIG
0.00	0.000	0.000	7.65	0.389	0.46
11.50	0.234	0.234	7.90	0.402	0.43
17.50	0.355	0.355	7.45	0.379	0.39
27.50	0.557	0.557	7.52	0.382	0.36
33.50	0.667	0.667	10.50	0.534	0.36
45.50	0.989	0.697	9.88	0.500	0.36
POROSITY				34.57 %	
AVERAGE Swi				11.49 %	
AVERAGE Sor				17.62 %	
ABSOLUTE PERMEABILITY				6.72 darcies	
Ko(Swi)				6.54 darcies	
Kw(Sor)				4.05 darcies	
VISCOSITY OF WATER				0.96 cp	
VISCOSITY OF OIL				1.51 cp	
MOBILITY RATIO				0.974	

TABLE A7. RUN NO. 7. WATER FLOOD.

TIME HRS.	CUM PV INJECTED	CUM PV PRODUCED	INJ RATE CC/MIN	INJ RATE CUFT/DAY	PRESS DROP PSIG
0.00	0.000	0.000	21.42	1.089	8.70
0.50	0.040	0.040	21.42	1.089	8.60
2.25	0.133	0.133	14.50	0.737	1.20
8.25	0.187	0.187	3.29	0.167	1.20
19.25	0.295	0.295	3.50	0.178	1.20
30.25	0.413	0.413	4.17	0.212	1.20
POROSITY				34.57 %	
AVERAGE Swi				11.16 %	
AVERAGE Sor				19.70 %	
ABSOLUTE PERMEABILITY				8.82 darcies	
Ko(Swi)				7.39 darcies	
Kw(Sor)				4.06 darcies	
VISCOSITY OF WATER				1.01 cp	
VISCOSITY OF OIL				21.40 cp	
MOBILITY RATIO				11.64	

TABLE A8. RUN NO. 8. WATER FLOOD.

TIME HRS.	CUM PV INJECTED	CUM PV PRODUCED	INJ RATE CC/MIN	INJ RATE CUFT/DAY	PRESS DROP PSIG
0.00	0.000	0.000	18.53	0.942	8.00
1.75	0.100	0.100	18.16	0.924	7.05
4.75	0.254	0.254	18.91	0.962	5.20
6.75	0.357	0.357	19.08	0.970	4.20
8.10	0.408	0.408	19.10	0.974	3.55
11.75	0.592	0.490	17.04	0.867	2.25
POROSITY				34.57 %	
AVERAGE Swi				14.03 %	
AVERAGE Sor				18.39 %	
ABSOLUTE PERMEABILITY				8.82 darcies	
Ko(Swi)				7.36 darcies	
Kw(Sor)				3.96 darcies	
VISCOSITY OF WATER				1.02 cp	
VISCOSITY OF OIL				21.90 cp	
MOBILITY RATIO				11.55	

TABLE A9. RUN NO. 9. WATER FLOOD.

TIME HRS.	CUM PV INJECTED	CUM PV PRODUCED	INJ RATE CC/MIN	INJ RATE CUFT/DAY	PRESS DROP PSIG
0.00	0.000	0.000	42.47	2.16	13.60
0.90	0.097	0.097	44.00	2.24	12.40
2.90	0.341	0.341	45.00	2.29	7.90
3.57	0.422	0.422	45.00	2.29	6.70
7.15	0.861	0.571	45.55	2.32	4.75
POROSITY				34.57 %	
AVERAGE Swi				14.74 %	
AVERAGE Sor				28.19 %	
ABSOLUTE PERMEABILITY				8.82 darcies	
Ko(Swi)				7.20 darcies	
Kw(Sor)				3.90 darcies	
VISCOSITY OF WATER				0.97 cp	
VISCOSITY OF OIL				19.90 cp	
MOBILITY RATIO				11.11	

TABLE A10. RUN NO. 10. WATER FLOOD.

TIME HRS.	CUM PV INJECTED	CUM PV PRODUCED	INJ RATE CC/MIN	INJ RATE CUFT/DAY	PRESS DROP PSIG
0.00	0.000	0.000	2.99	0.152	1.20
3.35	0.052	0.052	6.66	0.339	2.50
7.35	0.135	0.135	6.76	0.344	0.95
13.35	0.222	0.222	6.21	0.316	1.75
24.85	0.419	0.419	4.41	0.224	1.55
25.35	0.436	0.436	10.00	0.509	1.90
POROSITY			34.57 %		
AVERAGE Swi			18.75 %		
AVERAGE Sor			17.03 %		
ABSOLUTE PERMEABILITY			8.82 darcies		
Ko(Swi)			7.42 darcies		
Kw(Sor)			3.95 darcies		
VISCOSITY OF WATER			2.00 cp		
VISCOSITY OF OIL			18.40 cp		
MOBILITY RATIO			5.02		

TABLE A11. RUN NO. 11. WATER FLOOD.

TIME HRS.	CUM PV INJECTED	CUM PV PRODUCED	INJ RATE CC/MIN	INJ RATE CUFT/DAY	PRESS DROP PSIG
0.00	0.000	0.000	46.00	2.340	0.46
1.16	0.143	0.143	43.83	2.229	0.46
2.40	0.281	0.281	41.44	2.108	0.46
3.66	0.417	0.417	38.76	1.971	0.46
5.00	0.559	0.559	37.17	1.890	0.46
11.15	1.128	0.675	35.15	1.788	0.46
POROSITY				34.77 %	
AVERAGE Swi				9.11 %	
AVERAGE Sor				21.22 %	
ABSOLUTE PERMEABILITY				67.83 darcies	
Ko(Swi)				52.23 darcies	
Kw(Sor)				24.20 darcies	
VISCOSITY OF WATER				0.96 cp	
VISCOSITY OF OIL				1.40 cp	
MOBILITY RATIO				0.676	

TABLE A12. RUN NO. 12. WATER FLOOD.

TIME HRS.	CUM PV INJECTED	CUM PV PRODUCED	INJ RATE CC/MIN	INJ RATE CUFT/DAY	PRESS DROP PSIG
0.00	0.000	0.000	16.00	0.814	0.75
1.43	0.058	0.058	14.76	0.751	0.75
3.43	0.138	0.138	15.00	0.763	0.75
6.43	0.257	0.257	14.08	0.716	0.75
10.85	0.427	0.427	16.00	0.814	0.75
14.00	0.554	0.554	15.00	0.763	0.75
POROSITY				34.77 %	
AVERAGE Swi				10.29 %	
AVERAGE Sor				23.53 %	
ABSOLUTE PERMEABILITY				67.83 darcies	
Ko(Swi)				38.00 darcies	
Kw(Sor)				2.15 darcies	
VISCOSITY OF WATER				0.93 cp	
VISCOSITY OF OIL				1.37 cp	
MOBILITY RATIO				0.083	

TABLE A13. RUN NO. 13. WATER FLOOD.

TIME HRS.	CUM PV INJECTED	CUM PV PRODUCED	INJ RATE CC/MIN	INJ RATE CUFT/DAY	PRESS DROP PSIG
0.00	0.000	0.000	9.43	0.480	0.50
5.75	0.089	0.089	5.54	0.282	0.50
11.58	0.170	0.170	5.10	0.259	0.50
16.75	0.237	0.237	5.03	0.256	0.65
25.85	0.418	0.418	6.80	0.346	1.10
35.25	0.565	0.565	5.84	0.297	1.10
POROSITY				34.77 %	
AVERAGE Swi				9.08 %	
AVERAGE Sor				18.89 %	
ABSOLUTE PERMEABILITY				67.83 darcies	
Ko(Swi)				33.87 darcies	
Kw(Sor)				0.69 darcies	
VISCOSITY OF WATER				0.95 cp	
VISCOSITY OF OIL				1.40 cp	
MOBILITY RATIO				0.030	

TABLE A14. RUN NO. 14. WATER FLOOD.

TIME HRS.	CUM PV INJECTED	CUM PV PRODUCED	INJ RATE CC/MIN	INJ RATE CUFT/DAY	PRESS DROP PSIG
0.00	0.000	0.000	20.00	1.017	0.60
2.16	0.091	0.091	15.66	0.796	0.60
4.66	0.193	0.193	15.16	0.771	0.60
7.16	0.291	0.291	15.57	0.792	0.60
9.15	0.367	0.367	15.57	0.792	0.60
26.15	1.296	0.578	17.80	0.905	0.60
POROSITY				34.77 %	
AVERAGE Swi				7.80 %	
AVERAGE Sor				28.88 %	
ABSOLUTE PERMEABILITY				67.83 darcies	
Ko(Swi)				35.15 darcies	
Kw(Sor)				5.81 darcies	
VISCOSITY OF WATER				0.93 cp	
VISCOSITY OF OIL				17.80 cp	
MOBILITY RATIO				3.16	

TABLE A15. RUN NO. 15. WATER FLOOD.

TIME HRS.	CUM PV INJECTED	CUM PV PRODUCED	INJ RATE CC/MIN	INJ RATE CUFT/DAY	PRESS DROP PSIG
0.00	0.000	0.000	26.45	1.345	0.45
2.50	0.138	0.138	21.55	1.096	0.35
4.50	0.237	0.237	18.65	0.949	0.35
7.35	0.365	0.365	15.90	0.809	0.35
12.27	0.548	0.548	14.26	0.725	0.35
21.00	0.924	0.626	18.18	0.925	0.35
POROSITY				34.93 %	
AVERAGE Swi				9.68 %	
AVERAGE Sor				26.13 %	
ABSOLUTE PERMEABILITY				106 darcies	
Ko(Swi)				37.30 darcies	
Kw(Sor)				4.10 darcies	
VISCOSITY OF WATER				1.00 cp	
VISCOSITY OF OIL				1.46 cp	
MOBILITY RATIO				0.162	

TABLE A16. RUN NO. 16. WATER FLOOD.

TIME HRS.	CUM PV INJECTED	CUM PV PRODUCED	INJ RATE CC/MIN	INJ RATE CUFT/DAY	PRESS DROP PSIG
0.00	0.000	0.000	62.52	3.180	0.60
0.50	0.084	0.084	63.25	3.217	0.60
1.17	0.195	0.195	62.35	3.171	0.65
2.17	0.359	0.359	61.40	3.123	0.65
3.00	0.493	0.493	59.45	3.023	0.65
5.67	1.087	0.629	56.26	2.861	0.70
POROSITY				34.93 %	
AVERAGE Swi				10.17 %	
AVERAGE Sor				24.02 %	
ABSOLUTE PERMEABILITY				106 darcies	
Ko(Swi)				37.34 darcies	
Kw(Sor)				13.04 darcies	
VISCOSITY OF WATER				0.93 cp	
VISCOSITY OF OIL				1.40 cp	
MOBILITY RATIO				0.526	

TABLE A17. RUN NO. 17. WATER FLOOD.

TIME HRS.	CUM PV INJECTED	CUM PV PRODUCED	INJ RATE CC/MIN	INJ RATE CUFT/DAY	PRESS DROP PSIG
0.00	0.000	0.000	13.36	0.679	0.45
2.28	0.082	0.082	13.53	0.688	0.45
4.28	0.151	0.151	12.83	0.653	0.45
6.28	0.224	0.224	13.75	0.699	0.45
7.18	0.255	0.255	13.20	0.671	0.45
11.28	0.390	0.390	12.33	0.627	0.45
POROSITY				34.93 %	
AVERAGE Swi				8.76 %	
AVERAGE Sor				30.50 %	
ABSOLUTE PERMEABILITY				106 darcies	
Ko(Swi)				82.50 darcies	
Kw(Sor)				3.42 darcies	
VISCOSITY OF WATER				0.94 cp	
VISCOSITY OF OIL				11.00 cp	
MOBILITY RATIO				0.485	

TABLE A18. RUN NO. 18. WATER FLOOD.

TIME HRS.	CUM PV INJECTED	CUM PV PRODUCED	INJ RATE CC/MIN	INJ RATE CUFT/DAY	PRESS DROP PSIG
0.00	0.000	0.000	54.85	2.790	0.90
0.72	0.107	0.107	59.36	3.019	0.85
1.22	0.188	0.188	60.50	3.077	0.85
1.72	0.270	0.270	61.26	3.116	0.75
2.00	0.317	0.317	62.76	3.192	0.75
3.22	0.512	0.413	60.00	3.052	0.75
POROSITY				34.93 %	
AVERAGE S_{wi}				9.69 %	
AVERAGE S_{or}				28.99 %	
ABSOLUTE PERMEABILITY				106 darcies	
$K_o(S_{wi})$				103.73 darcies	
$K_w(S_{or})$				4.99 darcies	
VISCOSITY OF WATER				1.02 cp	
VISCOSITY OF OIL				12.30 cp	
MOBILITY RATIO				0.580	

APPENDIX B

NOMENCLATUREENGLISH SYMBOLS

A	:	Cross-sectional area of the model
$a = 1 / M$:	Inverse mobility ratio
C	:	Chuoke's constant
C^*	:	Wettability number
F_s	:	Stability factor
\vec{f}_w	:	Fractional flow vector
g	:	Gravitational acceleration
H	:	Height of model
J	:	Leverett function
k	:	Absolute permeability
k_{ro}	:	Relative permeability to oil
k_{rw}	:	Relative permeability to water
k'_o	:	Base permeability in the oil phase
k'_w	:	Base permeability in the water phase
k_{ocw}	:	Permeability to oil at connate water saturation
k_{wro}	:	Permeability to water at residual oil saturation
L	:	Length of model
M	:	Endpoint mobility ratio
m	:	Exponent in Archie equation
n	:	Wave number

P_C	:	Capillary pressure
P_O	:	Pressure in the oil phase
P_W	:	Pressure in the water phase
Q	:	Volumetric injection rate
Q_O	:	Volumetric oil flow rate
Q_W	:	Volumetric water flow rate
R_K	:	Known resistance
R_O	:	Resistance of brine saturated porous medium
R_t	:	Resistance of fluid saturated porous medium
ΔS	:	Difference in water saturation before and after water flooding
S_O	:	Oil saturation
S_{Or}	:	Residual oil saturation
S_W	:	Water saturation
S_{Wi}	:	Initial water saturation
t	:	Real time
T	:	Dimensionless time
V	:	Average velocity
\vec{V}	:	Dimensionless velocity vector
V_C	:	Critical velocity
V_{osc}	:	Voltage drop across the oscillator
\vec{v}	:	Total velocity vector
\vec{v}_O	:	Velocity vector in the oil phase

\vec{v}_w	:	Velocity vector in the water phase
v_x, v_y, v_z	:	Components of velocity vector in x-, y- and z-direction, respectively
W	:	Width of model
x, y, z	:	Rectangular cartesian coordinates
X, Y, Z	:	Dimensionless rectangular cartesian coordinates

GREEK SYMBOLS

α	:	Dip angle
λ	:	Wave length
λ_c	:	Critical wave length
λ_m	:	Most probable wave length
μ_o	:	Viscosity of oil
μ_w	:	Viscosity of water
ρ_o	:	Density of oil
ρ_w	:	Density of water
σ	:	Interfacial tension
σ^*	:	Effective interfacial tension
θ	:	Contact angle
ϕ	:	Porosity